EPRI

Oxidation and Reduction of PWR Steam Generator Secondary Side Deposits: Experimental Data and Predictive Models

Technical Report

Oxidation and Reduction of PWR Steam Generator Secondary Side Deposits: Experimental Data and Predictive Models

1003591

Final Report, July 2002

EPRI Project Manager
A. McIlree

EPRI • 3412 Hillview Avenue, Palo Alto, California 94304 • PO Box 10412, Palo Alto, California 94303 • USA
800.313.3774 • 650.855.2121 • askepri@epri.com • www.epri.com

DISCLAIMER OF WARRANTIES AND LIMITATION OF LIABILITIES

ORGANIZATION(S) THAT PREPARED THIS DOCUMENT

Dominion Engineering, Inc.

ORDERING INFORMATION

Requests for copies of this report should be directed to EPRI Orders and Conferences, 1355 Willow Way, Suite 278, Concord, CA 94520, (800) 313-3774, press 2 or internally x5379, (925) 609-9169, (925) 609-1310 (fax).

CITATIONS

This report was prepared by

Dominion Engineering, Inc.
6862 Elm Street, Suite 460
McLean VA 22101

Principal Investigators
C. Marks
R.D. Varrin

This report describes research sponsored by EPRI.

The report is a corporate document that should be cited in the literature in the following manner:

Oxidation and Reduction of PWR Steam Generator Secondary Side Deposits: Experimental Data and Predictive Models, EPRI, Palo Alto, CA: 2002. 1003591.

REPORT SUMMARY

This report builds on the work reported in *The Oxidation and Reduction of Copper in Steam Generator Deposits: Under Shutdown, Layup and Startup Conditions* (EPRI report 1001204). It completes the collection of fundamental kinetic data on oxidation and reduction of pressurized water reactor (PWR) secondary-side steam generator deposit species (copper and magnetite) and decomposition of oxygen scavengers (hydrazine and carbohydrazide). With these data, models were developed to predict the effect of various shutdown, layup, and startup activities on the oxidation state of steam generator deposits. These models were then used to analyze examples of specific plant practices as a guide to aid utility personnel in analyzing plant-specific shutdown, layup, and startup activities. A five-step analysis plan is recommended for evaluating the potential effect of oxidized deposit species on steam generator tube degradation.

Background

It has long been suspected that oxidation of secondary-side steam generator deposits may promote onset of intergranular attack and stress corrosion cracking (IGA/SCC) of mill-annealed Alloy 600 steam generator tubes. It is believed this same phenomenon could affect the possible future occurrence of IGA/SCC of thermally treated Alloy 600 and Alloy 690 tubes in newer steam generators. The working hypothesis that describes the influence of oxides on accelerated tube degradation is that deposits formed during normal operation are oxidized during shutdown, layup, or exposure to atmosphere during secondary-side maintenance and inspection. If not reduced during startup, these oxidized species could accelerate tube degradation during subsequent operation by raising the electrochemical potential of the secondary-side environment. Oxidation may occur in the aqueous phase (aqueous oxidation) or in the gas space above the steam generator water surface (atmospheric oxidation). To optimize outage and startup schedules and protocols, knowledge of these deposits' oxidation and reduction behavior is necessary.

Objectives

To complete an evaluation of the potential for oxidation and reduction of PWR secondary-side steam generator deposits under prototypical shutdown, layup, and startup conditions and to develop modeling tools to aid plant chemists in designing outage and startup protocols that will minimize reducible metal oxides in the steam generator during early full power operation.

Approach

This project was completed in three stages:

- Experimental work to obtain fundamental kinetic data on oxidation and reduction of steam generator deposits and decomposition of oxygen scavengers
- Modeling work to apply the kinetic data to specific plant situations
- Analysis of specific shutdown, layup, and startup protocols to provide examples of the application of the models developed.

Results

The project developed models to predict the degree of oxidation and reduction of deposits in various locations on the secondary-side of the steam generator (for example, freespan scale or packed crevices). Application of these oxidation and reduction models to typical shutdown/startup sequences indicates that it is possible to fully reduce oxides developed during an outage period by appropriate use of oxygen scavengers and limitation of oxidizing conditions during shutdown. A five-step program outlines how to develop a coherent strategy for evaluating the influence of reducible metal oxides on steam generator tube degradation. Several examples demonstrate how utility personnel can use these results to evaluate plant-specific shutdown, layup, and startup protocols.

EPRI Perspective

This work is part of EPRI's ongoing efforts to develop practical recommendations to extend steam generator life and reduce inspection and maintenance costs. Specifically, this report is expected to aid in developing and revising EPRI guidelines regarding control of oxides during shutdown, layup, and startup. Information in the document will aid utility personnel in assessing the impact of various shutdown, layup, and startup procedures on oxidation and reduction of steam generator deposits.

Keywords

Steam generator deposit
Pressurized water reactor (PWR)
Sludge
Corrosion product
Shutdown, layup, and startup
Oxidation and reduction
Oxygen scavenger (reducing agent)
Alternative amine (advanced amine)

ABSTRACT

The objective of this project was to complete an evaluation of the potential for oxidation and reduction of pressurized water reactor (PWR) secondary side steam generator deposits under prototypical shutdown, layup and startup conditions. It has long been suspected that oxidation of these deposits may promote the onset of intergranular attack and stress corrosion cracking (IGA/SCC) of mill annealed Alloy 600 steam generator tubes. It is believed that this same phenomenon could affect the possible future occurrence of IGA/SCC of thermally treated Alloy 600 and Alloy 690 tubes that are in newer steam generators. The working hypothesis that describes the influence of oxides on accelerated tube degradation is that deposits formed during normal operation are oxidized during shutdown, layup or exposure to atmosphere during secondary side maintenance and inspection. If not reduced during startup, these oxidized species could accelerate tube degradation during subsequent operation by raising the electrochemical potential of the secondary side environment.

Of particular concern, due to its high reactivity with oxygen, is copper. Copper is usually present in steam generator deposits as 1~3 μm inclusions close to the tube wall or in crevices. Of lesser, but significant, concern is the iron oxide magnetite (Fe_3O_4), the main component of most steam generator deposits. The oxidation products of these two species, *e.g.*, cuprite (Cu_2O), tenorite (CuO) and hematite (Fe_2O_3), are collectively referred to as reducible metal oxides.

In the present work, the kinetics of oxidation of deposit species, as well as subsequent reduction, have been investigated. The role of temperature and pH have been explored, as well as the effectiveness of hydrazine, carbohydrazide and catalyzed hydrazine in reducing oxidized species such as copper oxides and hematite. Oxidation tests were conducted under both aqueous and atmospheric (humid air) conditions. The purpose of these tests was to collect data for the construction of a model to predict oxidation and reduction of deposits in several geometries in several bulk environments as an aid to plant chemists in developing protocols to minimize the deposit oxide accelerated IGA/SCC of steam generator tubes.

Application of these oxidation and reduction models to typical shutdown/startup sequences indicates that it is possible to fully reduce the oxides developed during an outage period by appropriate use of oxygen scavengers and limitation of oxidizing conditions during the shutdown. A five-step program is outlined for developing a coherent strategy for evaluating the influence of reducible metal oxides on steam generator tube degradation. Several examples are given demonstrating how utility personnel can use the results of these studies to evaluate plant-specific shutdown, layup and startup protocols.

CONTENTS

LIST OF FIGURES

LIST OF TABLES

1
SUMMARY AND CONCLUSIONS

Objective and Scope

The objective of this project was to complete an evaluation of the potential for oxidation and reduction of pressurized water reactor (PWR) secondary side steam generator deposits under prototypical shutdown, layup and startup conditions. It has long been suspected that oxidation of these deposits may promote the onset of intergranular attack and stress corrosion cracking (IGA/SCC) of mill annealed Alloy 600 steam generator tubes. It is believed that this same phenomenon could affect the possible future occurrence of IGA/SCC of thermally treated Alloy 600 and Alloy 690 tubes that are in newer steam generators. The working hypothesis that describes the influence of oxides on accelerated tube degradation is that deposits formed during normal operation are oxidized during shutdown, layup or exposure to atmosphere during secondary side maintenance and inspection. If not reduced during startup, these oxidized species could accelerate tube degradation during subsequent operation by raising the electrochemical potential of the secondary side environment. The oxidation process may occur in the aqueous phase (*i.e.*, aqueous oxidation) or in the gas space above the steam generator water surface (*i.e.*, atmospheric oxidation). A schematic of this hypothesis is given in Figure 1-1.

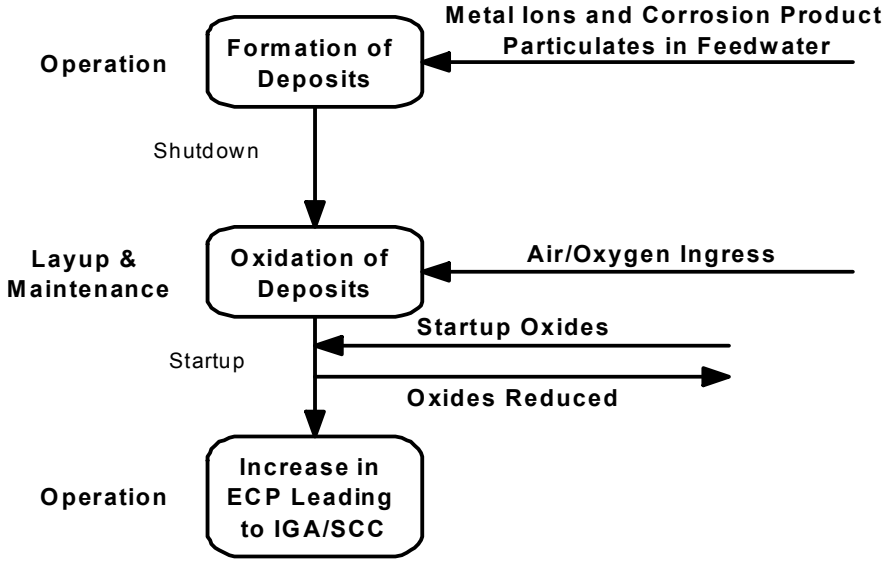

Figure 1-1
Schematic of the Working Hypothesis

Of particular concern in this regard is the oxidation of copper present in deposits. This is due in part to the high reactivity of copper with oxygen, as well as the significant influence of copper oxides on ECP. Although the concentration of copper in steam generator deposits varies widely from plant to plant (depending in large part on whether copper-bearing alloys have been used in the balance of plant), it typically manifests itself as distinct 1~3 μm metallic inclusions, often close to the tube wall or in crevices. Of lesser, but nevertheless still significant concern is the iron oxide magnetite (Fe_3O_4), the main constituent of most steam generator deposits. The oxidation products of these species, *e.g.*, cuprite (Cu_2O), tenorite (CuO) and iron oxides or hydroxides such as hematite (Fe_2O_3), are collectively referred to as reducible metal oxides (RMOs).

The purpose of this report is to present the results of experimental investigations of the kinetics of oxidation and reduction of deposit species under a variety of environments which reflect shutdown, layup and startup practices. The environmental conditions which were considered included temperature, pH and the concentration of oxygen scavenger, which may be used by the plant. From this kinetic data, it is then possible for a plant chemist to evaluate a particular outage sequence to determine the likelihood that a particular shutdown and layup scenerio could result in formation of RMOs, and then whether a startup sequence would fully reduce these oxides, thus reducing the potential for RMO-accelerated tube degradation.

Because RMOs are believed to accelerate IGA/SCC through elevation of the electrochemical potential (ECP), the fundamental measurement of their prevalence is the surface area exposed to the bulk chemistry. Therefore, the degree of oxidation is not necessarily relevant. For example, a 10 μm particle of copper with a 10 nm layer of copper oxide on its surface will not change the ECP any less than a 10 μm particle of pure copper oxide. Therefore, measurements of the degree of oxidation and reduction are best expressed in terms of the oxide thickness. In this way, the amount of oxide formed during an oxidation test can be directly compared to the degree of reduction during a reduction test and either can be directly compared to the degree of oxidation or reduction during any portion of an outage.

Summary of Experimental Results

In the present work, the kinetics of oxidation of deposit species, as well as subsequent reduction, have been investigated. In addition to these investigations, the decomposition of oxygen scavengers (specifically hydrazine and carbohydrazide) has also been examined both through experiments and through modeling. The topics explored in this project include the following:

- Aqueous Oxidation of Deposit Species
- Atmospheric Oxidation of Deposit Species
- Reduction of Deposit Species
- Decomposition of Oxygen Scavengers

The major conclusions from each of these four areas of the investigation are summarized below. Following the summaries of the experimental conclusions, guidance evaluating and improving a specific shutdown, layup and startup sequence is provided.

Aqueous Oxidation of Deposit Species

Rigorous feedwater chemistry control strategies have been developed by the nuclear industry to maintain reducing conditions on the secondary side of PWR steam generator during operation. Such reducing conditions are considered desirable in that they mitigate various forms of corrosion of both carbon steels and the Alloy 600, 690 or 800 tube materials. However, during an outage, steam generator deposits may be exposed to a variety of less reducing aqueous environments ranging from fully aerated water with no oxygen scavenger to solutions containing both amines and oxygen scavengers, but some residual oxygen. In addition, deposits can be exposed to oxygenated water during sludge lancing, bundle flushes or visual inspections, where water is often added to allow for underwater video use (a practice which is as generally performed as inspection in air). Based on the work described herein, the following conclusions were reached regarding oxidation of deposits in aqueous environments:

- In aerated water at neutral pH, which was the most aggressive (*i.e.*, oxidizing) environment tested, the oxidation of deposits appears primarily as the conversion of the copper portions of the deposits to copper oxides. The degree of oxidation of copper that can occur was found to be up to 1.2 nm/day at 60°C (140°F).
- The aqueous oxidation of copper at pH=9 is significantly retarded when the water is deaerated (dissolved oxygen less than 200 ppb) at relatively low temperatures (30°C—86°F). However, at higher temperatures (60°C—140°F) there is no retardation of the copper oxidation rate at low oxygen concentrations compared to the rates at high oxygen concentrations.
- The use of carbohydrazide (200 to 400 ppm) significantly suppressed the oxidation of copper at 30°C (86°F). For example, the amount of oxidation of copper was retarded by a factor of 3 to 4 in the presence of carbohydrazide. Replenishment of carbohydrazide was not required to achieve this retardation even for exposures of up to 30 days. This effect was observed to occur over a range of pH levels (7 to 10). This observation is in contrast with previous observations of similar experiments with hydrazine that found that hydrazine is quickly decomposed in such experiments and does not lead to long term retardation of oxidation.
- pH elevation using morpholine or ethanolamine was effective in retarding the rate of copper oxidation at 30°C (86°F), retarding the oxidation rate by a factor of two when the pH was raised fom 7 to 10. However, the use of these amines was less effective than the use of ammonia, which led to a five-fold retardation over the same pH change (7 to 10). For solutions containing each amine (except for ethanolamine, see Figure 3-4, between pH=8.5 and pH=10), the oxidation rate decreased as pH increased over a pH range of 7 to 10.
- While both tenorite (CuO) and cuprite (Cu_2O) were found in oxidized deposits, tenorite formation was found to be promoted by increased solution pH. The preferential formation of tenorite led to the slower formation of cuprite and an overall reduction in the rate of copper oxidation.
- Magnetite (Fe_3O_4) exposed simultaneously to air and unadjusted (*i.e.*, pH~6.5) deionized water for six months did not oxidize further to form hematite (Fe_2O_3) or any other iron oxides or iron hydroxyoxides at room temperature.

Atmospheric Oxidation of Deposit Species

At various times during plant outages, the secondary side of the steam generator may be exposed to air, either humid or dry. For this reason, the oxidation of deposits in air was studied. The following observations were made:

- Oxidation of copper in a humid air environment obeyed a logarithmic rate law, *i.e.*, the rate of oxidation decreased with time.
- As expected, the rate of oxidation of copper in humid air increases with increasing temperature. However, below approximately 60°C (140°F), the oxidation is a relatively slow process (*e.g.*, at 30°C or 86°F a one day exposure leads to a 1.0 nm oxide film) and is only mildly dependent on temperature. Above 60°C (140°F), oxidation rates increase significantly (*e.g.*, at 90°C or 194°F a one day exposure leads to a 24.2 nm oxide film) and the temperature dependence is more pronounced. If oxidation rates are examined separately in the two regions, Ahhrenius rate laws fit the observed reaction rates very well, allowing prediction of the degree of oxidation over a wide range of temperatures (30°C to 90°C or 86°F to 194°F) with reasonable accuracy.
- Increased moisture content in the air was found to mildly accelerate atmospheric oxidation of copper but was less important than temperature. Temperature increases of 60°C (140°F) can result in up to a hundred fold increase in the oxidation rate while relative humidity changes from 0 to 60% may increase the oxidation rate only by 50%.
- The atmospheric oxidation of magnetite was virtually undetectable (less than 0.1 nm of oxide based on weight gain measurements) below 50°C (122°F). Above this temperature, the oxidation followed a logarithmic rate law with rate constants that were well represented by an Ahhrenius rate law.

Reduction of Deposits

Since it is impossible to completely prevent the ingress of oxidants such as air or oxygen in the steam generators during layup or during activities such as sludge lancing, it is important to understand what steps can be taken to convert any RMOs formed in the steam generators back into less oxidized species. More specifically, one approach is to perform a reducing step during startup to convert reducible metal oxides to compounds with lower electrochemical potentials. In order to evaluate the effectiveness of this approach, experiments were conducted to investigate reduction of oxides of deposit species. The following conclusions were reached:

- Hydrazine is effective in reducing RMOs to less oxidized species over a range of temperatures (100°C to 288°C or 212°F to 550°F).
- The rate of reduction of copper oxides to copper metals by hydrazine has a highly complex temperature dependence due to competing reactions including decomposition of hydrazine and the reduction of metal oxides to metal.
- Lower temperatures (100°C—212°F) were found to be more effective in reducing of copper oxides by hydrazine when no hydrazine replenishment was made. Reactions at 150°C (302°F) led to less reduction over the course of 24 hours than did reactions at either 100°C

(212°F) or 200°C (392°F). This is attributable to competition between the various reactions occurring in a closed system of hydrazine, copper, copper oxide and oxygen.

- Reduction of copper oxides by carbohydrazide was found to be favored by intermediate temperatures (150°C—302°F) rather than high (200°C—392°F) or low (100°C—212°F) temperatures. This was especially true for short reaction periods (6 hours). At longer time periods (24 hours), reduction at 200°C (392°F) was nearly as effective as reduction at 150°C (302°F), but reduction at 100°C (212°F) was less effective.
- The rate of reduction of hematite (Fe_2O_3) to magnetite (Fe_3O_4) was slow in comparison to the rate of reduction of copper oxides. None of the solutions tested in this project was adequate for complete conversion of the hematite. However, the conversion that did occur was favored by increased temperature and increased concentrations of hydrazine and quinhydrone (a hydrazine catalyst). The maximum conversions achieved were on the order of 30%. This finding indicates that restricting the ingress of reducible iron species during startup may be an essential step in keeping steam generators free of these species during operation.
- In simulated startup sequences, significant conversion of copper oxides to copper metal was achieved for the three sequences tested. Based on these results, many startup procedures would be capable of converting up to 8 nm of copper oxide back to copper metal. More aggressive startup sequences could convert as much as 16 nm. A typical outage may produce from 4 nm to 20 nm of oxide, depending on the specific conditions experienced by the deposit species in the steam generator. Thus, the tests indicate that limiting oxidation during an outage, aggressively reducing oxides at startup or both will successfully eliminate all of the oxides formed during the outage before full power operation begins.

Scavenger Decomposition

One of the chief methods of retarding oxidation and promoting reduction of deposits and steam generator materials is to use oxygen scavengers, such as hydrazine or carbohydrazide, which lower the electrochemical potential of aqueous environments. It has long been known that these oxygen scavengers also undergo catalyzed decomposition in the presence of metals, metal oxides and metal ions, without promoting the reduction of these species. If the scavenger is consumed by decomposition it cannot perform the desired functions of reducing the electrochemical potential, consuming oxygen, retarding oxidation and promoting reduction. Therefore it is desirable to understand the competition between these reactions. To increase this understanding, both experimental and modeling investigations were conducted on the decomposition process. The experimental investigations were conducted to provide the relevant inputs (such as rate constants) to incorporate into the phenomenological models. In turn, the models provide a method by which various plant startup practices can be evaluated to determine their potential to reduce any oxidized species formed under prior stutdown or layup conditions. Specifically, the modeling was used to investigate the diffusion and decomposition of scavengers in three types of deposits: tube scale, deposits in packed crevices and sludge piles. The conclusions from these investigations are presented below.

Experimental Investigation

The following conclusions were drawn from the experiments conducted to evaluate oxygen scavenger decomposition and deposit reduction:

- The decomposition of both hydrazine and carbohydrazide in aqueous solutions was found to obey first order rate laws under a variety of conditions, including different temperatures, deposit concentrations and initial concentrations of scavenger.
- The deposit loadings (mass of deposits per mass of solution) did not significantly influence the decomposition rates of either hydrazine or carbohydrazide over a range of 1% to 2% (wt/wt).
- The presence of air above the aqueous solution (analogous to layup conditions without a nitrogen blanket) significantly enhanced the decomposition of hydrazine, leading to half-life values an order of magnitude lower than those without air (*e.g.*, 5 hours verses 90 hours for hydrazine at 60°C).
- The presence of steam generator deposits (removed during sludge lancing) or the presence of copper powder significantly accelerated the decomposition of both hydrazine and carbohydrazide relative to the presence of synthetic magnetite. For example, at 30°C the half-life of hydrazine in the presence of copper powder or steam generator deposits was on the order of 35 hours, while the half-life in the presence of synthetic magnetite was on the order of 170 hours.

The results from these experiments were used as inputs to the modeling investigation summarized below.

Model Development

Theoretical modeling of the simultaneous diffusion and decomposition of oxygen scavengers was conducted to determine the concentrations of scavenger in crevices and within porous deposits. The results of the modeling were as follows:

- The diffusion resistance in free span tube scale is negligible, leading to oxygen scavenger concentrations at the tube/tube scale interface equivalent to those in the bulk water.
- In crevices and sludge piles, diffusion can significantly retard the transport of hydrazine and carbohydrazide from the bulk to the inner regions of the deposit. For a prototypical crevice (0.5 cm deep), the scavenger concentrations were predicted to be on the order of 15% to 20% of the bulk concentration. In a prototypical sludge pile (1.5 cm deep), concentrations on the order of 1% of the bulk concentration were predicted.

The modeling results demonstrate that there are likely to be locations in the steam generator where the concentration of the oxygen scavenger during layup is low, even if the bulk layup solution contains high concentrations of scavenger (on the order of 400 ppm). Therefore, when evaluating the degree of reduction of oxides formed during an outage, separate consideration must be given to deposits in crevices and sludge piles.

Evaluating Shutdown, Layup and Startup Practices

As described in the previous summary sections, the goals of this project were as follows:

- to improve the overall understanding of the formation of oxidized species (RMOs) on the secondary side of PWR steam generators during typical shutdown, layup and startups
- to investigate the role of oxygen scavengers in mitigating oxidation processes and possibly promoting direct reduction of RMOs (for example, during startup)
- to develop models that can be used as tools to predict the formation and reduction of RMOs at a particular plant

With regard to the plant-specific evaluations, the following steps are suggested:

- Review plant deposit characterization reports and summarize the following:
  - total deposit loading
  - copper concentrations in deposits by deposit type (powder, tube scale, hard top-of-tubesheet sludge or collars)
  - information on deposit oxidation state (copper metal versus copper oxides or hematite versus magnetite, for example)
- Summarize the plant's shutdown, layup and startup protocols noting the following for each exposure environment:
  - air (humid or dry) or aqueous
  - duration
  - temperature
  - pH
  - oxygen scavenger type and concentration
  - oxygen concentration
- Estimate oxidation of deposit species during shutdown and layup. The data on oxidation rates presented in this report can be used to evaluate the thickness of the oxide layer formed during each activity. The rates for neutral pH water can be used to predict the thickness of oxide formed during sludge lancing; the rates for humid air oxidation can be used to predict the thickness of the oxide formed during tube sleeving; *etc.*
- Estimate the reduction of the deposit RMOs formed during shutdown, layup and startup in light of the information gathered in the summarizing of the startup protocol (duration, temperature, pH, *etc.*). More specifically, the plants practices can be evaluated to determine the oxide thickness that is likely to be reduced during the startup sequence. For example, the experiments conducted for this project indicate that an oxide layer 8 nm thick can be reduced by a mildly reducing startup sequence (~0.5 ppm hydrazine) while more aggressive startups (~50 ppm hydrazine) can reduce twice as much.
- Estimate the reduction of any residual deposit RMOs during subsequent power operation.

Using the above steps, an estimate of the total inventories of RMOs by location in the steam generator is in theory available to the plant. While no specific guidelines exist for defining an "acceptable" concentration of RMOs, Section 2 does provide general information on the role of RMOs in promoting the corrosion of several materials including Alloys 600, 690 and 800.

Application of these oxidation and reduction models to typical shutdown/startup sequences indicates that it is possible to fully reduce the oxides developed during an outage period by appropriate use of oxygen scavengers and limitation of oxidizing conditions during the shutdown. However, the margin for some typical sequences is not large. Considering the importance of avoiding oxidizing conditions, increasing the margin by limiting exposure to oxidizing conditions and maximizing the strength of reducing conditions during startup is considered prudent.

Based on the work done in this report, it appears that oxides formed in place by exposure of steam generator deposits to oxidizing conditions during shutdown and layup can be adequately reduced by the use of low oxygen levels and high levels of oxygen scavengers during startup. However, this work did not address reduction of RMOs brought into the steam generators from the secondary system during startup and early power operation. It is known that the levels of RMOs brought into the steam generator from the balance of the plant during these periods are high relative to transport during steady-state full power operation, both in absolute concentration and as a fraction of the total transport. Reducing these RMOs to less oxidized species before they concentrate in crevice areas (*e.g.*, by the use of high levels of hydrazine during early phases of operation) may be of even more importance with respect to maintaining tube integrity than reducing the RMOs developed in place in the steam generators.

2
INTRODUCTION

The concentration and eventual precipitation of feedwater impurities is an unavoidable consequence of steam production. In pressurized water reactors (PWRs), the boiling of water on the secondary side of the steam generator (SG) results in significant deposition of impurities. These deposits can form in many locations within the steam generator, for example, on the SG tubes as scale, in the support plate crevices or on the top of the tube sheet as hard piles, collars or powder. In PWR steam generators, tube scale and powder are generally composed of iron species, which typically constitute more than 80% of the deposit weight. After iron, copper is often the most plentiful element in tube scale and powders, particularly at plants that use copper alloys as materials of construction in the feedwater and condensate systems. Copper concentrations in deposits range from 0.3% to 1% at plants with nominally copper-free secondary systems, and up to 2% to 20% at copper-bearing plants. Iron is usually present in the form of magnetite (Fe_3O_4), while deposited copper is usually present in the form of copper metal (Cu).

Because deposits are often found in direct contact with SG tubes (either as free-span scale or crevice deposits), these materials are expected to strongly influence the local chemistry conditions experienced by the tube surface. One of the chief influences of deposits is the alteration of the electrochemical potential (ECP). A kinetically active electrochemical reaction will maintain the local ECP at the potential of the reaction couple. For example, if copper is being converted to cuprous oxide (Cu_2O or cuprite), then the local ECP will be the potential of the Cu/Cu_2O reaction since this is the only potential at which both species can exist. The difference between local ECP and bulk ECP will depend on the kinetics of the reaction, the ratio of the reacting surface area to the reaction volume, the other species present and other situation-specific factors. Figure 2-1 shows the calculated [1] ECP of several chemical reactions or couples associated with the species most common in deposits. The ECP is shown relative to the ECP of the Ni/NiO reaction. (The values in Figure 2-1 are those for neutral pH. However, the potentials of these couples and that of the Ni/NiO reaction are roughly parallel when plotted as functions of pH in the alkaline region. Therefore, the relative potential values given in Figure 2-1 are valid over a range of pH levels.)

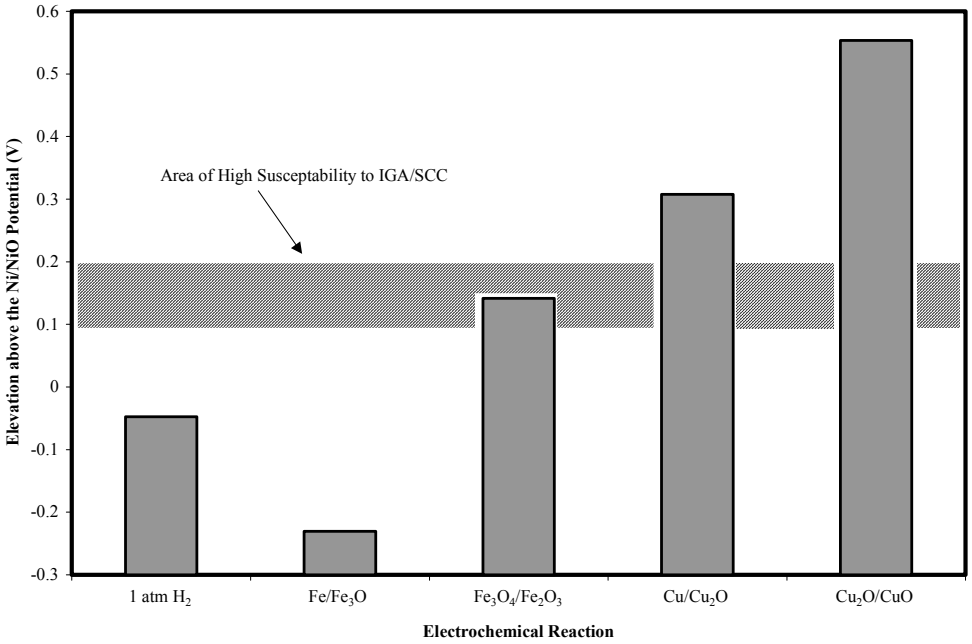

Figure 2-1
Potentials of Several Electrochemical Reactions at 300°C at Neutral pH

Experiments have shown that Alloy 600 is most susceptible to IGA/SCC at potentials of 100 to 200 mV above the Ni/NiO potential [2, 3 and 4]. Figure 2-1 shows this range, with respect to the Ni/NiO potential with a shaded band. If the ECP of the local environment is below the area of susceptibility, corrosion is expected to be too slow to support IGA/SCC. However, if the ECP of the bulk environment is below the area of susceptibility and the local area is above, there exists a location between the local chemical reaction (high potential) and the bulk environment (low potential) that is in the area of susceptibility. Since SGs are typically operated at low potential (perhaps as low as the potential of the one atmosphere hydrogen electrode or the Ni/NiO reaction, but possibly higher), the presence of equilibria with elevated potentials will likely lead to some portions of the SG being exposed to potentials which may accelerate IGA/SCC. Thus from an electrochemical analysis, cuprous oxide (Cu_2O or cuprite), cupric oxide (CuO or tenorite) and hematite (Fe_2O_3) would all be expected to promote IGA/SCC.

Because of the many variables associated with operating and controlling the chemistry in SGs, absolute confirmation that oxidants in SG deposits are a significant cause of IGA/SCC is difficult, if not impossible, to obtain. However, considerable anecdotal evidence exists to support this hypothesis. A detailed summary of much of the data present in the literature is given in Reference 5. Some of the most convincing cases given in that reference include the following:

- Low IGA/SCC rates at Swedish and Japanese plants where strict controls on oxides were in place during the plants' entire life.
- An evaluation of Belgian plants indicating that IGA/SCC is related to the number of shutdowns and startups rather than the operating life.
- A rapid increase in circumferential cracking at a plant after a chemical cleaning that may have left oxidized copper in the SG (no copper/copper oxide removal step was performed).

- The absence of accelerated IGA/SCC after chemical cleanings that included a high-temperature oxide reduction step.
- The successful amelioration of severe IGA/SCC when strict controls over startup oxides (along with other remedial measures) were imposed.

Together, anecdotal evidence from plants and theoretical evidence from evaluation of electrochemistry form a strong indication that deposit oxides can contribute to the acceleration of IGA/SCC.

Today, secondary side systems are operated at low oxygen concentrations (<1 to 10 ppb) with small but significant concentrations of a reducing agent, typically hydrazine. It is therefore unlikely that oxidizing conditions in the SGs will develop during long-term operation. This conclusion is confirmed by analysis of deposits from SGs, which generally consist of compounds (almost wholly magnetite and copper metal, to the extent that typical analysis methods, such as XRD or Mössbauer spectroscopy, can determine concentrations of other species) which exhibit low potentials. However, during layup and startup of the SG, deposits may be exposed to an oxidizing environment. Such an environment may arise through any of the following situations:

- Sludge lancing with aerated water
- Exposure to humid air after draining
- Layup with aerated or partially oxygenated water
- Additions of aerated or partially oxygenated auxiliary feedwater

When the deposits are exposed to an oxidizing environment, reducible metal oxides may be formed through one of the following reactions (simplified herein for clarity):

$$2Fe_3O_4 + ½O_2 \rightarrow 3Fe_2O_3 \quad (2\text{-}1)$$

$$2Cu + ½O_2 \rightarrow Cu_2O \quad (2\text{-}2)$$

$$Cu + ½O_2 \rightarrow CuO \quad (2\text{-}3)$$

In addition to the oxidized species that may be formed by these reactions, reducible metal oxides may be transported to the steam generator from the feedwater train or other balance of plant systems, especially during startup when these systems may be in a more oxidizing condition than would exist during full power operation.

Due to the competition between different reactions and diffusion limitations through the deposits, some reducible metal oxides may survive startup and influence the high temperature electrochemical environment in a way that accelerates IGA/SCC during operation. This is despite attempts to reduce species during plant startup. For example, hydrazine can reduce copper oxides back to copper metal. However, this reaction, as well as the decomposition of hydrazine and the reaction of hydrazine with oxygen, is temperature dependent. The reaction rate under a layer of tube scale or at the bottom of a crevice can be limited by the diffusion of hydrazine through deposits. Furthermore, thermal expansion differences may close crevices after startup, trapping oxides near the tube surface and making them inaccessible to hydrazine.

The complex chemistry of deposit oxidation and subsequent reduction can be represented by the three-stage process shown in Figure 1-1. In the first step, during normal operation, reduced deposits (magnetite and copper metal) are formed. These deposits are generally benign with respect to acceleration of tube degradation. In the second step, during layup, the deposits are exposed to oxidizing conditions and undergo a chemical reaction (to form hematite or copper oxides). At the low temperatures associated with layup, there is likely to be no tube degradation during this stage. However, in step three, the tubes are heated in the presence of reducible metal oxides that, due to incomplete reduction, accelerate IGA/SCC of the SG tubes.

If the working hypothesis outlined in the previous paragraph is valid, then there are two ways in which the deleterious effects of deposit oxides can be mitigated. These are as follows:

- Minimize the oxidation of species during layup
- Take steps to ensure reduction of the oxidized deposits back to their low potential form before the temperature of the system increases to a point where these species could cause the deposits to accelerate IGA/SCC

The first of these goals requires data on oxidation kinetics. The second requires data on reduction kinetics. In addition, data on the decomposition of oxygen scavengers is required to accurately assess the local environment experienced by the secondary side deposits. These data were collected during the course of this investigation and are presented in the next section.

Note that an additional source of oxidizing agents are those species entering the steam generator from the feedwater train during startup and early phases of operation. This report deals primarily with alteration of deposits present in the steam generator at shutdown and does not specifically address the ingress of additional species during startup and early operation. However, the data collected during this project indicates the following:

- Ingress during startup may be the prime source of hematite on the secondary side (specifically, it was found that oxidation of magnetite deposits already in the steam generator is not a likely source of hematite).
- Hematite, once present in the steam generator, will be difficult to reduce to magnetite using conventional startup sequences.

Investigation of the ingress of oxides during startup was not within the scope of this project. However, reduction kinetics data collected for this project are expected to apply to reducible metal oxides regardless of their source.

3
EXPERIMENTS AND DISCUSSION

Introduction

The prevention of reducible metal oxide accelerated tube degradation depends on two separate, but related actions. These are as follows:

- Retarding oxidation during shutdown and layup
- Promoting reduction during startup

However, these are not the only (nor even, in general, the most important) goals of layup and startup sequence design. Numerous other activities, such as reactor physics testing, must also be included in the outage schedule and the economics of the various choices must be evaluated. In order for plant personnel to make rational decisions with respect to minimizing reducible metal oxides, data are required regarding the rates of deposit oxidation and reduction. The experiments conducted during this investigation provide those data. In order to accurately apply these data to actual plant conditions, knowledge of the local environment experienced by the secondary side deposits is required. One way that the local and bulk environments may differ is in the concentration of oxygen scavenger. This possible difference arises because of the deposit-accelerated decomposition of oxygen scavengers.

Thus, three types of data are required to accurately assess the likelihood that reducible metal oxides will be present after startup is complete. These types are:

- Deposit oxidation rates
- Deposit reduction rates
- Scavenger decomposition rates

Deposit oxidation rates differ both quantitatively and qualitatively in aqueous and atmospheric environments. Therefore it is useful to treat these two conditions separately. Likewise, the decomposition of oxygen scavengers can be investigated both experimentally and through modeling, and these interrelated investigations are also more easily examined when separated. In the remainder of this section five sets of experiments and modeling efforts are discussed. These are as follows:

- Aqueous oxidation experiments
- Atmospheric oxidation experiments
- Reduction experiments

- Scavenger decomposition experiments
- Scavenger decomposition modeling

Each of these sets is discussed in detail in the sections below.

Aqueous Oxidation Experiments

Secondary side deposits in steam generators may be exposed to a variety of environments during shutdown and layup. These range from slightly acidic, aerated sludge lancing water to high pH, deaerated layup water. In a previous EPRI-sponsored study [6] it was found that the oxidation rate of copper was a function of temperature and pH, as shown in Figure 3-1. It was also found that the presence of hydrazine did not particularly retard oxidation. It was also found that the oxidation of magnetite, Fe_3O_4, (in general, the primary constituent of secondary side deposits) was negligible over the course of one month.

Note that the oxidation and reduction rates in this and in the previous EPRI study [6] are reported as surface conversions in nanometers per day. This distinguishes this work to some degree from other studies reported in the literature, where often *percent oxidation* or *percent reduction* are used to characterize converting deposit species. However, the use of surface conversions is considered more appropriate as the oxidation and reduction phenomena are in fact surface effects, similar to corrosion phenomena. For example, a 10 nm oxidation of a plant deposit containing 3 wt% copper, which is present as 1 μm particle inclusions, corresponds to 0.12 wt% copper oxide (as a fraction of the entire deposit). Likewise, a 20 nm oxidation of powdered sludge with a 10 μm particle size corresponds to 1.2 wt% conversion to hematite.

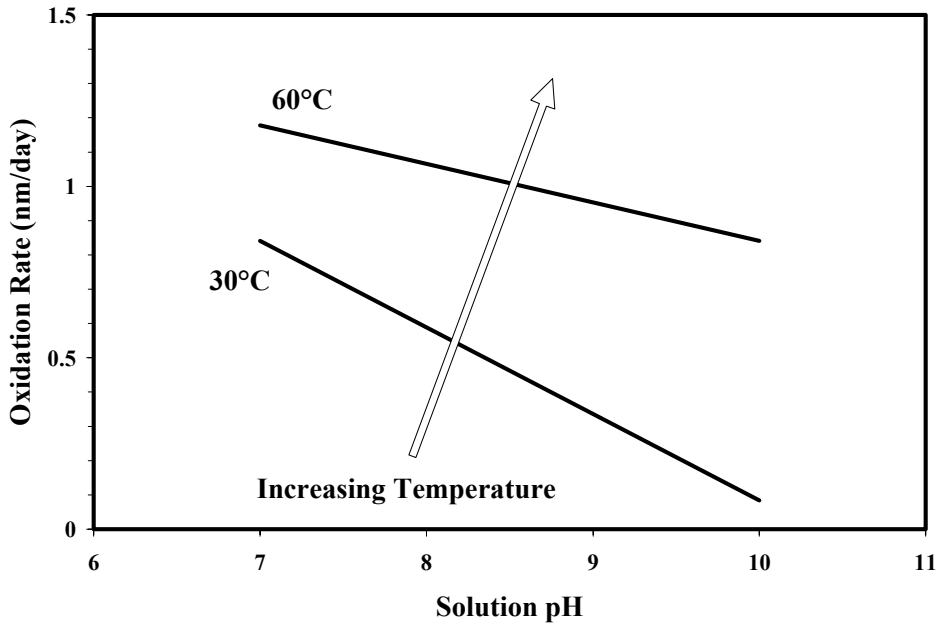

Figure 3-1
Effect of pH and Temperature on the Aqueous Oxidation of Copper

The experiments reported below expanded upon those previously reported. Specifically, they addressed the following issues:

- The effect of dissolved oxygen concentration on copper oxidation
- The effect of carbohydrazide addition on copper oxidation
- The effect of alternate amines on elevated-pH retardation of copper oxidation
- Long-term oxidation of magnetite

Each of these issues was addressed by an independent investigation. The details of the procedures and results of these investigations are given below.

Low Oxygen Aqueous Environments

One way to reduce the oxidation of secondary side deposits during layup is to reduce the amount of oxygen available to react with the copper in the deposits. Theoretically, eliminating oxygen altogether from the secondary side will completely stop the oxidation of copper in the steam generator deposits [7]. However, in practice, complete deaeration is not possible. It is therefore useful to know whether moderate amounts of deaeration can retard oxidation of deposits.

To determine the effects of reduced oxygen levels on the oxidation of steam generator deposits a series of aqueous oxidation experiments was performed using copper powders. The use of copper powder in lieu of copper particles distributed in a magnetite matrix was justified in the previous EPRI work [6], as mass transport limitations in the deposit matrix were shown to be low. Briefly, these experiments involved a series of batch reactions in which copper powder was exposed to a specified aqueous environment. At a pre-determined time point, the experiment was ended and the degree of oxidation was assessed using X-ray diffractometry (XRD). By conducting several experiments with different duration and identical environments, kinetic data was obtained. This experimental technique is discussed in more detail in Reference 6.

A source of mildly deaerated water was created by sparging de-ionized water with nitrogen followed by addition of hydrazine. The oxygen concentration of this water was about 200 ppb, measured colorometrically. This level of oxygen is considerably lower than that of water in equilibrium with the atmosphere (about 7 ppm at room temperature) and higher than that which is readily achieved during wet layup in some secondary water systems (less than 100 ppb) [8]. The pH of the deaerated water was 9.2, while the hydrazine level was initially at 200 ppm (6.25 mM). Oxidation experiments were conducted at 30°C (86°F) and 60°C (140°F).

Figure 3-2 shows the average oxidation rates observed in the low oxygen studies compared with those previously determined [6] for high oxygen solutions. The oxide form of the copper was primarily cuprite (Cu_2O) with traces of tenorite (CuO). (Note that CuO has a higher potential than Cu_2O, see Figure 2-1.) As can be seen in this figure, at lower temperatures, even mild deaeration can provide significant reduction of oxidation. In Figure 3-2, the oxidation rate for copper at 30°C (86°F) in low oxygen (200 ppb) water is statistically indistinguishable from zero. However, at higher temperatures, the advantages of deaeration are reduced. These results reflect similar findings regarding pH [6], which showed that the advantages of raising the pH are lost at higher temperatures (60°C—140°F).

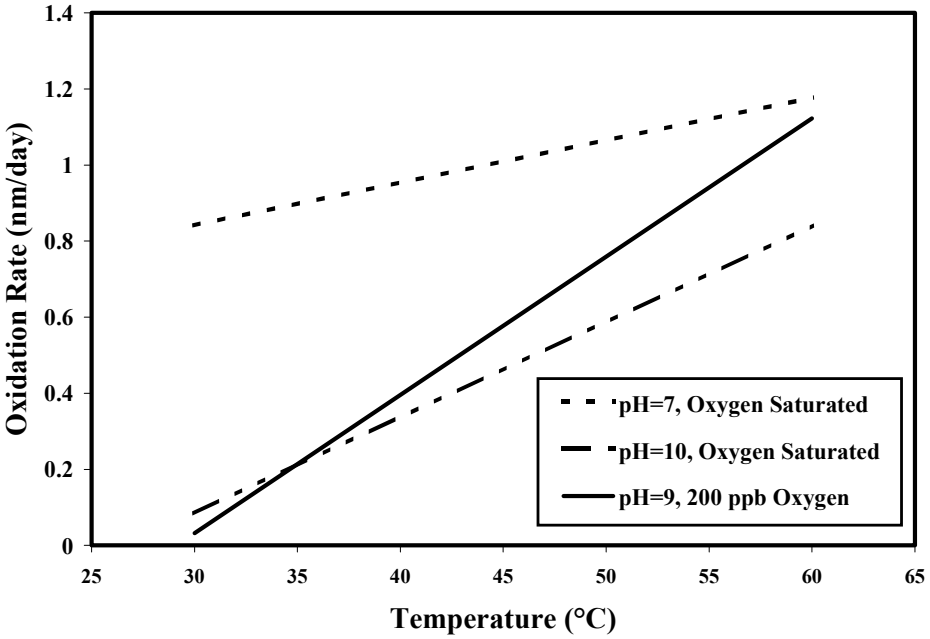

Figure 3-2
Effect of Lower Dissolved Oxygen on the Oxidation of Copper

From these findings, it can be concluded that lowering the oxygen content of layup water to levels at or below about 200 ppb can significantly reduce the rate of oxidation of copper in the steam generator deposits. However, the advantages of lower oxygen levels may be lost if the layup water increases in temperature much above 30°C (86°F). At higher temperatures, more significant deaeration of the secondary side layup water may be necessary.

The current version of the EPRI PWR secondary water chemistry guidelines specifies an upper limit for dissolved oxygen of 100 ppb for layup water [9]. Other investigations into the oxidation of copper have indicated that the peak oxidation rate occurs at a dissolved oxygen concentration of about 200 ppb [10]. Therefore, the concentration of dissolved oxygen chosen for the experiment was 200 ppb, which will conservatively overestimate the degree of oxidation expected during layup in an actual steam generator. Below 200 ppb, the oxidation rate is expected to decrease linearly with the oxygen concentration.

Carbohydrazide as an Oxidation Inhibitor

In the previous study [6] it was determined that hydrazine (N_2H_4) was an ineffectual inhibitor of copper oxidation under batch conditions. When present, hydrazine would prevent oxidation. However, over the course of a few days, copper powder or plant deposit powder would accelerate the decomposition of hydrazine so that after a brief inhibition period the oxidation rate would attain the same level as that observed in tests in which hydrazine was not present initially. This finding lead to the consideration of alternate oxygen scavengers for oxidation inhibitors in layup conditions.

Aqueous oxidation experiments were performed with copper powder to investigate the efficacy of carbohydrazide ($H_2NNHCONHNH_2$—Aldrich Chemical Co.) as an oxidation inhibitor. These experiments were similar to those used in the previous study and are described in detail in Reference 6. Briefly, these experiments involve batch reactions of copper powder in de-ionized water. At the end of each experiment, the powder was removed and analyzed using X-ray diffraction (XRD) to determine the degree to which it has oxidized. By conducting several experiments in the same environments for varying lengths of time, kinetic data were obtained.

In these experiments, copper powder was submersed in de-ionized water containing carbohydrazide at either 200 ppm (2.2 mM) or 400 ppm (4.4 mM). These levels are comparable to the weight percent levels of hydrazine used at some plants to control oxidation during wet layup. The pH levels of the solutions containing carbohydrazide were adjusted using ammonium hydroxide to either pH=7 or pH=10. The temperature was maintained at 30°C (86°F).

The measured oxidation rates are shown in Figure 3-3 along with data from Reference 6 regarding oxidation of copper in the absence of carbohydrazide. In general, the oxide form was cuprite (Cu_2O) with trace levels of tenorite (CuO). As can be seen in this figure, carbohydrazide has significant efficacy as an oxidation inhibitor. As discussed earlier, the previous investigation [6] showed that hydrazine was not an effective oxidation inhibitor if it was not continuously replenished. Together, these results indicate that the use of carbohydrazide instead of hydrazine during wet layup has the potential of reducing the extent to which secondary side steam generator deposits are oxidized.

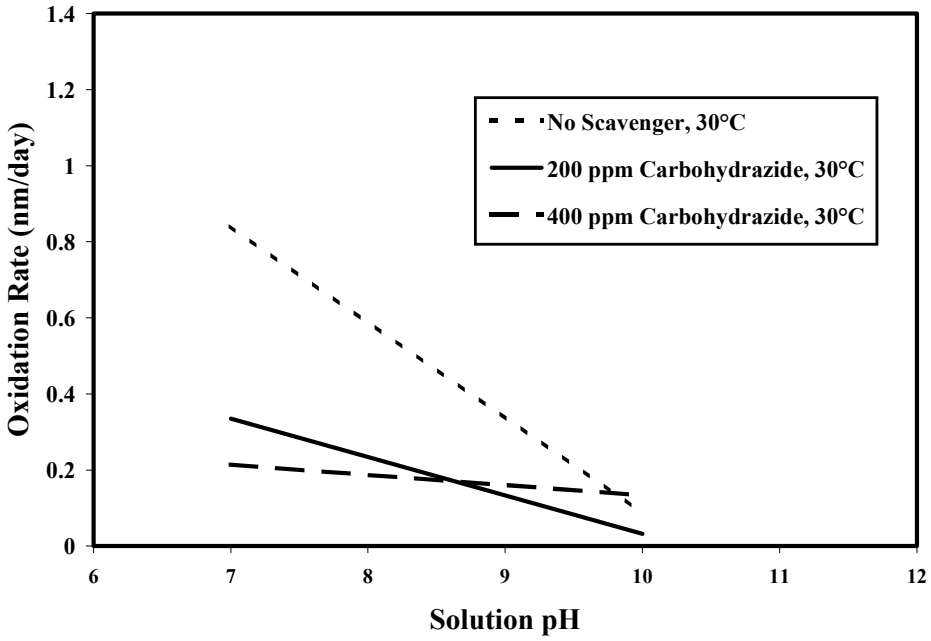

Figure 3-3
Effect of Carbohydrazide on the Oxidation of Copper

As the pH is increased, the effect of carbohydrazide addition becomes less distinct due to the large effect of pH in suppressing copper oxidation. However, at lower pH, the effect of carbohydrazide is quite strong. Similar reductions in oxidation rates can thus be achieved either by pH elevation or by carbohydrazide addition. Carbohydrazide addition thus tends to lower the dependence of oxidation rates on pH. This is consistent with literature data regarding the inhibition of oxidation of other metals by carbohydrazide. For example, it has been demonstrated that, at sufficiently high levels of carbohydrazide (>125 ppm), pH has little influence on the corrosion rates of carbon steel [11].

The reduction in oxidation rates due to raising the carbohydrazide level from 200 ppm to 400 ppm is smaller than that due to raising the concentration from zero to 200 ppm. This indicates that increased levels of carbohydrazide may produce diminishing decreases in oxidation rates. This implies that given additional data regarding the material and other usage costs for implementation of carbohydrazide addition, an optimum concentration of carbohydrazide could be found. However, the determination of such optima would require further data regarding intermediate carbohydrazide levels.

Alternate Amines as Oxidation Inhibitors

Previously [6] it has been shown that elevation of the pH from 7 to 10 using ammonium hydroxide can significantly decrease the oxidation rate of copper powders and, by implication, secondary side steam generator deposits containing copper. Increasingly, consideration is being given to the use of advanced amines for pH control in secondary water systems. Thus, it is useful to know whether the oxidation inhibition previously observed was due solely to changes in pH or if the use of an alternative amine would affect the oxidation rate.

Experiments were conducted in which copper powders were exposed to environments with a range of pH levels generated by the following three different amines:

- ammonia hydroxide
- morpholine
- ethanolamine

These experiments were conducted according to the procedures developed in Reference 6. In brief, batch reactions of copper powder submersed in de-ionized water were performed. At the end of the experiment, the oxidation state of the copper powder was determined by X-ray diffraction. Kinetic data were obtained by conducting several experiments with the same environmental conditions and different durations.

The oxidation rates measured are shown in Figure 3-4. Except for one anomalous experiment for ethanolamine at pH=10, the oxidation rates decline with increasing pH. The effect of ammonium hydroxide is the most pronounced, while that for morpholine is the least. Note that even for the low pH experiments at pH=7, some amine was added to adjust the pH from the slightly acidic level arising from the absorption of carbon dioxide from the atmosphere.

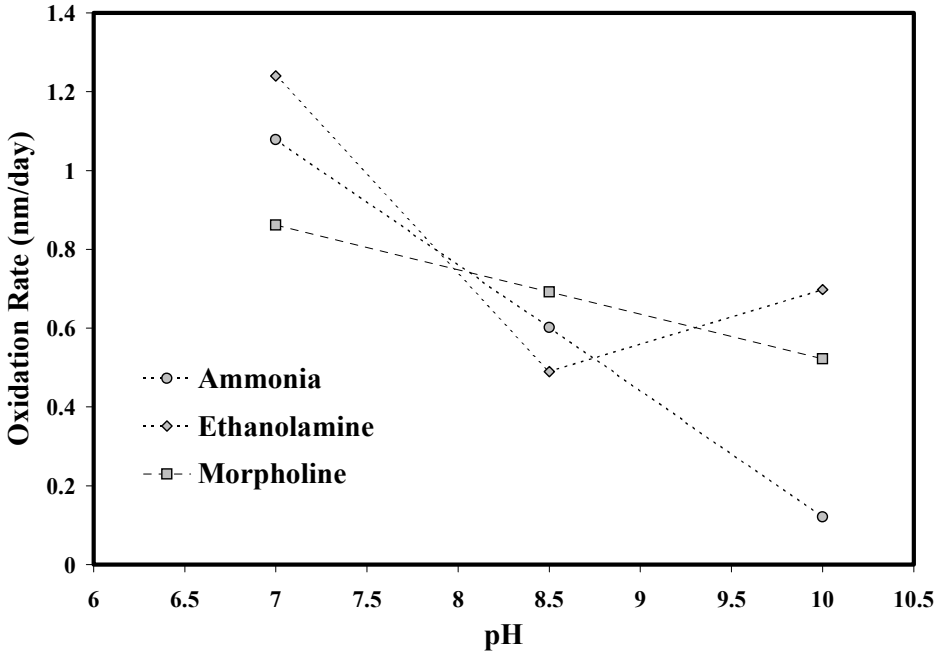

Figure 3-4
Copper Oxidation Rate as a Function of pH for DI Water with Three Additives

At low pH values, the morpholine was more effective than ammonium hydroxide at lowering the oxidation rate while ethanolamine was less effective. At high pH values, both advanced amines were less effective. Since most layup chemistries are in the pH range of 9 to 10, this implies that ammonium hydroxide may be more effective in preventing the oxidation of steam generator deposits during wet layup. The data shown in Figure 3-4 also suggest that raising the pH of the layup environment from moderately high values (8.5) to still higher values (10) can further inhibit the oxidation of deposits.

Figure 3-5 shows the relationship between the amount of cuprite (Cu_2O) detected and the amount of tenorite (CuO) detected. (Note that oxide contents are expressed as thicknesses, which are calculated from the weight fraction measured by XRD and the specific surface area.) As this figure shows, increasing amounts of tenorite lead to decreasing amounts of cuprite. There is a rough correlation between the oxide formed and the pH of the environment. At low pH values (7), nearly all of the oxide formed is cuprite (regardless of the amine used to adjust the pH). At higher pH values the oxide formed is increasingly tenorite (with ethanolamine again displaying anomalous behavior). This trend is most pronounced in the cases where ammonium hydroxide was used to adjust the pH. These data roughly correspond to the equilibrium observation that increased pH makes tenorite more stable than cuprite [12].

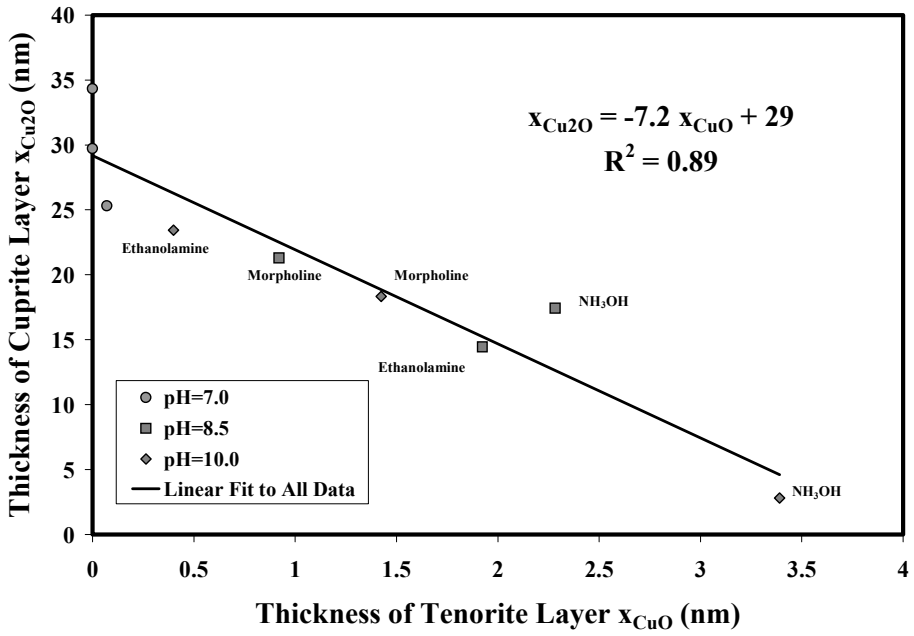

Figure 3-5
Cuprite (Cu_2O) Thickness as a Function of Tenorite (CuO) Thickness

The kinetic data shown in Figure 3-5 offer evidence that tenorite formed under these conditions can lead to the development of a passivation layer which protects the copper metal from further oxidation. Thus it appears that the mechanism for oxidation inhibition of copper at high pH levels is not due to an absence of oxidation, but rather a shift from the development of an unprotective cuprite (Cu_2O) film to a protective tenorite (CuO) film.

Magnetite Oxidation in Aqueous Environments

Previous investigations [6] showed no evidence of magnetite oxidation in aqueous solutions over the course of one month. These experiments included tests with synthetic magnetite as well as secondary side deposit powder from a commercial nuclear plant. The harshest condition studied was 60°C (140°F) and pH=7. During this experiment, magnetite powders where fully submersed in oxygen saturated water. This condition was considered to bound the more aggressive aqueous environments that might be found in a steam generator during wet layup.

In addition to wet conditions bounded by the previous experiments, steam generator deposits can be exposed to dry or moist conditions due to outage activities such as draining and refilling for hideout return or sludge lancing. It is well known that the three-way interface between the liquid, solid and gas phases can be a highly aggressive environment for oxidation. Therefore, in order to test the most severe conditions to which deposits might be exposed during layup, an experiment was devised for testing the oxidation of magnetite in contact with both air and water.

In this experiment, porous pellets and powders composed of synthetic magnetite and magnetite obtained from sludge lancing at two commercial nuclear plants were used. The magnetite from Plant A was in the form of sludge pile powder. The magnetite from Plant B was obtained by

grinding flakes collected during sludge lancing. From their initial characteristics, these flakes were determined to be secondary side tube scale. These pellets and powders were simultaneously exposed to both air and distilled water as shown in Figure 3-6 and Figure 3-7. The deionized water was not pH adjusted and so had a slightly acidic (pH ~ 6) nature due to adsorption of carbon dioxide from the air.

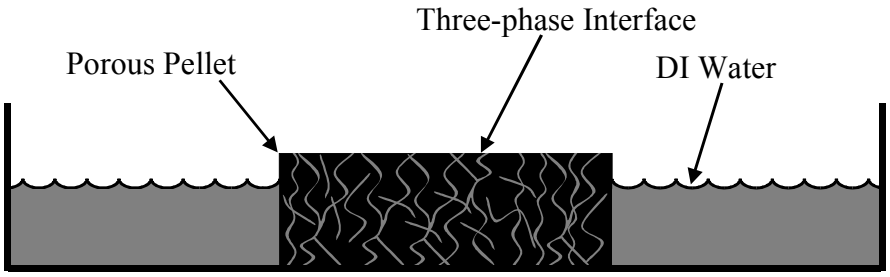

Figure 3-6
Schematic of Pellet Experiment Showing the Three-Phase Interface

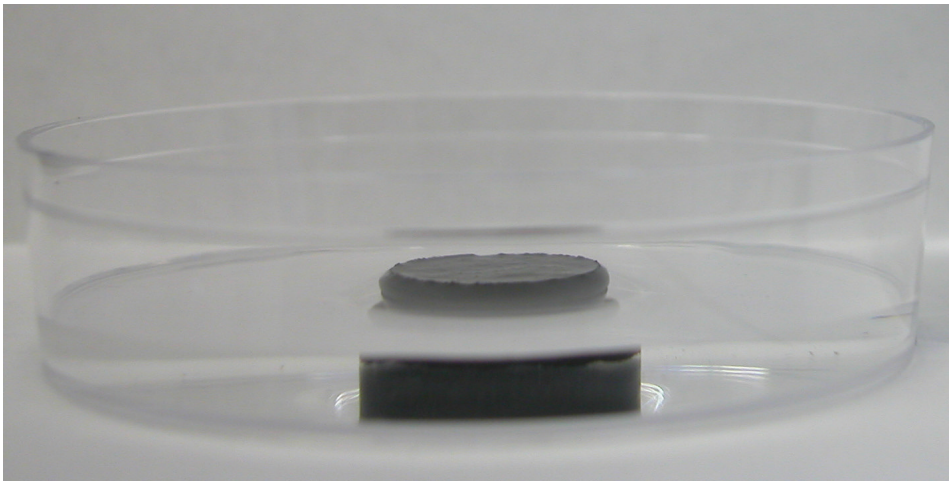

Figure 3-7
Magnetite Experiment Setup; Pellet in Petri Dish

After three months and after six months, portions of the pellets and powders were analyzed using X-ray diffractometry (XRD). The spectra obtained were compared to unexposed samples of the same magnetites as well as library spectra for magnetite, hematite and aluminum (the metal comprising the sample holders used for XRD). Figure 3-8 through Figure 3-15 show that no detectable oxidation of magnetite occurred, indicating that oxidation of magnetite in steam generator secondary side deposits during layup is extremely unlikely. (The expected detection limit using the XRD technique has been calculated to correspond to 1 nm of conversion of magnetite to hematite.)

The details of the experimental procedure are given on Page 3-14, following the figures below.

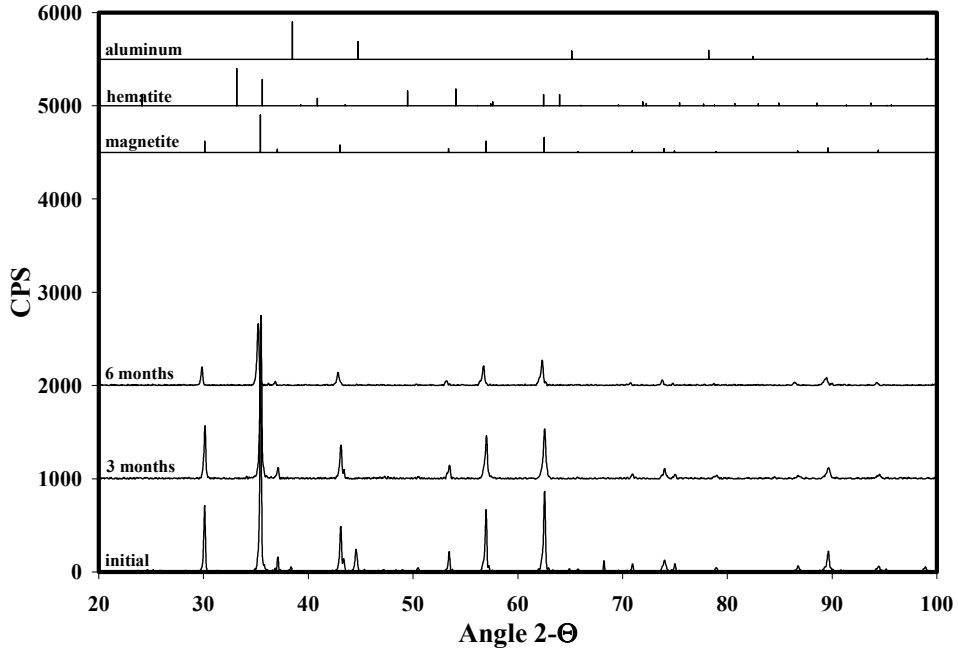

Figure 3-8
XRD Spectra of Plant A Pellets

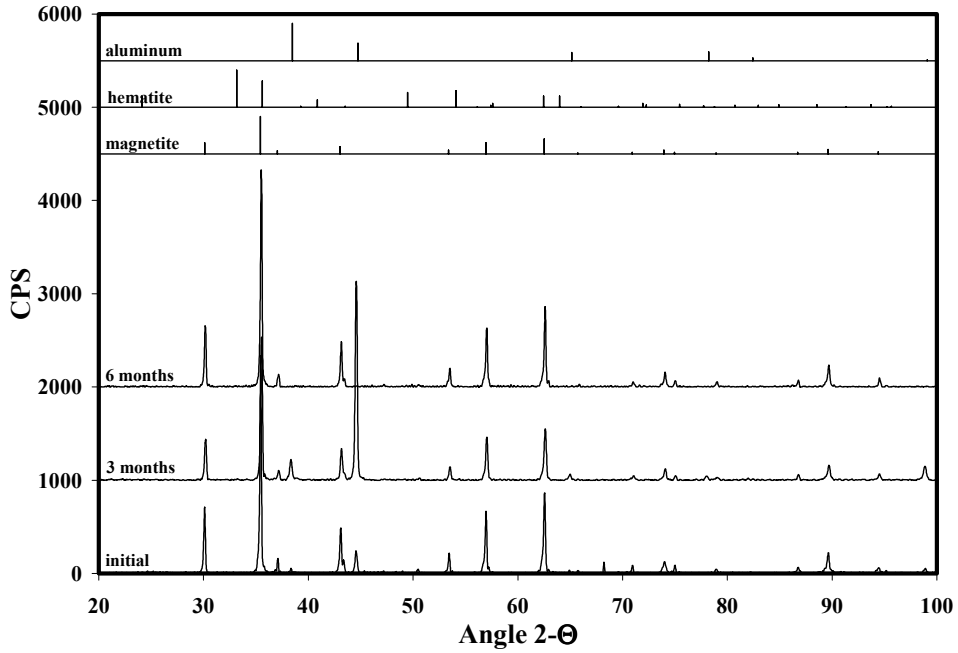

Figure 3-9
XRD Spectra of Plant A Powder

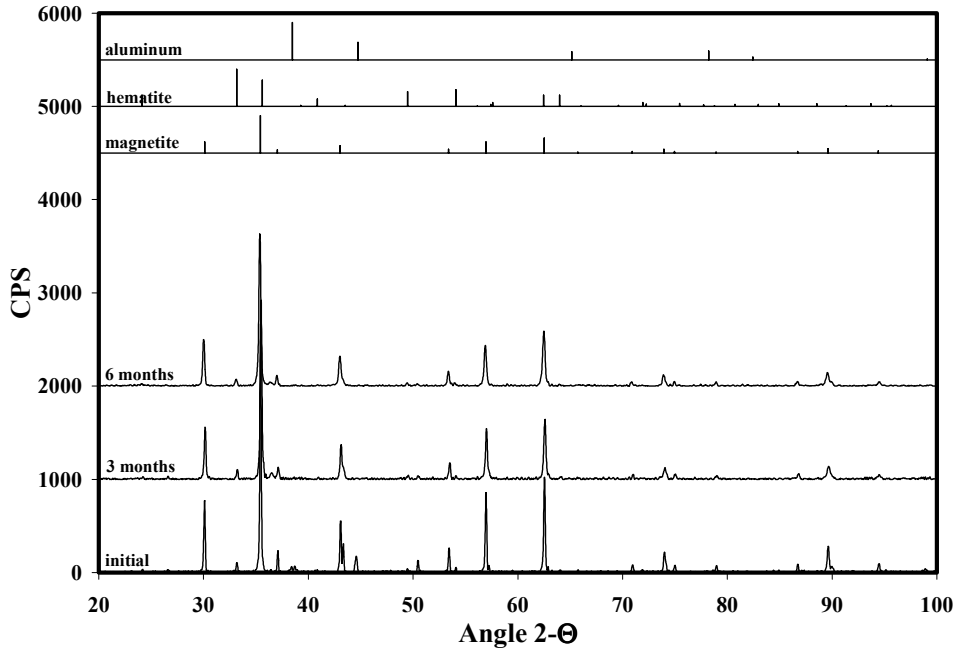

Figure 3-10
XRD Spectra of Plant B Pellets

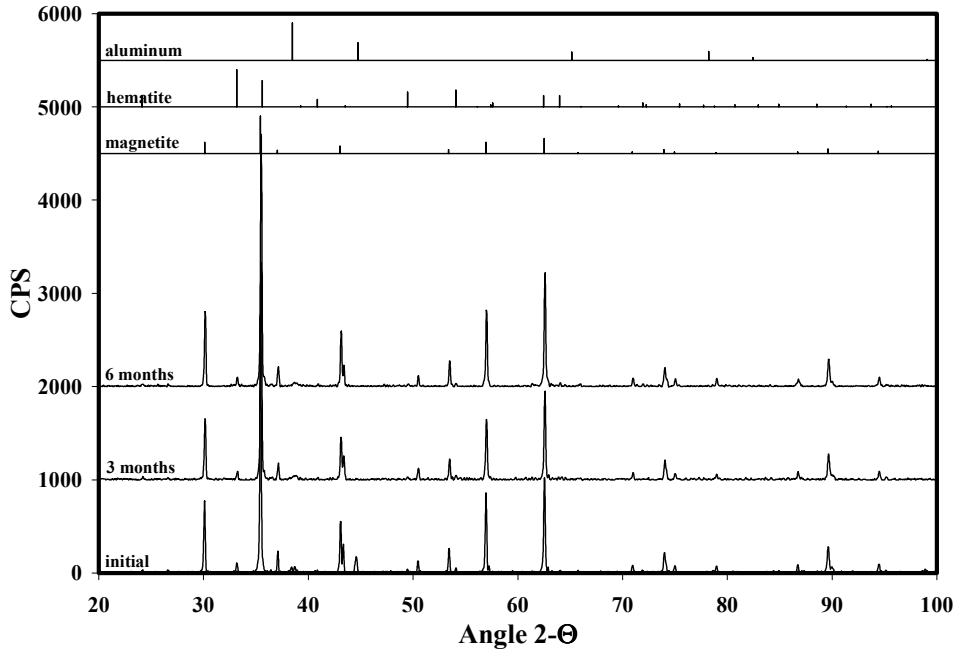

Figure 3-11
XRD Spectra of Plant B Powder

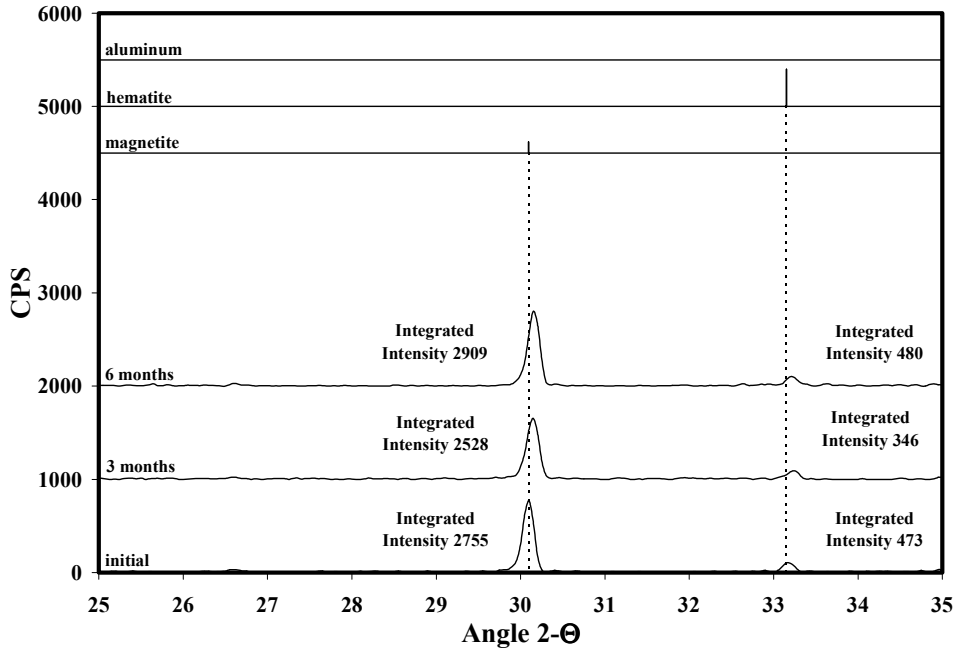

Figure 3-12
XRD Spectra of Plant B Powder; Closeup

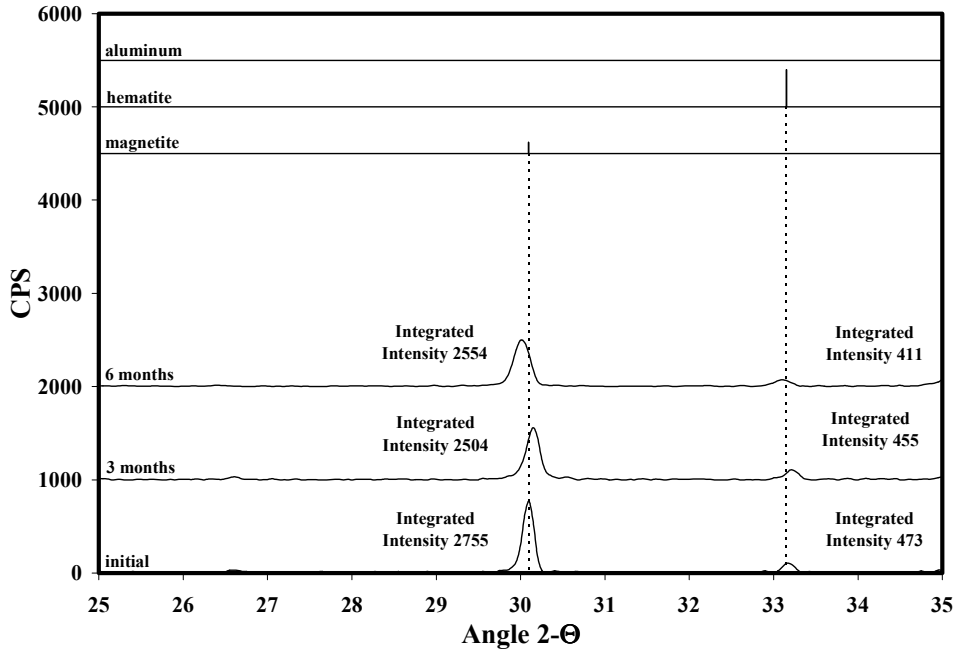

Figure 3-13
XRD Spectra of Plant B Pellets; Closeup

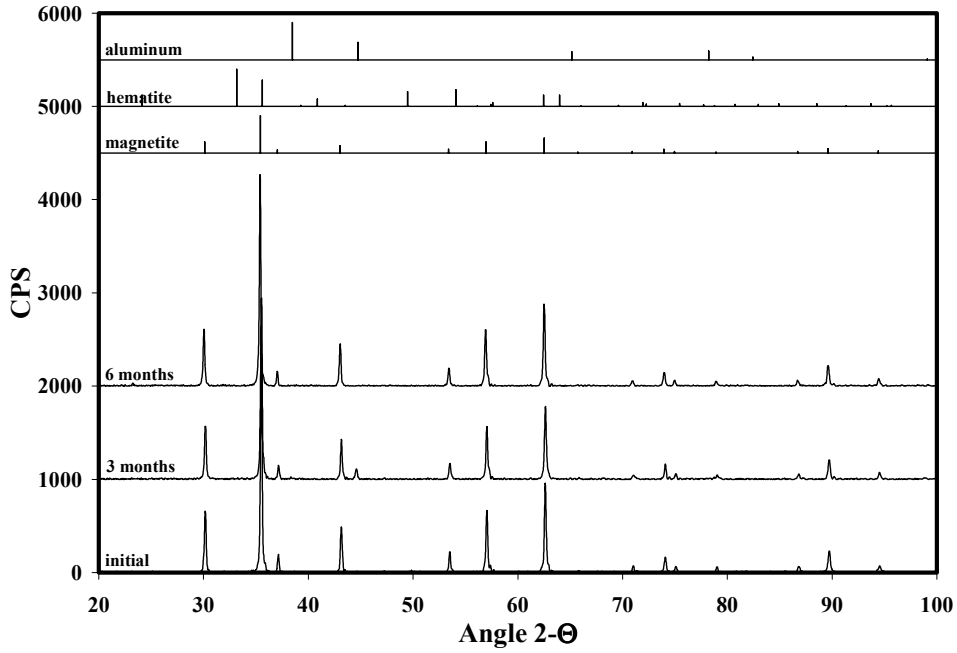

Figure 3-14
XRD Spectra of Synthetic Magnetite Powder

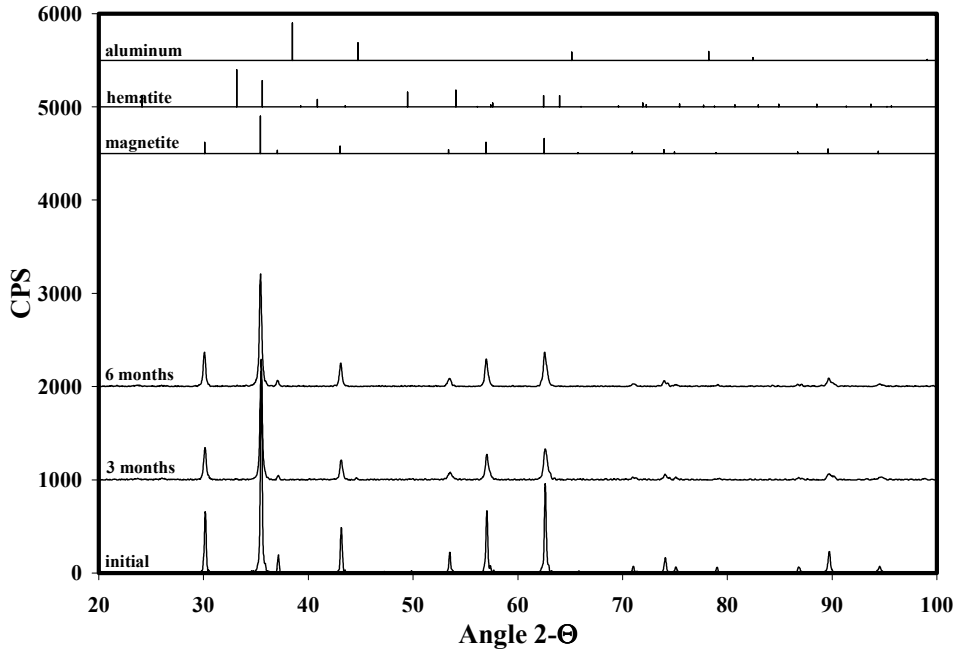

Figure 3-15
XRD Spectra of Synthetic Magnetite Pellets

Experimental Details

Powders were obtained from three sources:

- Synthetic magnetite, Fisher I119, Lot 986192 (area average particle diameter ~100 nm)
- Plant A powder obtained from steam generator sludge lancing at a commercial nuclear power plant (area particle diameter ~ 800 nm)
- Plant B powder consisting of flakes, judged former tube scale, obtained from steam generator sludge lancing at a commercial nuclear power plant and ground into a powder (area particle average diameter ~ 1200 nm)

Portions of these powders were examined using XRD to obtain a base line characterization of the oxidation state of iron. Figure 3-8 through Figure 3-15 show the powder spectra, labeled in these figures as *initial*. The initial state of iron in the synthetic magnetite and the ground flakes from Plant B proved to be entirely magnetite, to the extent that this analytical technique could determine (<1% hematite). Powder from Plant A showed the presence of a small quantity of hematite in the initial scan (see Figure 3-9). From the XRD spectra, hematite was judged to make up less than five per cent of the powder from Plant A.

Each of the three powders was formed into pellets. These pellets were made by compressing the materials in a Corverlab press equipped with a KBr die mold at 15, 000 psi. The curing temperature was 60°C (140°F).

The mold used for these experiments produced pellets cylindrical in shape, with a diameter of approximately 10 mm and a length of about 5 mm. A small amount of phosphate binder was also added to improve the structural integrity of the pellet. This process produces a structurally sound, highly porous pellet. The process does not cause oxidation of the magnetite.

Pellets and powder samples of the three magnetites were added to petri dishes and partially covered with de-ionized water as shown in Figure 3-6 and Figure 3-7. The porous pellets adsorbed the water through capillary action ensuring that the un-submersed suface of the pellet was exposed simultaneously to both air and water. The volume to surface area ratio of the water in the petri dishes was approximately half a centimeter, ensuring that the water was continuously in equilibrium with the surrounding air. To correct for evaporation, fresh de-ionized water was added to the petri dishes on a regular basis. The water level in the dishes varied, but always kept the pellets and powders wet and never completely submersed the samples. The samples were kept at room temperature.

After three months, portions of the pellets and powders were removed from the petri dishes and dried in a desiccator for two weeks. Once dried, the pellets were ground into powders. The powders (both those tested as powders and those tested as pellets) were examined using XRD. The XRD spectra are shown in Figure 3-8 through Figure 3-15. The spectra taken after three months are labeled *3 months* and are offset from the actual values by a factor of 1000 counts per second (CPS) to distinguish them from the other spectra. The three month spectra showed no hematite in the synthetic magnetite or the powder from Plant B and no change in the initial hematite level for the powder from Plant A. There were no detectable differences between the powder spectra and the pellet spectra.

After six months, the remaining powder and pellets were removed from the petri dishes and dried for two weeks. The samples were examined by XRD. The XRD spectra are shown in Figure 3-8 through Figure 3-15 and are labeled *6 months*. These spectra are offset from the actual values by a factor of 2000 CPS to allow comparison with the other spectra. XRD analysis showed no change in hematite levels over the course of six months. The samples did not show the development of any color change. Surface conversion of magnetite to hematite would be accompanied by a change in color from black (magnetite) to rust red (hematite) even at levels of less than one per cent conversion.

The environment to which these samples were subjected, low pH and oxygen saturation, is considered to be the most oxidizing that secondary side deposits would experience during layup. This environment is similar to those that might accompany sludge lancing or draining and refilling for hideout return and other cleanup measures. The time scale of the experiment, six months, is longer than the exposure likely in a commercial power plant by approximately an order of magnitude. Therefore, the conclusion drawn from this experiment, that magnetite does not oxidize to hematite under wet layup conditions is considered quite robust.

Atmospheric Oxidation Experiments

The atmospheric oxidation of secondary side deposits was explored using thermogravimetric analysis (TGA). The details of the method used are given in Reference 6. In brief, TGA uses a high resolution mass balance to measure the change in mass of a sample when exposed to a flowing gas stream at a controlled temperature. The instrumentation used allows a wide range of test temperatures (room temperature to over 1000°C—1832°F) and a variety of reaction gasses. The oxidation of copper powder in dry and humid air was measured as well as the oxidation of magnetite to hematite. These two sets of tests are described more fully in the following two sub-sections.

Copper Oxidation at Various Humidities

In the previous study [6] a limited number of experiments were performed to analyze the rate of copper oxidation as a function of temperature and humidity. These tests were supplemented with additional tests at various temperatures and humidities. As reported in detail in Reference 6, the humidity was controlled in these experiments by saturating the reaction gas (bottled air) with water at a temperature lower than the test temperature. When temperature of the saturated air stream was raised to the test temperature, the relative humidity fell to the desired value.

The oxidation of the copper sample was monitored by measuring the increase in weight due to the addition of oxygen. Figure 3-16 shows an example test. As indicated in the figure, the data is well fit by a logarithmic rate law taking the following form:

$$x = A\ln(Bt + 1) \tag{3-1}$$

where x is the oxide thickness, t is the elapsed time and A and B are empirically determined constants obtained by fitting the experimental data to Equation 3-1. Logarithmic rate laws

generally indicate that the oxidation rate at the surface is controlled by diffusion of metal atoms through a semiprotective oxide layer.

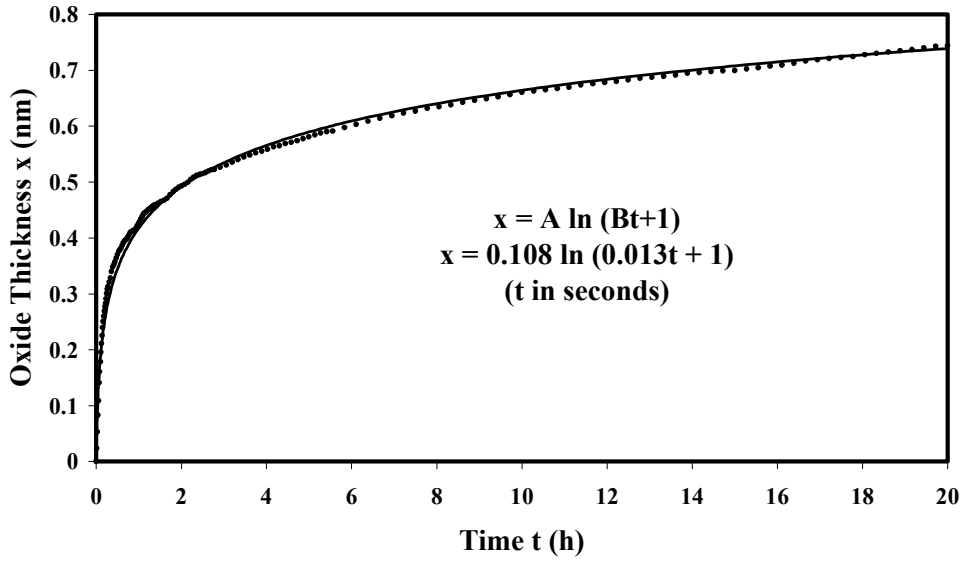

Figure 3-16
Typical Copper Oxidation Experiment; Weight Gain Expressed as Oxide Thickness

The constants *A* and *B* were determined for each test using a least squares fitting routine. The effects on oxidation of the two parameters studied (temperature and relative humidity) were evaluated based on the degree to which they influenced the constants *A* and *B*.

In typical chemical reactions, the reaction rate (characterized by a rate constant, *k*) is a function of the temperature, following an Ahhrenius rate law according to the following equation:

$$k = k_o e^{\frac{-E_{act}}{RT}} \tag{3-2}$$

where k_o (pre-exponential constant) and E_{act} (activation energy) are empirical constants, *R* is the ideal gas constant and *T* is the absolute temperature. Rearranging Equation 3-2 yields the following equation:

$$\ln(k) = \ln(k_o) - \frac{E_{act}}{R}\frac{1}{T} \tag{3-3}$$

The advantage of Equation 3-3 is that it has a linear form when ln(*k*) is plotted against 1/*T*. The values of the empirical constant *A* from tests at several temperatures and humidities are plotted in

Figure 3-17. From this figure, there appear to be two different regions following different Ahhrenius relationships. Below a temperature of about 57.5°C or 135.5°F (~0.003 1/K), an Ahhrenius relationship is followed with an activation energy of about 16.3 kJ/mol (3.89 kcal/mol). Above a temperature of about 57.5°C (135.5°F), an Ahhrenius relationship is followed with an activation energy of about 100.6 kJ/mol (24.03 kcal/mol). The following relationship was used to describe the data:

$$A = \begin{Bmatrix} if\ T < T_o : A_{low\,T} e^{\frac{-E_{act\ A\,low\,T}}{RT}} \\ if\ T > T_o : A_{high\,T} e^{\frac{-E_{act\ A\,high\,T}}{RT}} \end{Bmatrix} \tag{3-4}$$

The empirical constants T_o, $A_{low\,T}$, $E_{act\,A\,low\,T}$ and $E_{act\,A\,high\,T}$ were determined using a least squares fitting routine. The constant $A_{high\,T}$ was determined by equating the high and low temperature equations at $T=T_o$ according to the following equation:

$$A_{high\,T} = A_{low\,T} e^{\left(\frac{E_{act\ A\,high\,T} - E_{act\ A\,low\,T}}{RT_o}\right)} \tag{3-5}$$

The following values of the constants in Equation 3-4 were found to fit the data well:

$$A_{high\,T} = 1.45 \text{ x } 10^{16}\ nm \qquad E_{act\ A\,high\,T} = 1.06 \text{ x } 10^{5}\ \frac{J}{mol}$$

$$A_{low\,T} = 93.2\ nm \qquad E_{act\ A\,low\,T} = 1.63 \text{ x } 10^{4}\ \frac{J}{mol}$$

$$T_o = 57.5°\,C \tag{3-6}$$

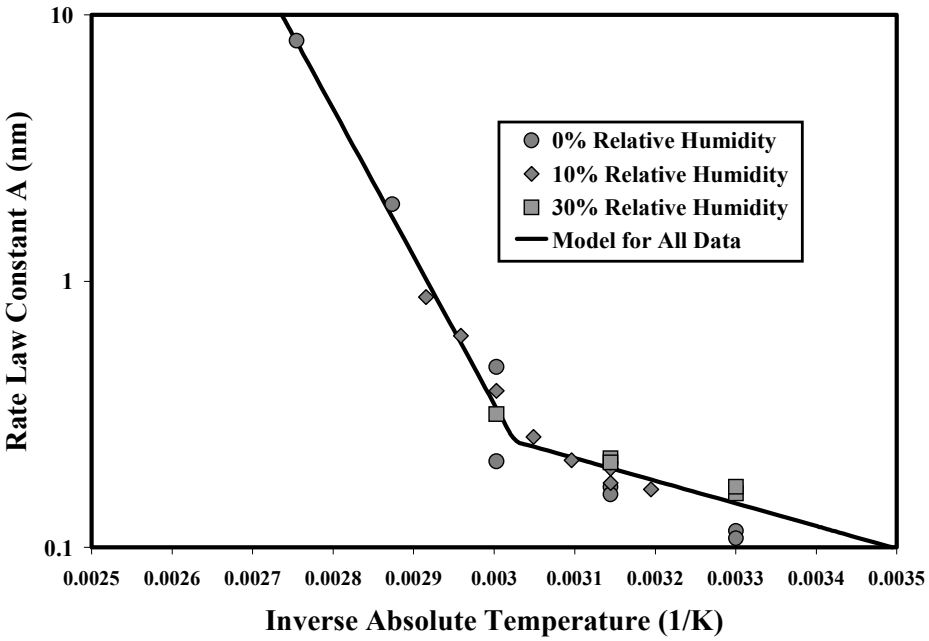

Figure 3-17
Empirical Constant *A* as a Function of Temperature—Copper Oxidation

A similar analysis of the data on the empirical constant *B* was performed, save that the value of the transition temperature was fixed at that determined for Equation 3-5. The equation defining *B* is as follows:

$$B = \begin{Bmatrix} if\ T < T_o : B_{low\ T} e^{\frac{-E_{act\ B\ low\ T}}{RT}} \\ if\ T > T_o : B_{high\ T} e^{\frac{-E_{act\ B\ high\ T}}{RT}} \end{Bmatrix} \tag{3-7}$$

The values of the fitting parameters in Equation 3-7 are as follows:

$$B_{high\ T} = 3.29 \text{ x } 10^{-19}\, s^{-1} \qquad E_{act\ B\ high\ T} = -1.03 \text{ x } 10^{5}\, \frac{J}{mol}$$

$$B_{low\ T} = 1.57 \text{ x } 10^{-5}\, s^{-1} \qquad E_{act\ B\ low\ T} = -1.60 \text{ x } 10^{4}\, \frac{J}{mol}$$

$$T_o = 57.5° C \tag{3-8}$$

The values of the constant *B* for the experiments conducted and the empirical fit described by Equation 3-7 are shown in Figure 3-18.

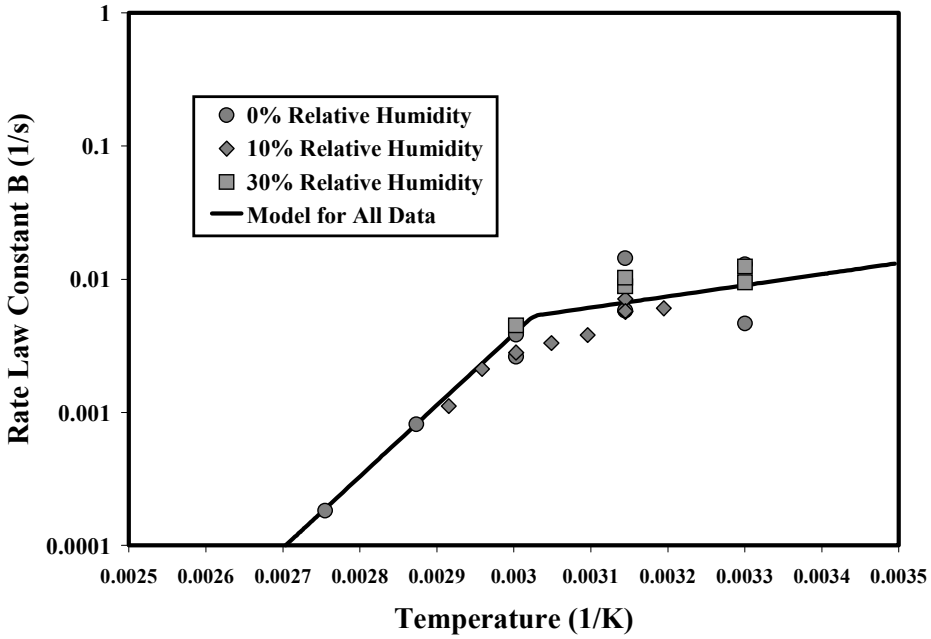

Figure 3-18
Empirical Constant *B* as a Function of Temperature—Copper Oxidation

The behavior of the variable *B* with respect to temperature is atypical of chemical reaction rate constants because the value of *B* decreases with increasing temperature, implying a negative activation energy. One explanation for this unusual feature is that the constant *B* is characteristic of the density of the oxide film. As the temperature increases, the film density becomes greater, creating a higher barrier to the diffusion of copper atoms through the film to react with oxygen at the oxide film surface. This leads to slower oxidation. However, although diffusion is more difficult through the dense film, it is faster, due to the increased vibration of molecules in the film. This leads to faster oxidation. On this basis, the rate constant *A* may be assumed to be related to the increased thermal motion of the molecules in the oxide film. The measured activation energies for the constant *A* (both at high and low temperatures) are consistent with an increase in rate due to increased thermal activity. The rate constant *B* is most likely an indication of the density of the oxide film. This interpretation is consistent with the measured negative activation energy.

The values of *A* and *B* measured in the various tests were also examined as a function of humidity. Because the different test temperatures lead to widely varying rates, the effect of humidity was examined using relative values of *A* and *B* as calculated using the following equations:

$$Relative\ Rate\ Constant\ A = \frac{measured\ A}{A(T)} \tag{3-9}$$

$$Relative\ Rate\ Constant\ B = \frac{measured\ B}{B(T)} \tag{3-10}$$

where *A(T)* and *B(T)* are the values calculated using Equations 3-4 and 3-7. Figure 3-19 shows the value of the relative rate constant *A/A(T)* as a function of humidity. Figure 3-20 shows the value of the relative rate constant *B/B(T)* as a function of humidity. These figures indicate that the effect of humidity, if significant, is small compared to that of temperature. For example, increasing the relative humidity from 0% (dry) to 60% increases the oxidation rate by about 50% while increasing the temperature from about 20°C (68°F) to 90°C (194°F) increased the oxidation rate by about a factor of 100.

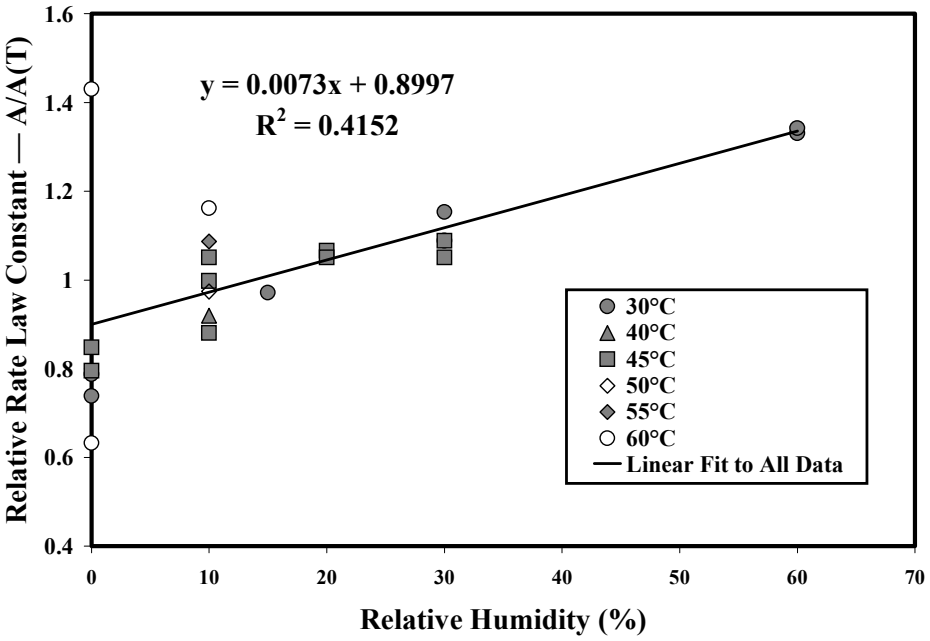

Figure 3-19
Relative Empirical Constant *A/A(T)* as a Function of Humidity

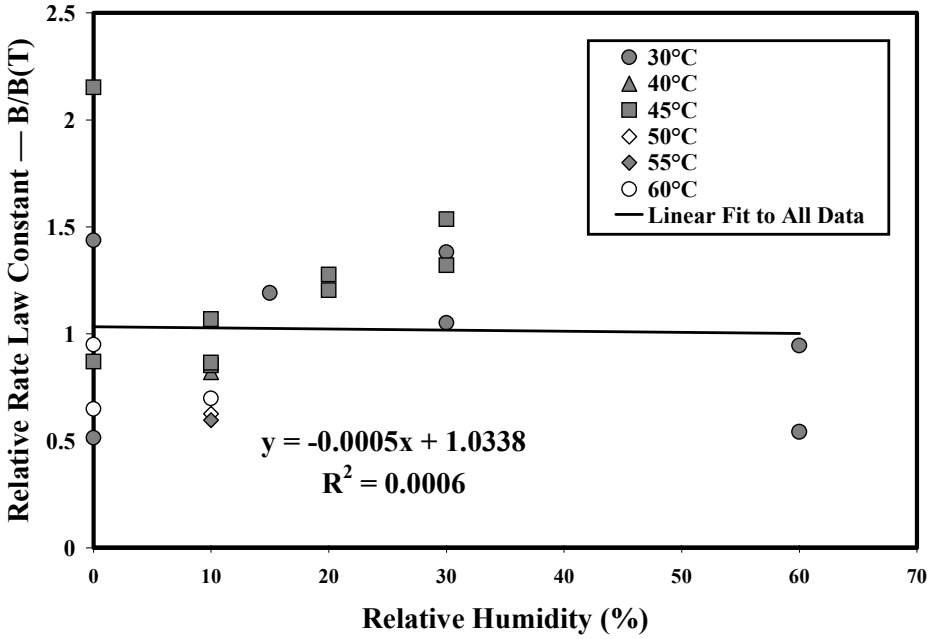

Figure 3-20
Relative Empirical Constant *B/B(T)* as a Function of Humidity

Because the rate of oxidation does not depend heavily on the humidity, Equations 3-4 and 3-7 can be used to predict the degree of oxidation at a given time. Figure 3-21 shows the thickness of the oxide layer that would develop over the course of 12 hours, 72 hours and 10 days as a function of temperature calculated using Equations 3-4 and 3-7. The data plotted in the figure demonstrate that, once the initial phases of oxidation have passed, the oxide layer thickness is much more dependent on the temperature than the duration of exposure.

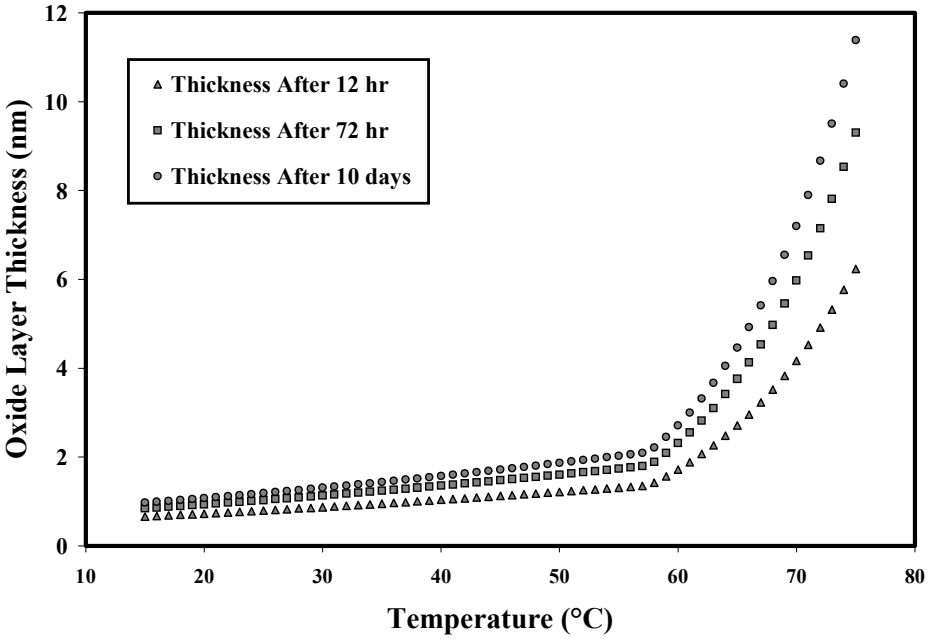

Figure 3-21
Oxide Thickness at 12 hours, 72 hours and 10 days as a Function of Temperature

Magnetite Oxidation

In most PWR steam generators, secondary side deposits are composed primarily of magnetite (Fe_3O_4). This is especially true for sludge pile powder and freespan tube scale. Under some conditions, it is possible that magnetite may undergo additional oxidation to form hematite (α-Fe_2O_3). If hematite is present on the secondary side during operation, it may raise the electrochemical potential enough to accelerate degradation of the steam generator tubing. Thus, hematite is one species that should be considered when attempting to reduce the presence of oxides on the secondary side. Magnetite, by contrast, is not expected to significantly raise the electrochemical potential (see Figure 2-1).

One source of hematite is the atmospheric oxidation of magnetite during layup. In order to determine the extent to which hematite may form during layup several TGA tests, similar to those performed with copper, were conducted. As magnetite was exposed to air at a controlled test temperature, the weight gain due to additional oxidation was measured. This weight gain was then converted into an oxide thickness based on the measured specific surface area of the sample.

Magnetite from three different sources was used in these studies. These sources were as follows:

- Synthetic magnetite, Fisher I119, Lot 986192
- Plant A powder obtained from steam generator sludge lancing at a commercial nuclear power plant
- Plant B powder consisting of flakes, judged former tube scale, obtained from steam generator sludge lancing at a commercial nuclear power plant and ground into a powder

Note that these were the same sources that were previously used in the aqueous magnetite oxidation studies (see above, page 3-8). Most of the work conducted used the synthetic magnetite, since the quantities of plant powders were limited. In the discussion below, only the synthetic powder was used to determine the nature of the reaction rate law constants. The plant powders were only used for comparison.

As with copper oxidation, the oxidation of magnetite to hematite was found to follow a logarithmic rate law function. One example of a set of experimental data is shown in Figure 3-22. Each of the experiments conducted was analyzed to determine the rate constants *A* and *B*. As can be seen in Figure 3-23, with the exception of one experiment at 50°C (122°F), the value of *A* is constant with respect to temperature. The average value measured for *A* was 1.751 nm/s (which is comparable to the temperature dependent values observed for copper).

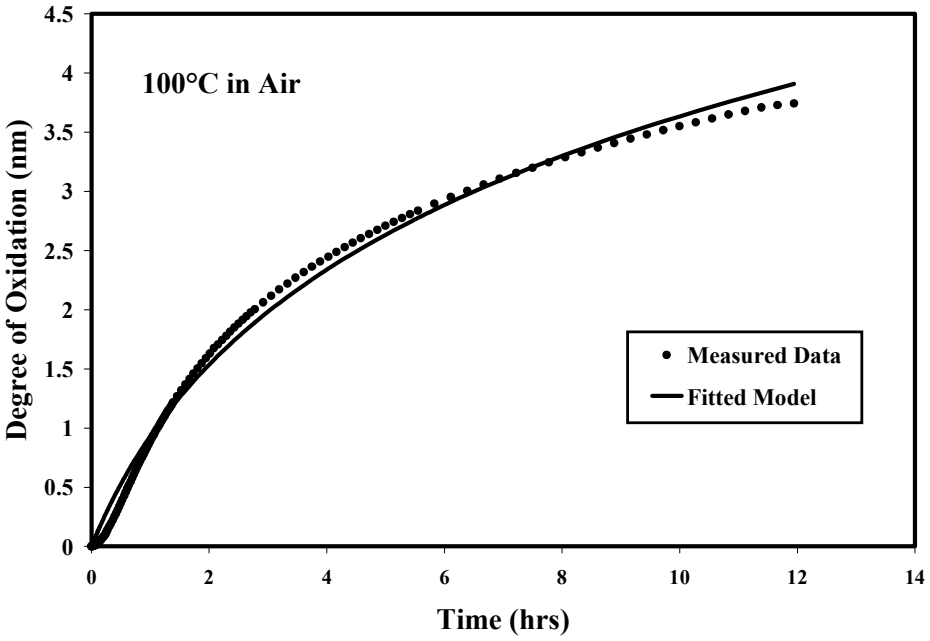

Figure 3-22
Magnetite Oxidation in Air at 100°C, Experimental Data and Fitted Model

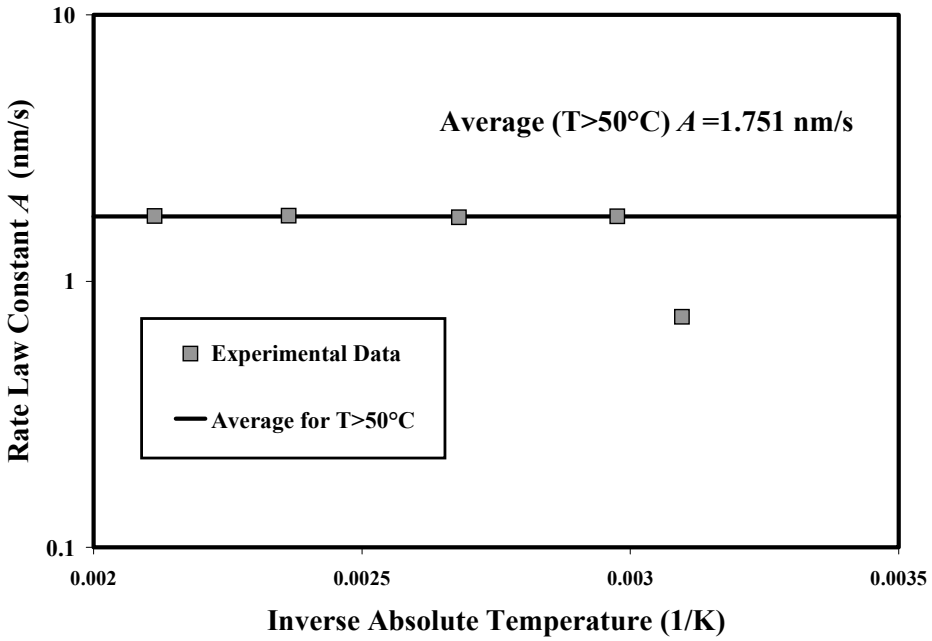

Figure 3-23
Rate Law Constant *A* for Magnetite Oxidation as a Function of Temperature

Using the average value of *A*, the value of *B* was determined for each experiment by a least squares fitting routine. The values obtained are shown in Figure 3-24 as a function of the inverse absolute temperature. From this plot, it is clear that the data are well fitted by an Ahhrenius type rate law as given by the following equation:

$$B = B_o e^{\frac{-E_{act\ magnetite}}{RT}} \tag{3-11}$$

where $E_{act\ magnetite}$ is the activation energy of the oxidation reaction. The calculated activation energy (91.496 kJ/mol—21.858 kcal/mol) is a reasonable value for surface reactions indicating the validity of the test technique.

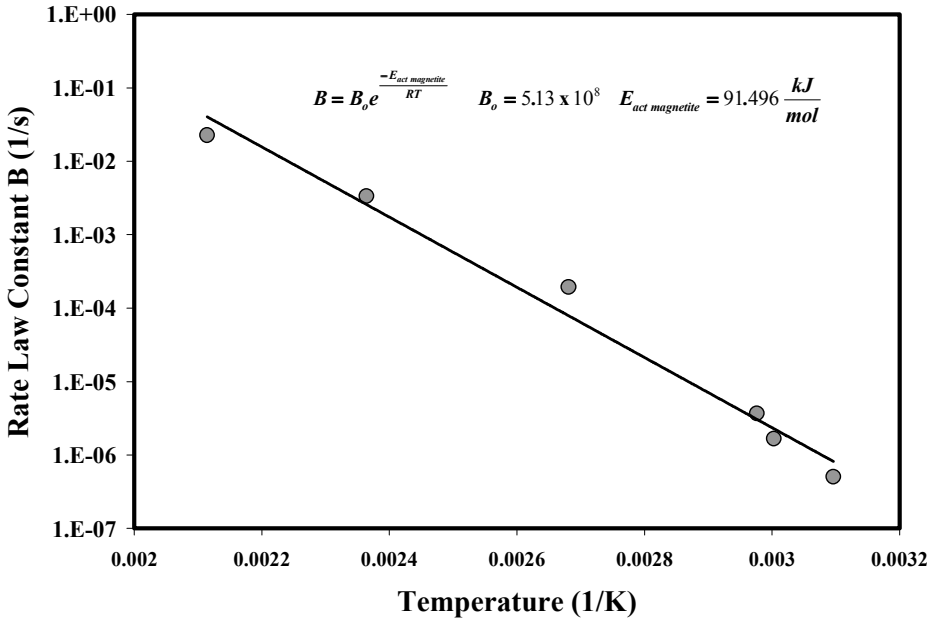

Figure 3-24
Rate Law Constant *B* for Magnetite Oxidation as a Function of Temperature

In order to illustrate the degree of oxidation that might be experienced during the dry layup of steam generators, an oxide thickness was calculated for 12 hours and 72 hours of exposure, based on the values of *A* and *B* determined by experimentation. The results of these calculations are shown in Figure 3-25 and Figure 3-26. Results of similar calculations based on experiments with plant powders are also shown in these figures. The oxide thicknesses for the plant powders are roughly similar to those of the synthetic powder. It is possible that the powder obtained from grinding flakes is less susceptible to oxidation than the synthetic powder. Note, however, that the oxidation of magnetite to hematite is virtually undetectable if the temperature remains below 50°C (122°F).

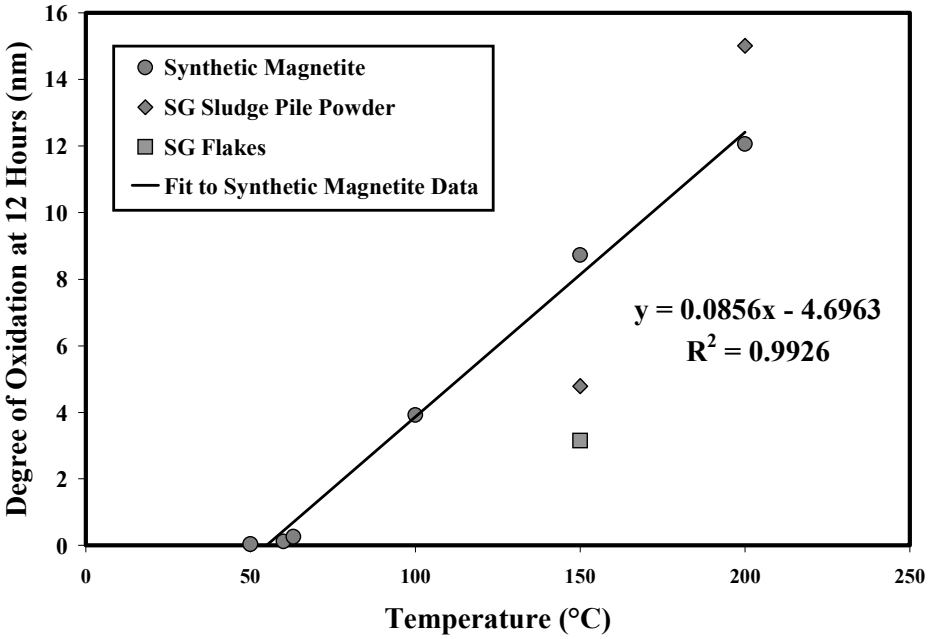

Figure 3-25
Degree of Oxidation at 12 hours as a Function of Temperature

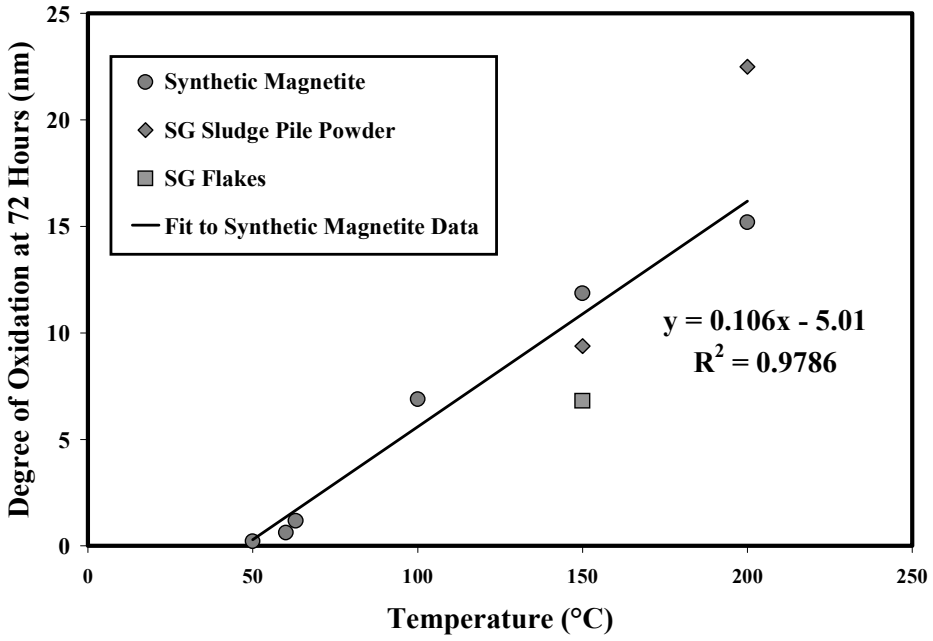

Figure 3-26
Degree of Oxidation at 72 hours as a Function of Temperature

Reduction Experiments

In practice, it is often unpractical to completely prevent the formation of oxides in the steam generator during layup. Thus, prevention of oxide-accelerated tube degradation may rely on promoting the reduction of such oxides during startup. Therefore, it is of interest to understand the kinetics of oxide reduction so that current startup sequences can be assessed with respect to reducing capacity and optimized sequences can be designed.

This project investigated the following reduction phenomena:

- Reduction of copper oxides by hydrazine
- Reduction of copper oxides by carbohydrazide
- Reduction of hematite to magnetite
- Reduction of deposits during simulated startup sequences

The techniques and results of the investigations into these phenomena are described below.

Copper Oxide Reduction with Hydrazine

Previously [6] it had been shown that copper oxides could be reduced to copper metal at moderate temperatures (100°C to 200°C or 212°F to 392°F) with stoichiometric excesses of hydrazine. Additional testing was carried out to determine if an intermediate temperature (150°C—302°F) would provide enhanced reduction of copper oxides.

The reduction tests are fully described in Reference 6. In brief, previously oxidized copper powder is loaded into a small test cylinder which is subsequently filled with deaerated water containing 2.2% hydrazine (equivalent to ten times the hydrazine required by the reaction stoichiometry to reduce the copper oxide present). The test cylinder is then sealed and heated to the test temperature. After a predetermined interval, the test cylinder is cooled, and the powder is dried and examined by XRD to determine the quantity of oxide remaining. (It should be noted that 400 ppm hydrazine, a typical concentration of hydrazine for layup of a steam generator, represents a ten-fold stoichiometric mass of hydrazine relative to the mass of copper oxide present, if it is assumed that there is a 1% by weigh deposit loading, that the deposit is approximately 10% by weight copper and that 10% of the copper is oxidized.)

Figure 3-27 shows the results of reduction tests at 150°C (302°F) along with those previously reported for 100°C (212°F) and 200°C (392°F). From the figure, it appears that reduction is less complete at 150°C (302°F) than at either 100°C (212°F) or 200°C (392°F).

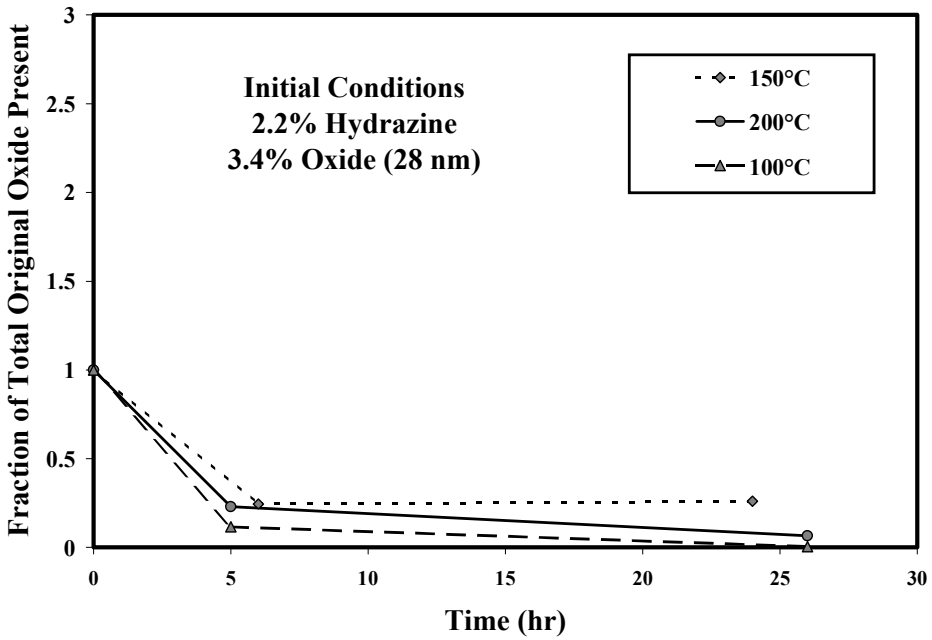

Figure 3-27
Reduction of Copper Oxides by Hydrazine at Three Temperatures

The observation that reduction is least at an intermediate temperature can be explained by the complex combination of reactions occurring during the test. These reactions include:

- Reduction of copper oxide by hydrazine
- Additional oxidation of copper by residual oxygen
- Consumption of hydrazine by residual oxygen
- Consumption of hydrazine by decomposition

The observed reduction of copper oxides is in fact the net result of both reduction and additional oxidation. The rate of reduction is influenced by the concentration of hydrazine, which is affected by three different reactions. The following scenarios may explain the observed results:

- At low temperatures, all reactions rates are slowed. If reduction is slowed the least, then significant reduction is achieved.
- At high temperatures, all reactions are increased. Because of the observations at low temperatures, the reduction reaction is expected to increase the least. Therefore, oxidation might be expected to dominate. However, if the rate of consumption of residual oxygen is increased the most, then oxidation of copper is slowed and the net reduction remains high.
- At intermediate temperatures, the rate of reduction remains low (based on the first observation) but the rate of hydrazine decomposition has increased. This further decreases the reduction rate lowering the net rate of reduction.

This interpretation is further supported by the observations at intermediate times. Early in the experiment, the hydrazine has not been completely degraded even at high temperatures. Thus the rate of reduction in the intermediate and high temperature tests is comparable in the early stages. As the data in Figure 3-27 show, this is the case.

Copper Oxide Reduction with Carbohydrazide

Reduction experiments similar to those performed in hydrazine solutions were conducted in carbohydrazide solutions. Tests at six conditions were conducted covering two concentrations of carbohydrazide (0.57% and 2.89%) and three temperatures (100°C, 150°C and 200°C—212°F, 302°F and 392°F, respectively). The concentrations used correspond to twice and ten times the carbohydrazide stoichiometrically required to reduce the copper oxide present in the experiment. The results of these experiments are shown in Figure 3-28 and Figure 3-29.

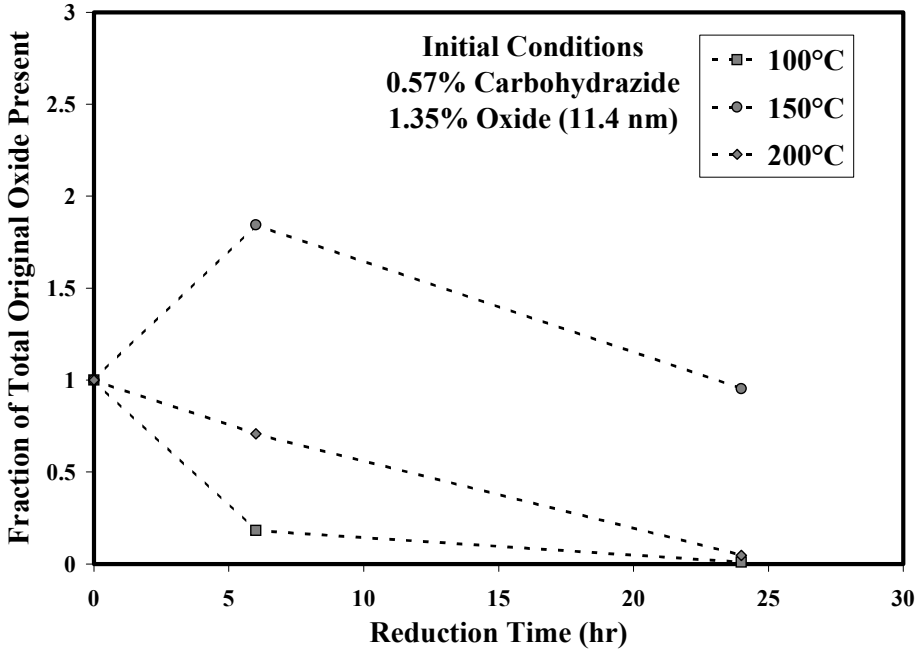

Figure 3-28
Reduction of Copper Oxides by 2x Stoichiometric Carbohydrazide

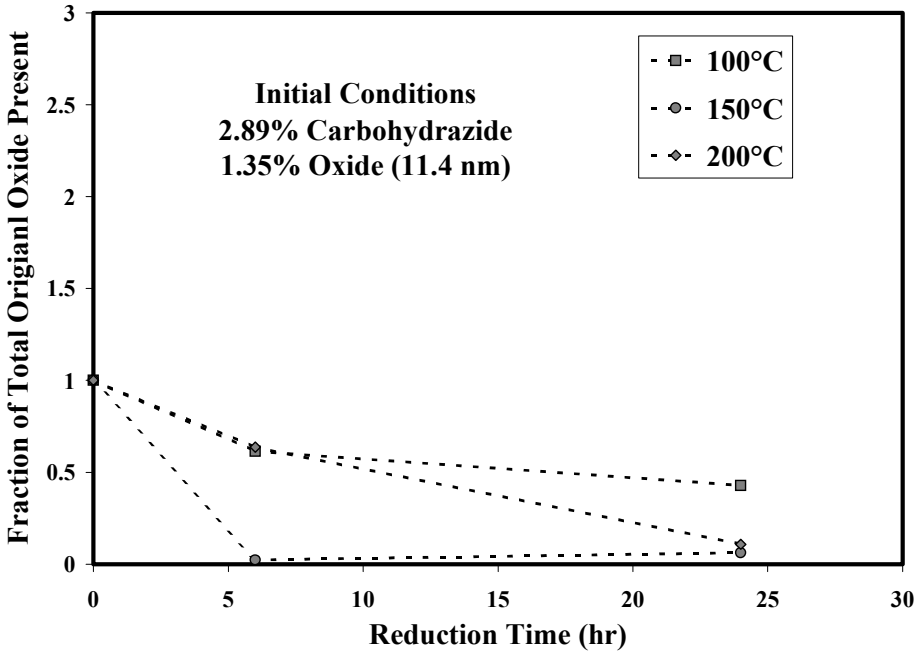

Figure 3-29
Reduction of Copper Oxides by 10x Stoichiometric Carbohydrazide

As was the case for reduction in hydrazine solutions, Figure 3-28 shows a minimum in the degree of reduction at an intermediate temperature. The reason for this is most likely the same as that hypothesized for hydrazine solutions: at intermediate temperatures, the rate of scavenger decomposition is increased, lowering the reduction rate. This hypothesis is further supported by the contrast with the data shown in Figure 3-29 for higher initial carbohydrazide concentrations. In these tests, the carbohydrazide concentration remains high even at intermediate temperatures, leading to optimal reduction of copper oxides at the intermediate temperature.

Hematite Reduction

Although testing indicates that magnetite in secondary side deposits, once formed, will not convert to hematite under normal layup conditions (see above, page 3-8 and 3-22), typical startup conditions may result in the accumulation of hematite from the secondary system waters due to the partially oxidizing conditions in the feedtrain during startup. For example, during startup elevated levels of hematite have been detected in the feedwaters of several steam generator types, indicating that hematite could accumulate in SGs during this phase of operation [5]. Thus, even though the magnetite from deposits formed during normal operation may not oxidize, hematite may still be present due to ingress during less reducing operating conditions. Therefore, it is desirable to understand the kinetics of hematite reduction so that increases in electrochemical potential due to the presence of hematite can be avoided.

During a recent steam generator chemical cleaning at a US nuclear power plant, residual deposits were removed from the steam generators. This powder was analyzed by XRD and found to consist of a mixture of magnetite and hematite. The hematite concentration was about 38% by

weight. Laboratory tests were conducted using this powder to investigate the kinetics of its reduction to magnetite.

The initial phase of this study investigated the relative reducing power of the following three different reducing agents:

- Hydrazine (Hz)
- Carbohydrazide (Cz)
- Catalyzed hydrazine (hydrazine supplemented with quinhydrone (QH), a fifty-fifty mixture of hydroquinone and benzoquinone)

Note that the catalyzed hydrazine used in this test contains quinhydrone in a 1:175 ratio to hydrazine and approximates the composition of Amerzine® and Scavox II®, two commercially available catalyzed hydrazine solutions.

Table 3-1
Magnetite Reduction Test Conditions

Reducing Agent	Reducing Agent Concentration (ppm)	Temperature (°C)	Test Duration (hr)	Hematite Converted to Magnetite (%)
Hydrazine	500	260	24	7
Carbohydrazide	500	260	24	-10
Catalyzed Hydrazine	300	288	4	29

In each test approximately 0.3 g of the hematite/magnetite mixture were dispersed in 150 mL of test solution (for a powder loading of 2 g/L). The conditions of these tests are given in Table 3-1. The results are shown graphically in Figure 3-30. In these tests a negative conversion percentage corresponds to the conversion of magnetite to hematite. (Note that in these tests the temperature is significantly higher than the temperature of the previous magnetite oxidation test—pages 3-8 and 3-22—and so the observance of oxidation does not contradict the previous findings.)

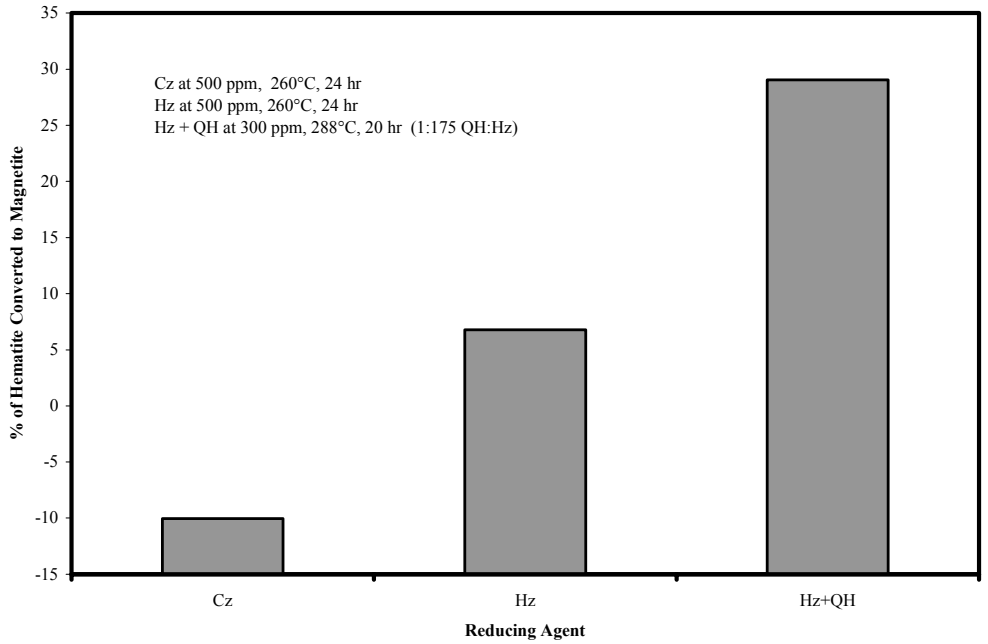

Figure 3-30
Reduction of Hematite to Magnetite by Three Different Reducing Agents

From Figure 3-30 it is clear that the greatest conversion of hematite to magnetite was obtained using catalyzed hydrazine. In order to explore this reaction further, the effects of temperature, hydrazine concentration and ratio of quinhydrone to hydrazine were explored in a second round of testing. Figure 3-31 shows the results of this second round of testing. From this data the following conclusions can be made:

- The reduction of hematite to magnetite is accelerated by increased temperature.
- At moderate (77°C—171°F) and elevated (163°C—325°F) temperatures, reduction is accelerated by increasing levels of quinhydrone.
- At room temperature there is no reduction of hematite to magnetite.

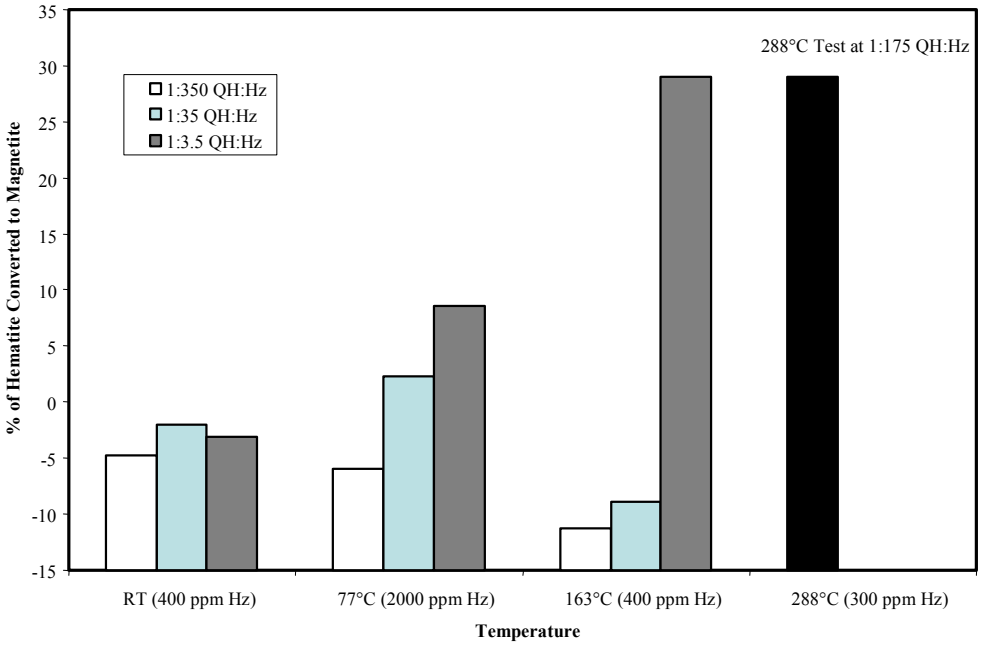

Figure 3-31
Reduction of Hematite to Magnetite by Catalyzed Hydrazine

Simulated Startups

In the studies described previously (page 3-27) examining the reduction of copper oxide by hydrazine and carbohydrazide, the experiments were limited to the investigation of high hydrazine concentrations due to the batch nature of the experiment. That is, the quantity of hydrazine available for the reaction was limited by the initial concentration. Under plant startup conditions, the hydrazine concentrations are generally much lower than those previously considered (on the order of ppm's rather than percent's). However, the total available hydrazine can be much larger due to the large ratio of the volume of secondary side water to the mass of oxides in the deposits and the continuous or periodic replenishment of hydrazine. In order to investigate the possible effects of concentration, as opposed to availability, startup sequences were simulated in an autoclave facility. The details of the experimental procedures are described below, followed by an analysis of the results.

Experimental Procedure

In this round of testing, partially oxidized copper powder was wrapped in filter paper and secured with stainless steel wire mesh. These packets of powder were suspended in a glass autoclave that was subsequently filled with the test solution. The packets were designed to simulate deposits that were exposed directly to the bulk chemistry environment. The test solution consisted of deaerated, de-ionized water with ammonium hydroxide added to adjust the pH and hydrazine added per the sequence protocol, described below. The test solution was continuously withdrawn from the autoclave through a measurement loop. The measurement loop contained an on-line oxygen monitor. The loop also contained an injection port for adding supplemental

hydrazine to the autoclave. Liquid samples were obtained from a separate sampling port for pH and hydrazine measurement. At the conclusion of the test, the autoclave was drained and the powder packets were removed and dried in a desiccator. They were then examined by XRD to determine the degree of oxide reduction obtained during the experiment. Additional sample packets were included containing iron oxides, sludge lancing powder from a commercial power plant and synthetic copper oxide powders. No significant changes were observed in these supplemental samples.

Based on the input from a small informal survey (see Appendix C) of industry startup practices, three prototypical startup sequences were designed. The temperature and hydrazine profiles of these sequences are shown in Figure 3-32 through Figure 3-34. Brief descriptions of these profiles are given in the following paragraphs.

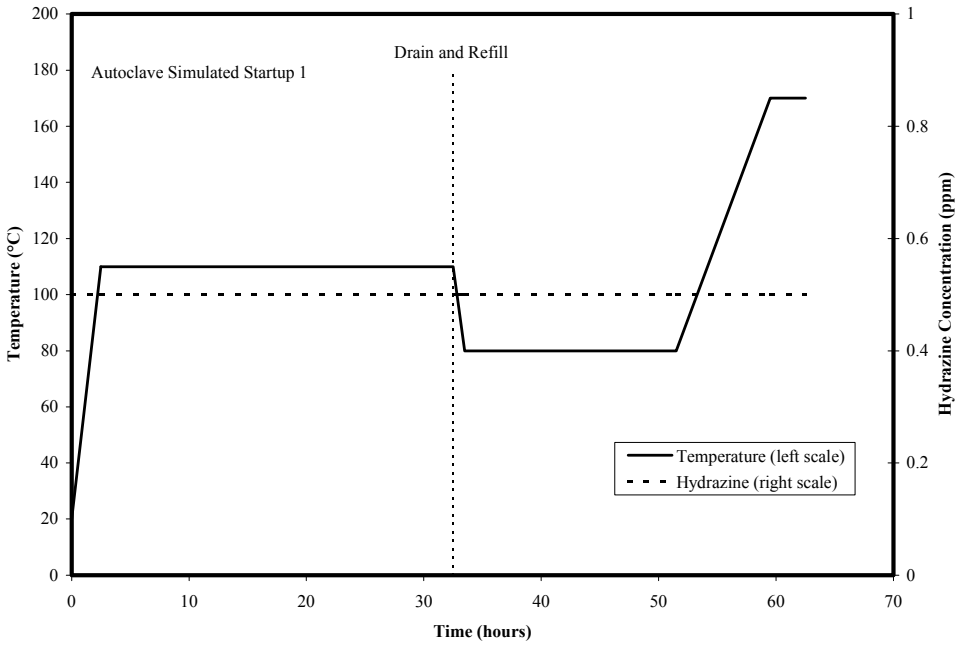

Figure 3-32
Autoclave Simulated Startup Test 1

The Test 1 sequence began with a hot soak at 110°C (230°F). After 30 hours at temperature, the autoclave was drained and refilled, with a new temperature of 80°C (176°F). There was a hold at this temperature for approximately 18 hours. After the hold, the temperature was raised to 170°C (338°F) over the course of 8 hours. The last stage was a hold for 3 hours at 170°C (338°F). The hydrazine concentration was maintained at 0.5 ppm during the entire test sequence. The room temperature pH for the entire test was 9.5±0.3.

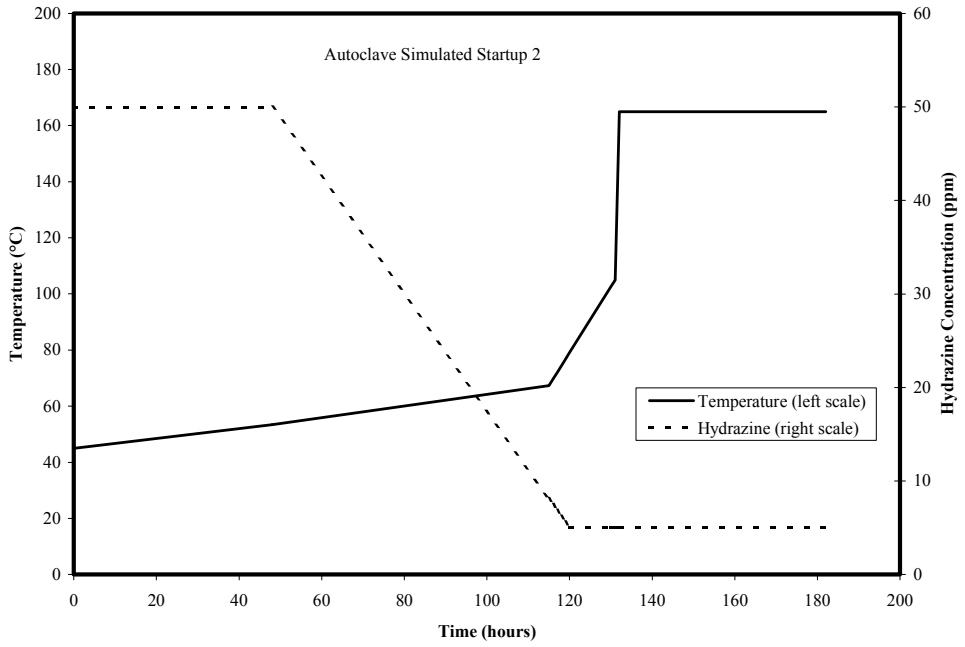

Figure 3-33
Autoclave Simulated Startup Test 2

In Test 2, the temperature was raised from 45°C (113°F) to 70°C (158°F) over the course of approximately 5 days. After this slow heatup, the temperature was raised to 165°C (329°F) and held at that temperature for approximately 2 days. After the high temperature hold, the test was terminated. The hydrazine concentration was held at 50 ppm for the first 2 days. Over the course of the next 3 days, the hydrazine concentration was allowed to fall to 5 ppm. The concentration of hydrazine was then held at 5 ppm for the remainder of the test. The room temperature pH for the entire test was 9.5±0.3.

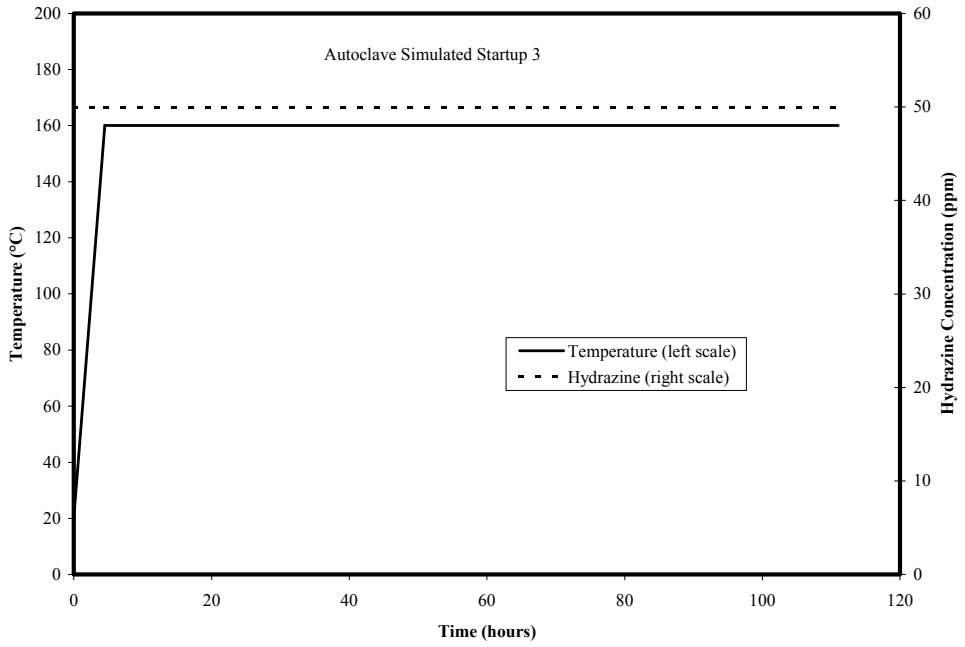

Figure 3-34
Autoclave Simulated Startup Test 3

In the third test, the temperature was raised to 160°C (320°F) over the course of 4.5 hours. The temperature was then held at 160°C (320°F) for approximately 4.5 days. The hydrazine concentration was held at 50 ppm throughout the test. The room temperature pH for the entire test was 9.5±0.3.

Results

The oxide fractions of the powder samples were measured before and after the startup tests. These measurements were converted into oxide thickness and are shown in Figure 3-35 through Figure 3-37. These figures indicate that a large portion of the tenorite initially present on the surface of the copper particles was reduced to cuprite. Some of this cuprite was further reduced to copper metal. Comparison of the three tests show that the startup sequence in Test 1 reduced significantly less oxide to metal than the sequences in Tests 2 and 3. However, the difference between Test 2 and Test 3 was not significant.

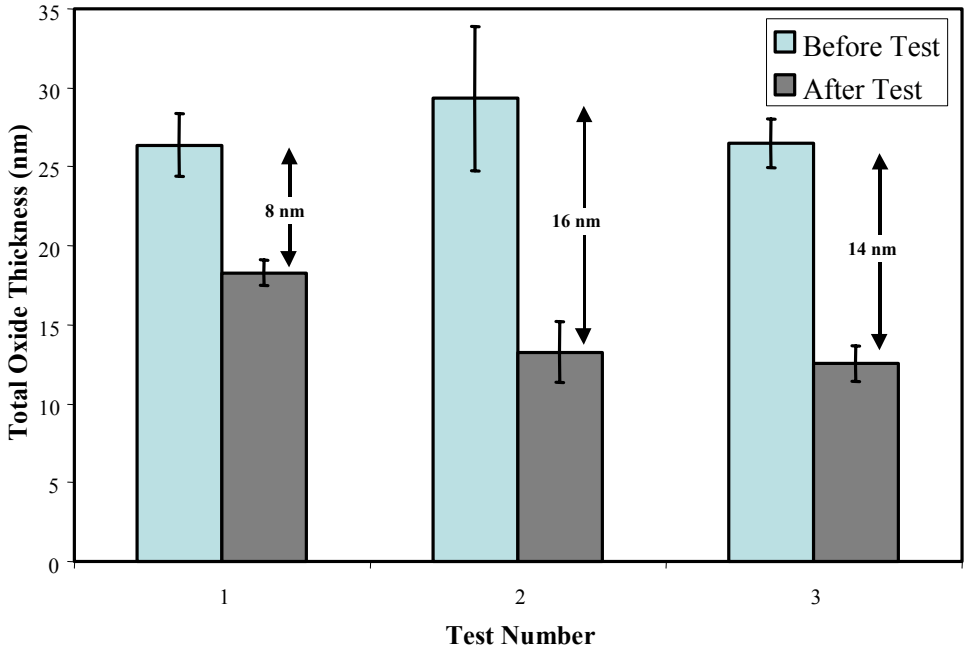

Figure 3-35
Autoclave Simulated Startup Tests—Total Oxide Thickness Before and After

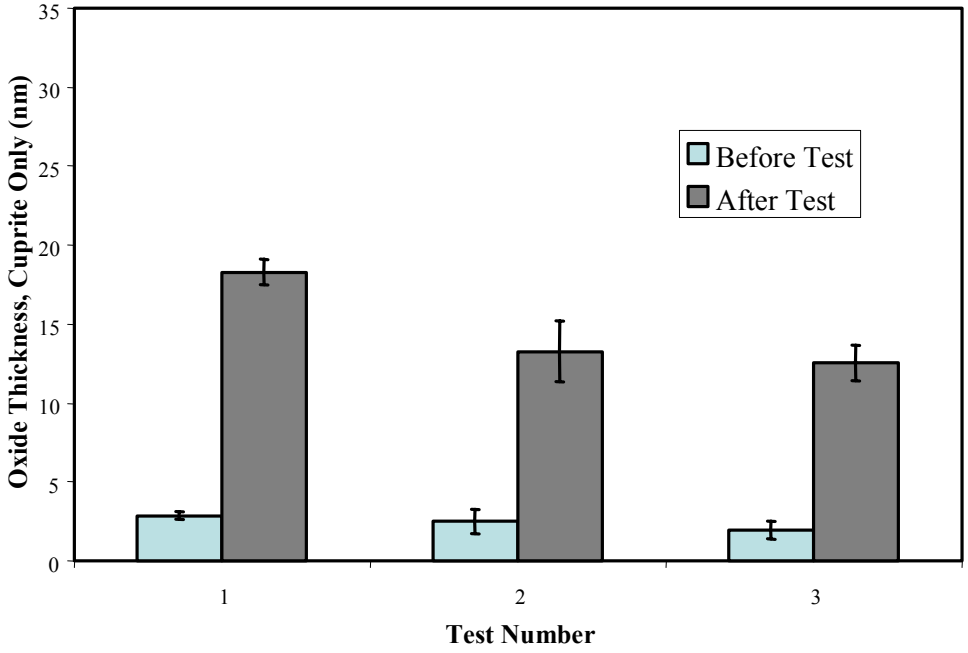

Figure 3-36
Autoclave Simulated Startup Tests—Cuprite Thickness Before and After

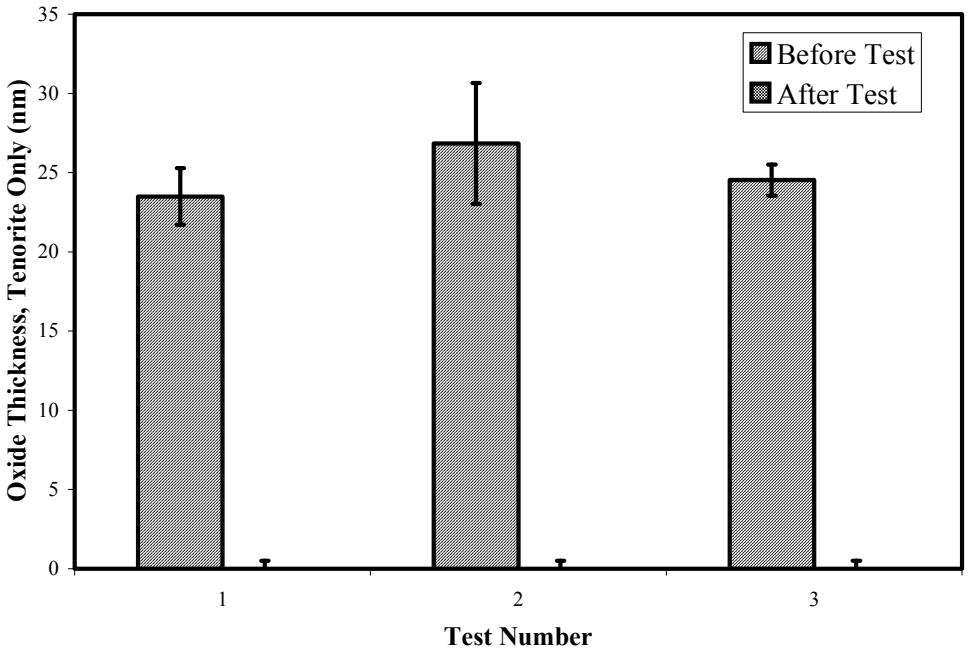

Figure 3-37
Autoclave Simulated Startup Tests—Tenorite Thickness Before and After

Figure 3-38 shows the percent of the total oxide thickness reduced in each test. This figure shows how the sequence used in Test 1 reduced significantly less oxide that the sequences used in Tests 2 and 3. Figure 3-39 shows the total oxide thickness reduced in each test. This figure shows that even the sequence used in Test 1 is capable of reducing a significant amount of copper oxide. Evaluation of the adequacy of a given startup sequence in reducing copper oxide must be made from an estimate of the degree of oxidation occurring during layup. If the startup practices can reduce more oxide than is formed during layup, then the sequence is appropriate with respect to deposit oxide reduction. For comparison, exposure to approximately 6 days of low pH, aerated water at 30°C (86°F) (such as might be used during sludge lancing) would lead to approximately 8 nm of oxide.

For the copper in deposits above the wet layup water level, which will be exposed to humid air, the expected oxide layer thickness would be 5 nm at most. Accordingly, each of the startup sequences tested would in theory be able to convert the cuprous or cupric oxide back to copper metal. Note that these results apply to fairly exposed deposits such as those on tube freespans or powders at the top-of-tubesheet. The next section discusses the effects on deposits in more restricted geometries such as in crevices at tube supports or at the top-of-tubesheet.

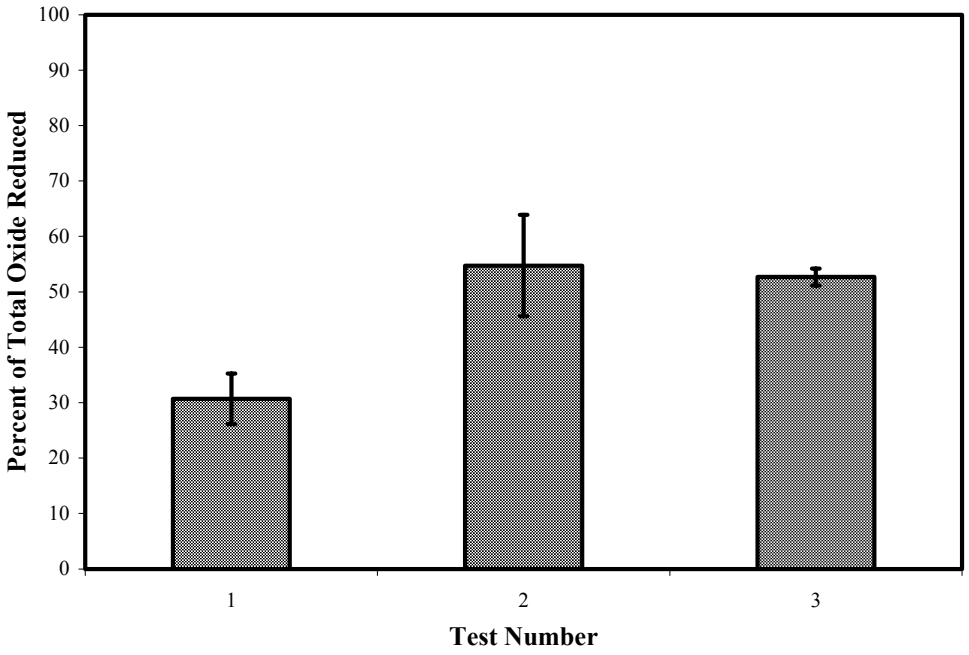

Figure 3-38
Autoclave Simulated Startup Tests—Percent of Total Oxide Reduced

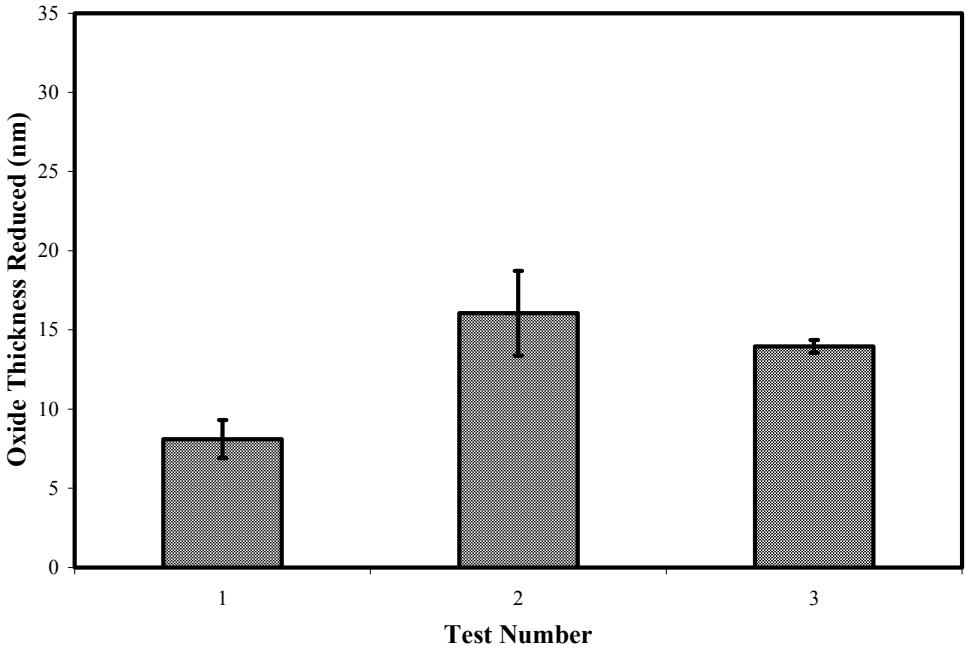

Figure 3-39
Autoclave Simulated Startup Tests—Oxide Thickness Reduced

Scavenger Decomposition—Effect on Crevice and Sludge Pile Reduction

During wet layup of steam generators, oxygen scavengers such as hydrazine or carbohydrazide are used to maintain a reducing environment [9]. In the previous EPRI sponsored study [7], it was found that hydrazine can be decomposed relatively quickly in solutions in contact with steam generator deposits. This raised the concern that hydrazine diffusing into a crevice or into a deposit layer might be decomposed before reaching the regions close to the steam generator tubes. This would leave the critical regions of the steam generator secondary side in an oxidizing environment. Note that the previous process, oxidation of the deposits, was not found to be diffusion limited, as discussed in Reference 6.

To evaluate the possibility of excessive scavenger decomposition, a diffusion-reaction model of a crevice was developed. The primary parameter governing the decomposition of scavengers in a crevice was the Thiele Modulus, a nondimensional parameter defined as follows:

$$\phi = L\sqrt{\frac{k_d}{D_{eff}}} \tag{3-12}$$

where L is the depth of the crevice, k_d is the decomposition reaction constant (equal to $ln(2)/t_{½}$, where $t_{½}$ is the scavenger half life) and D_{eff} is the effective diffusivity. While the depth of the crevice can be determined from steam generator geometry and the diffusivity of hydrazine in water can be determined from the literature, the decomposition rate of hydrazine in the presence of secondary side deposits is largely unknown. Therefore, before implementing the model, experiments were performed to determine the decomposition rates of hydrazine and carbohydrazide under various conditions.

The experimental techniques used to determine the scavenger decomposition rates are presented in the next section. The results of the experiments are then presented, followed by the results of the diffusion-reaction modeling.

Experimental Techniques

Decomposition Monitoring

Several tests were performed to determine the decomposition rate of hydrazine and carbohydrazide. In general, these tests involved making a solution with a known scavenger concentration, adding deposit powder and maintaining a constant temperature. Periodically, an aliquot of the test solution was removed and the scavenger concentration was measured by the methods descibed in the sections below. In this manner, the concentration of scavenger was determined as a function of time.

In most cases, the concentration decreased in a manner consistent with a first order decomposition reaction, characterized by an exponential decay:

$$\frac{C}{C_o} = e^{-k_d t} \tag{3-13}$$

where C is the measure concentration at time t, C_o is the initial concentration and k_d is the decomposition reaction rate constant (equivalent to $ln(2)/t_{½}$, where $t_{½}$ is the scavenger half life). Figure 3-40 shows one example of the concentration profile of the scavenger concentration.

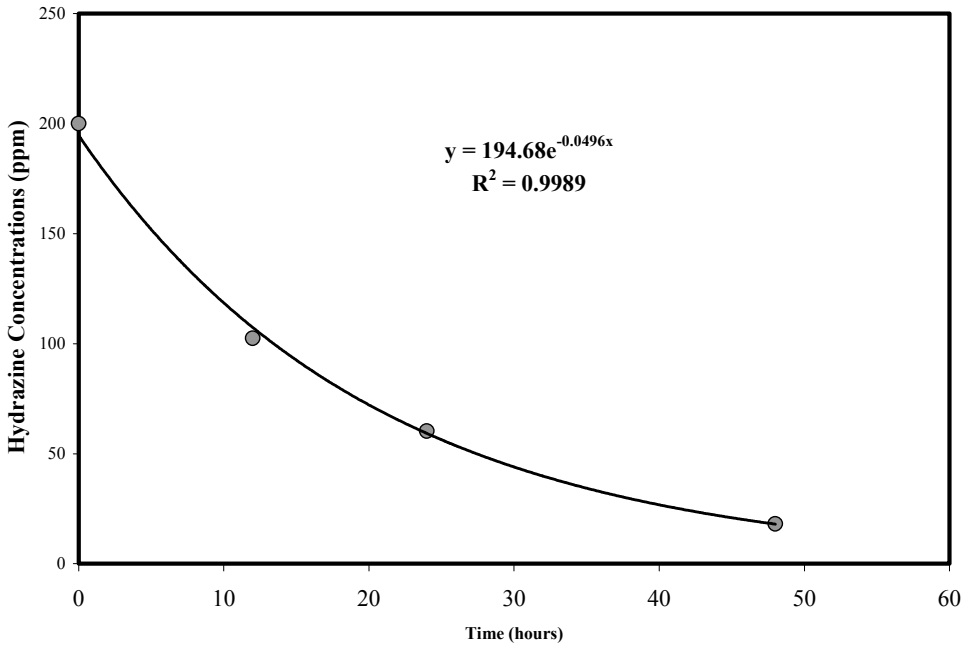

Figure 3-40
Decay of Hydrazine—Concentration as a Function of Time

The following parameters were varied from test to test:

- initial concentration
- temperature
- deposit loading
- deposit source

The details of these experimental parameters are discussed below.

Initial concentrations of 200 ppm and 400 ppm hydrazine or carbohydrazide were used to determine if the absolute concentration of scavenger had an effect on the relative decomposition rates.

Two temperatures were examined: 30°C (86°F) and 60°C (140°F).

Two different powder loadings (1% and 2% weight per volume of solution, equivalent to 10 g/L and 20 g/L) were used to test for an effect of deposit concentration. These loading are considerably lower than those that might be representative of crevices or sludge piles. The lower concentrations were chosen to magnify any dependence on powder loading, since at lower loadings the concentration of powder was more likely to limit the reaction and thus influence the decomposition rates. However, testing revealed that even at these low loadings, the decomposition rate was not affected by the powder density, indicating that there would be no change in the kinetics at higher loadings.

Four powder types were used: synthetic copper powder, synthetic magnetite powder, deposit powder from the secondary side of a commercial steam generator (Plant A) and ground flakes which were at one time tube scale from the secondary side of a commercial steam generator (Plant B). The powder from Plant A had approximately 10% copper by weight. The scale from Plant B had about 5% copper by weight.

The parameter variations described above were tested with both hydrazine and carbohydrazide, yielding a complete matrix of 64 tests, as shown in Table 3-2, below.

Table 3-2
Test Conditions for First Round of Scavenger Decomposition Tests

Scavenger	Hydrazine								Carbohydrazide							
Initial Concentration (ppm)	200				400				200				400			
Temperature (°C)	30		60		30		60		30		60		30		60	
Deposit Loading (%)	1	2	1	2	1	2	1	2	1	2	1	2	1	2	1	2
Powder Type	Cu, Fe_3O_4, Plant A and Plant B															
Total # of Tests	64															

In addition to the sixty-four tests described above, three additional investigations were made into the effects of air in the “head space” above the scavenger solution. In one test, experiments were conducted at 30°C (86°F) with no powder but at three different initial concentrations of hydrazine (100, 200 and 400 ppm) and four different head space volumes. The head space volume was varied by changing the volume of solution used in a single size reaction tube. The total tube volume used was 55 ml. The solution volumes were 10, 25, 40 and 55 ml (resulting in 45, 30, 15 and 0 ml of headspace, respectively). This additional experiment thus consisted of twelve individual tests, as shown in Table 3-3. Note that the volume ratios of head space to solution range from zero to about 4.5. During layup of an actual steam generator, this ratio is typically in the range of 0.25 to 1. However, it should be noted that the head space in these experiments was filled with air. Currently, the EPRI secondary chemistry guidelines [9] recommend a nitrogen blanket whenever practical to prevent the exposure of the layup water to oxygen.

Table 3-3
Hydrazine Tests with Different Head Space Volumes without Deposits at 30°C

Solution Volume	10	25	40	55
Head Space Volume	45	30	15	0
Volume Ratio of Head Space to Solution	4.5	1.2	0.375	0
Initial Concentrations	100, 200 and 400 ppm			

In the second additional investigation, the temperature was 60°C (140°F). Two different reaction tube volumes were used, one in which the solution charge filled the entire tube and one in which the solution charge filled approximately one quarter of the tube. Two different initial concentrations (200 and 400 ppm) and two different powder loadings (1% and 2% or 10 and 20 g/L, respectively) were used. This resulted in eight individual tests in this experiment, as shown Table 3-4.

Table 3-4
Hydrazine Tests with Different Head Space Volumes with Deposits at 60°C

Volume Ratio of Head Space to Solution	0		2.67	
Initial Concentration (ppm)	200	400	200	400
Powder Loading	1% and 2%			

In the third additional investigation, the temperature was also 60°C (140°F). Two different reaction tube volumes were used as well as two different charge volumes. Initial hydrazine concentrations were either 200 or 400 ppm. No deposits were added. Table 3-5 summarizes the tests performed in this investigation. A total of six tests were performed in this investigation.

Table 3-5
Hydrazine Tests with Different Head Space Volumes without Deposits at 60°C

Tube Volume (ml)	15		55
Solution Volume (ml)	15	7.5	15
Volume Ratio of Head Space to Solution	0	1	2.67
Initial Concentrations	200 and 400 ppm		

Hydrazine Detection

The hydrazine concentrations in these experiments were determined using a colorometric technique based on *ASTM Method D1385, Standard Test Method for Hydrazine in Water* [13]. This method measures the absorbance of a 5:1 mixture of acidified sample to indicator. The indicator is a 1.8% acidified solution of p-dimethylaminobenzalehyde in methyl alcohol. The absorbance at 458 nm is directly related to the hydrazine concentration. This method is appropriate for hydrazine concentrations up to 200 ppb. Higher concentrations were measured

using dilution of the original sample. Figure 3-41 shows a calibration curve indicating the absorbance measured for a number of standard solutions.

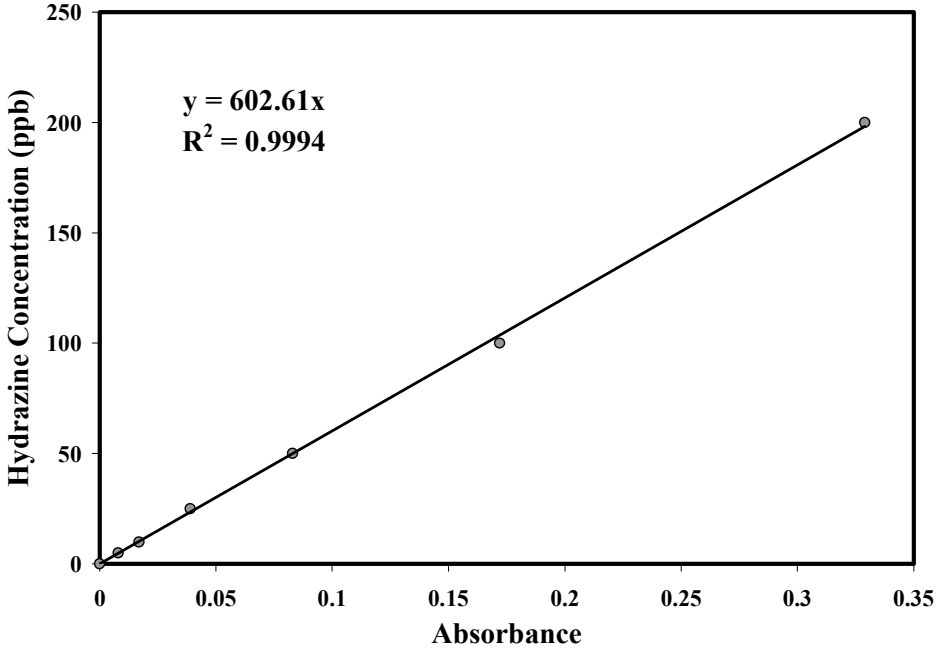

Figure 3-41
Hydrazine Detection Calibration Curve

Carbohydrazide Detection

The carbohydrazide concentrations were measured using a modification of the method presented in Reference 14. This method uses two chemical reactions. First, carbohydrazide reacts with ferric ions (Fe^{3+}) converting them to ferrous ions (Fe^{2+}). Second, the ferrous ions react with an indicator molecule, ferrozine (3-(2-pyridyl)-5,6-bis(4-phenylsulphonic acid)-1,2,4-triazine). This produces a solution whose absorbance at 562 nm is a function of the initial carbohydrazide concentration. Figure 3-42 shows the calibration of this method. For carbohydrazide concentrations up to 700 ppb, a parabolic relationship between the concentration and the absorbance fits the data well. Above this level, concentrations of carbohydrazide can be determined by dilution of the initial solution.

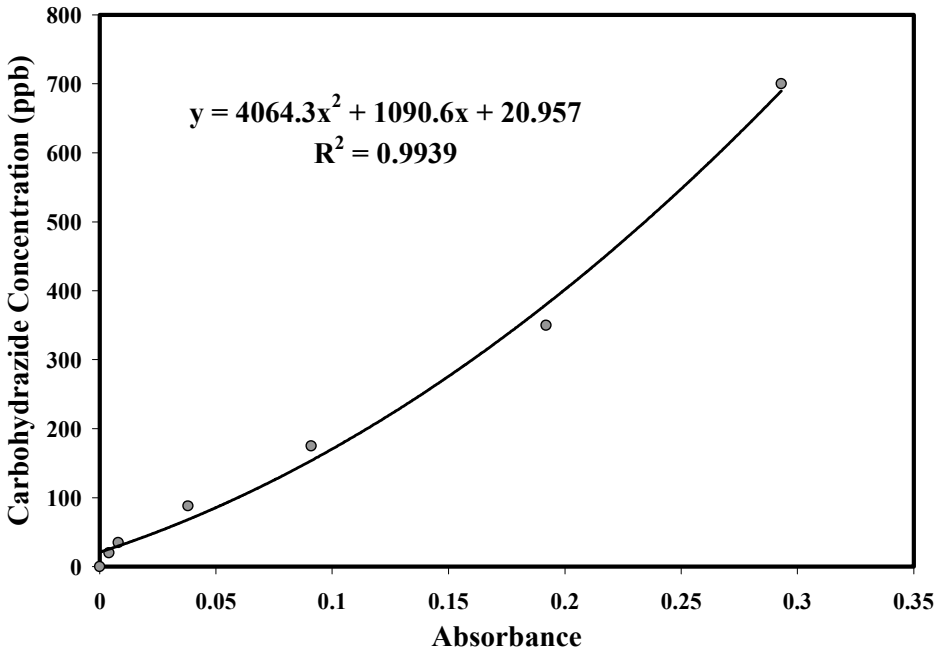

Figure 3-42
Carbohydrazide Detection Calibration Curve

Decomposition Rate Results

As stated above in the experimental description, this investigation examined the effects on scavenger decomposition of the following five parameters:

- initial concentration
- deposit loading
- deposit source
- temperature
- head space

The influence of each of these parameters is discussed in the sections below. Specifically, the half-life of the scavenger molecule in each test was determined and the various values of the half-life were compared.

Initial Concentration

The half-life of scavenger was calculated for each of the 64 experiments described in Table 3-2. For the purpose of examining the influence of the initial concentration, it was assumed that the deposit loading was not an influential factor. This allowed the creation of a set of 32 average half-life values, each with a standard deviation. It was then possible to assess the effect of initial concentration.

Figure 3-43 shows the measured half-life of hydrazine in solutions of different initial concentrations at 30°C (86°F) for the four different deposit types. The standard deviations shown in Figure 3-43 by error bars are calculated from the results of experiments at two different deposit loadings. From this figure it is clear that the initial hydrazine concentration does not strongly influence the half-life for solutions exposed to copper or to secondary side deposits. In the case of synthetic magnetite, it is possible that the initial concentration does make a significant difference in the hydrazine half-life. If hydrazine decomposition were to follow a first order rate law such as that given by Equation 3-13, the initial concentration would make no difference. Thus the data shown in Figure 3-43 suggest that the decomposition of hydrazine may proceed by a different mechanism in the absence of copper powder or secondary side deposits.

Figure 3-44 shows a similar analysis for hydrazine decomposition at 60°C (140°F). The conclusion that initial concentration has no strong effect is largely supported by this analysis. However, firm conclusions are more difficult to make because there is considerably more variability in the data for higher temperature decomposition.

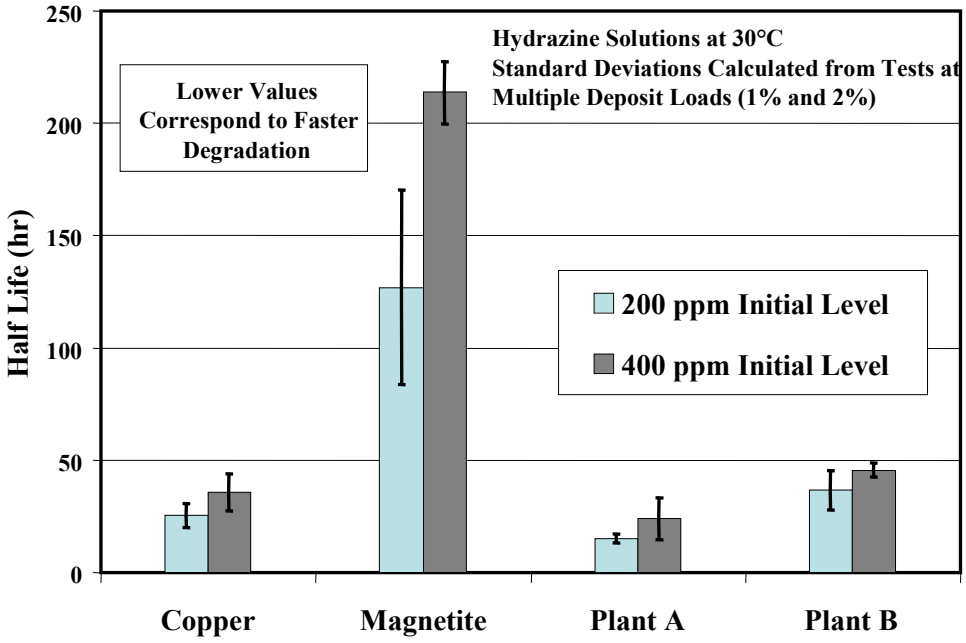

Figure 3-43
Hydrazine Decomposition at 30°C, Effect of Initial Concentration

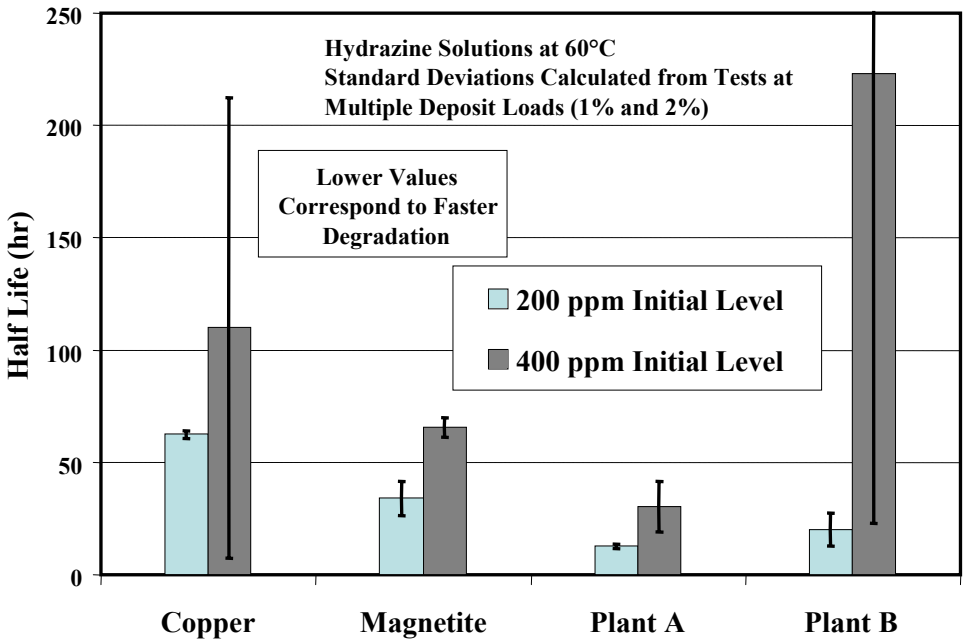

Figure 3-44
Hydrazine Decomposition at 60°C, Effect of Initial Concentration

Figure 3-45 and Figure 3-46 show the half-life values for carbohydrazide in solutions at 30°C (86°F) and 60°C (140°F), respectively. The data are similar to those for hydrazine, indicating that, except for the case of solutions exposed to synthetic magnetite at 30°C (86°F), initial concentration of scavenger makes little difference. This conclusion indicates that carbohydrazide, as well as hydrazine, follows first order decay kinetics as given by Equation 3-13.

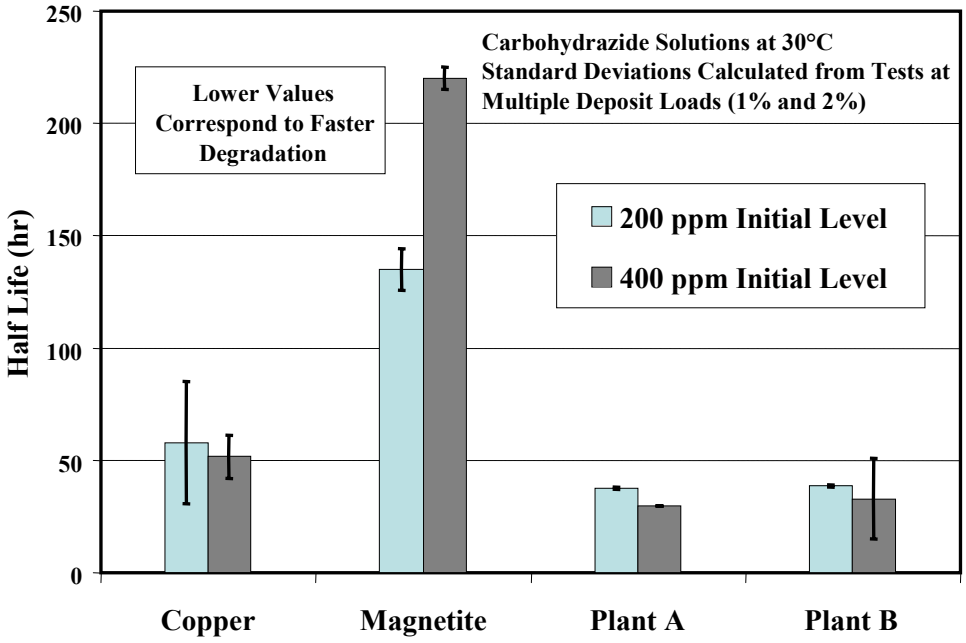

Figure 3-45
Carbohydrazide Decomposition at 30°C, Effect of Initial Concentration

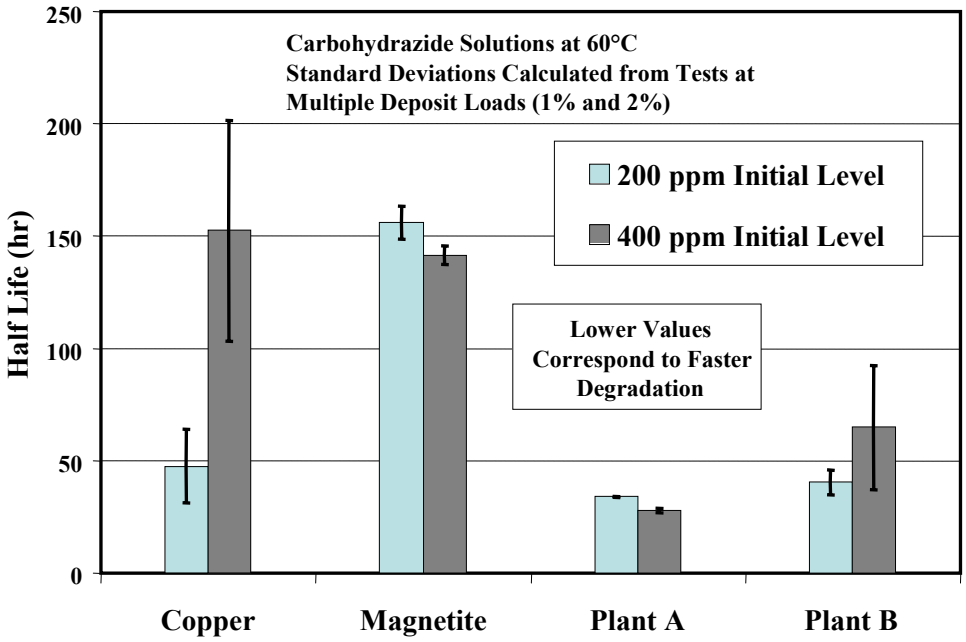

Figure 3-46
Carbohydrazide Decomposition at 60°C, Effect of Initial Concentration

Powder Loading

As indicated in Table 3-2, experiments were run with both a 1% and a 2% deposit loading (1% is equivalent to 1 g of powder per 100 ml of liquid or 10 g/L, which is typical of a moderately loaded steam generator). Because the previous examination showed that the initial concentration does not affect the decomposition kinetics, the two experiments at different initial concentrations can be used to evaluate the variability between experiments. This allows the evaluation of the influence of deposit loading with respect to the random variability of the experiment.

Figure 3-47 and Figure 3-48 show the hydrazine half-life values measured in the experiments described in Table 3-2 for 30°C (86°F) and 60°C (140°F), respectively. The error bars in these plots show the standard deviation calculated from the results of tests at different initial concentrations of hydrazine. From these plots it is evident that the deposit loading does not influence the reaction kinetics of hydrazine decomposition. Figure 3-49 and Figure 3-50 show similar data for carbohydrazide decomposition at 30°C (86°F) and 60°C (140°F), respectively. Carbohydrazide decomposition is also not influenced by the deposit loading.

Figure 3-51 and Figure 3-52 show the effect of headspace on decomposition in the absence of deposits. The experiments with no headspace are comparable to those shown in Figure 3-47 to Figure 3-50. A comparison of the hydrazine half-life values with and without deposits shows that the presence of deposits can decrease the half-life of hydrazine by a factor of about 10. Therefore, there are some limits to the conclusion that the deposit loading does not affect decomposition. In a PWR steam generator during wet layup, two extremes of deposit loading are present. In the bulk fluid, there are essentially no deposits. In the regions near the tubes, on the tube sheet or in crevices the deposit concentration may be considered to be quite high due to the presence of tube scale, sludge and collars, respectively. Therefore, it is likely that there will be a fairly sharp division between regions where the decomposition rate is slow (as indicated by long half-life values such as those in Figure 3-51 and Figure 3-52) and regions where the decomposition rate is fast (as indicated by short half-life values such as those in Figure 3-47 to Figure 3-50).

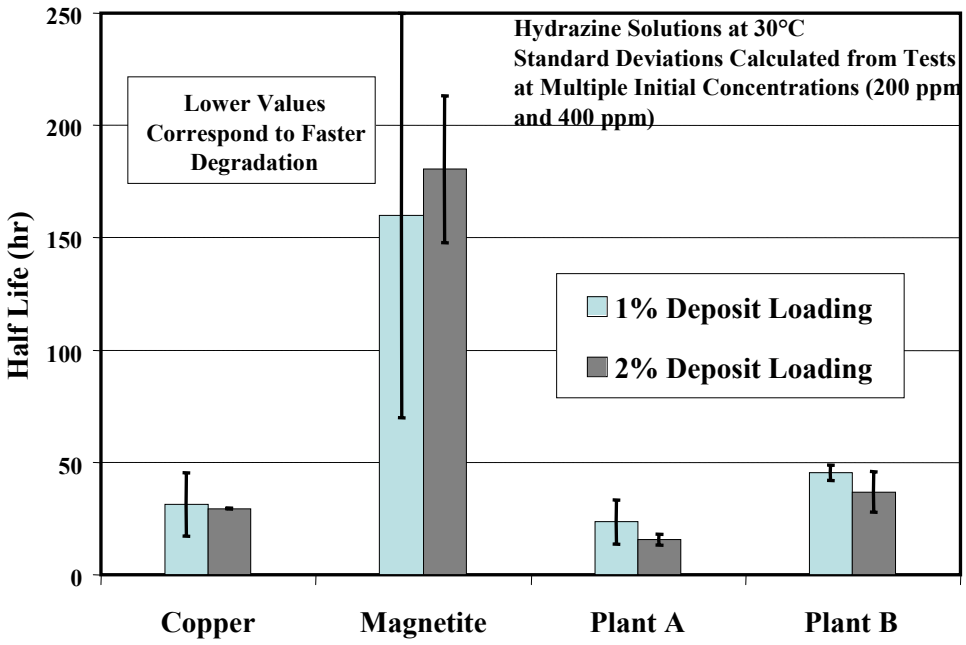

Figure 3-47
Hydrazine Decomposition at 30°C, Effect of Deposit Loading

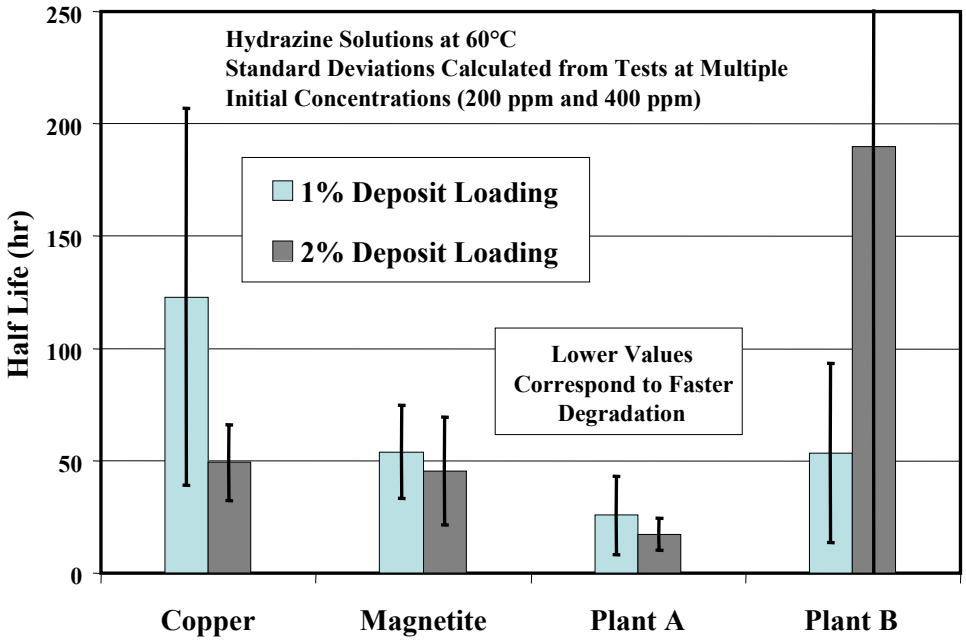

Figure 3-48
Hydrazine Decomposition at 60°C, Effect of Deposit Loading

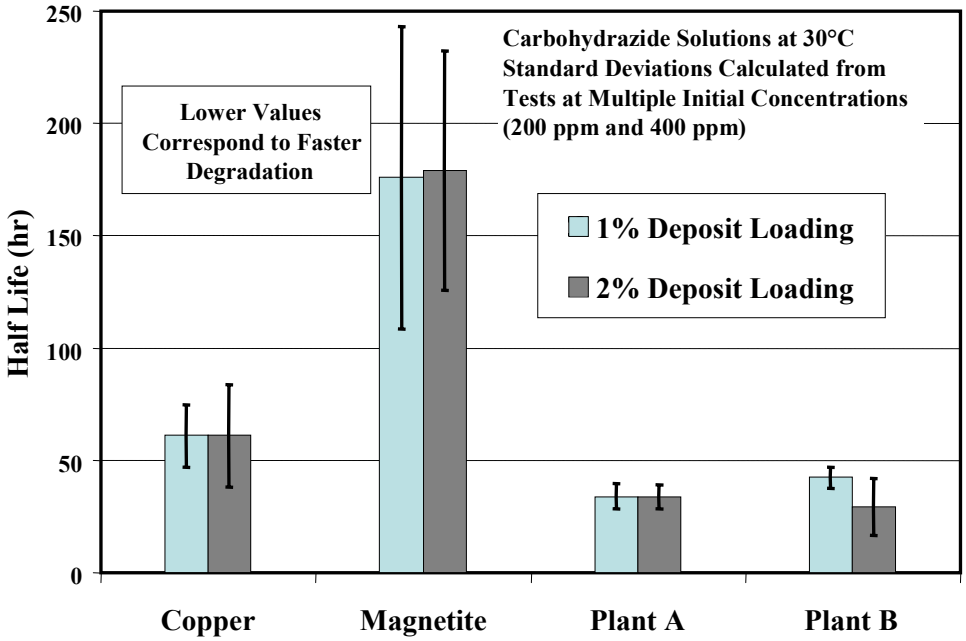

Figure 3-49
Carbohydrazide Decomposition at 30°C, Effect of Deposit Loading

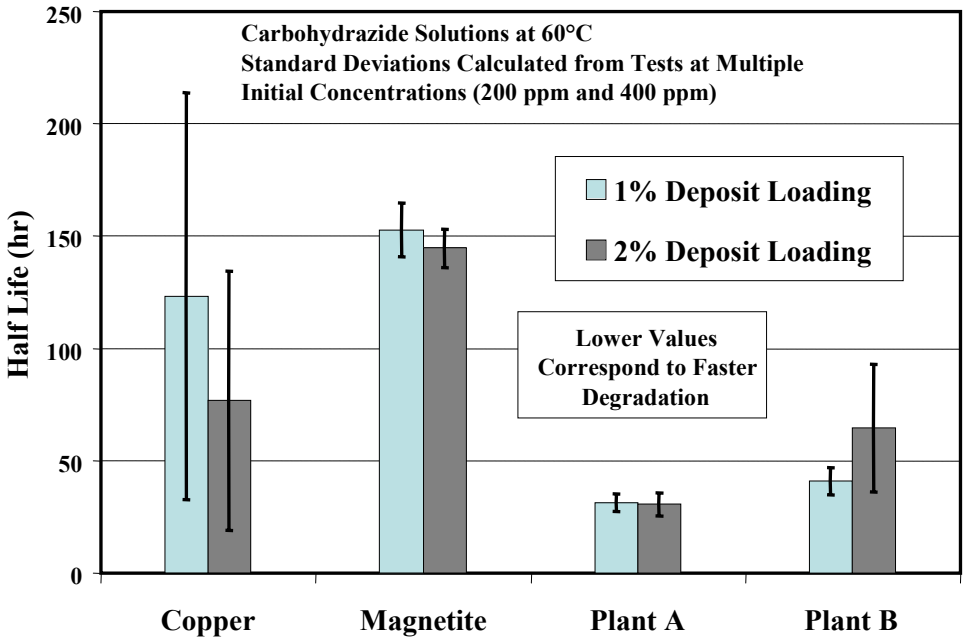

Figure 3-50
Carbohydrazide Decomposition at 60°C, Effect of Deposit Loading

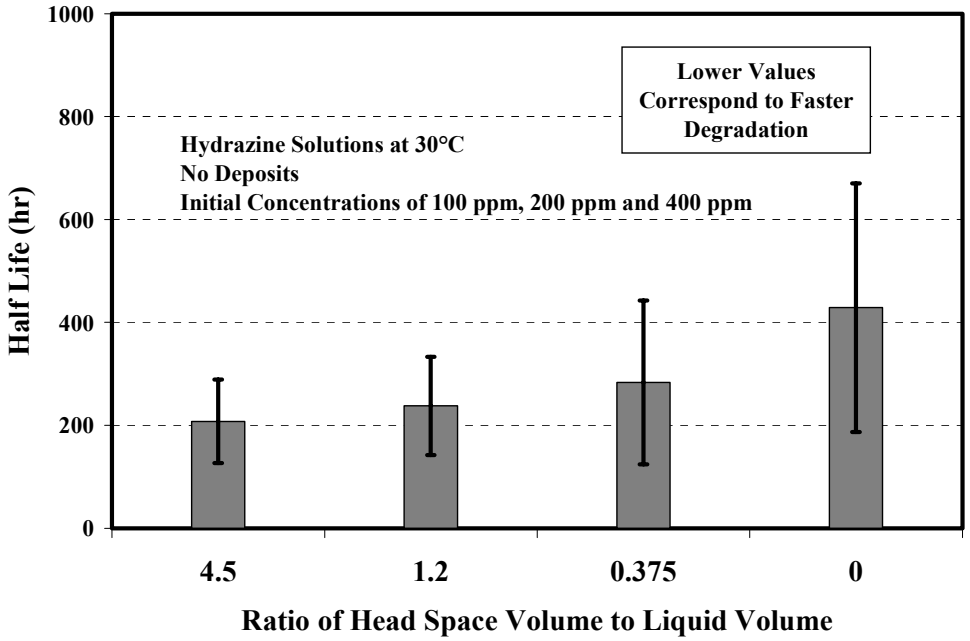

Figure 3-51
Hydrazine Decomposition at 30°C, Effect of Head Space, No Deposits

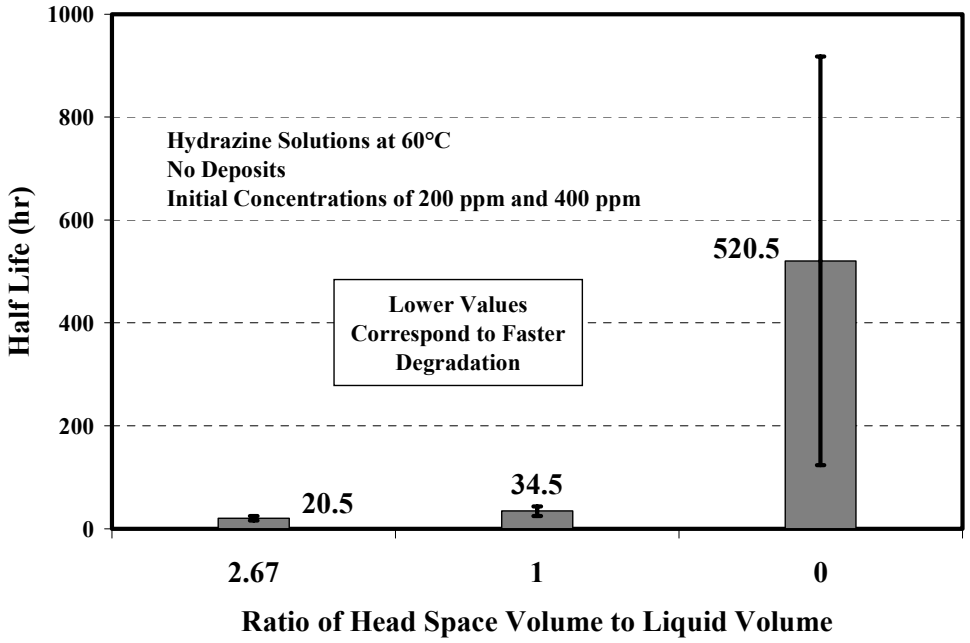

Figure 3-52
Hydrazine Decomposition at 60°C, Effect of Head Space, No Deposits

Powder Type

Because the powder loading and the initial concentration were not found to have a significant influence on the decomposition of either hydrazine or carbohydrazide, the 64 experiments described in Table 3-2 can be analyzed as 16 experimental conditions with four replicates of each condition. Figure 3-53 to Figure 3-56 show this analysis with error bars representing the standard deviations calculated from the results of the four replicates.

At 30°C (86°F), the decomposition of hydrazine (Figure 3-53) is significantly faster in the presence of copper powder or secondary side deposits than in the presence of synthetic magnetite. There appears to be no significant difference between pure copper powder and secondary side deposits with respect to hydrazine decomposition at 30°C (86°F). At 60°C (140°F) (Figure 3-54) there is considerably more scatter in the data. The specific deposit type appears to influence the decomposition rate less at 60°C (140°F) than at 30°C (86°F). Similar results (Figure 3-55 and Figure 3-56) are found with carbohydrazide, with the exception that at 60°C (140°F), carbohydrazide appears to retain a relative stability in the presence of synthetic magnetite. These results are in agreement with preliminary conclusions drawn in Reference 6.

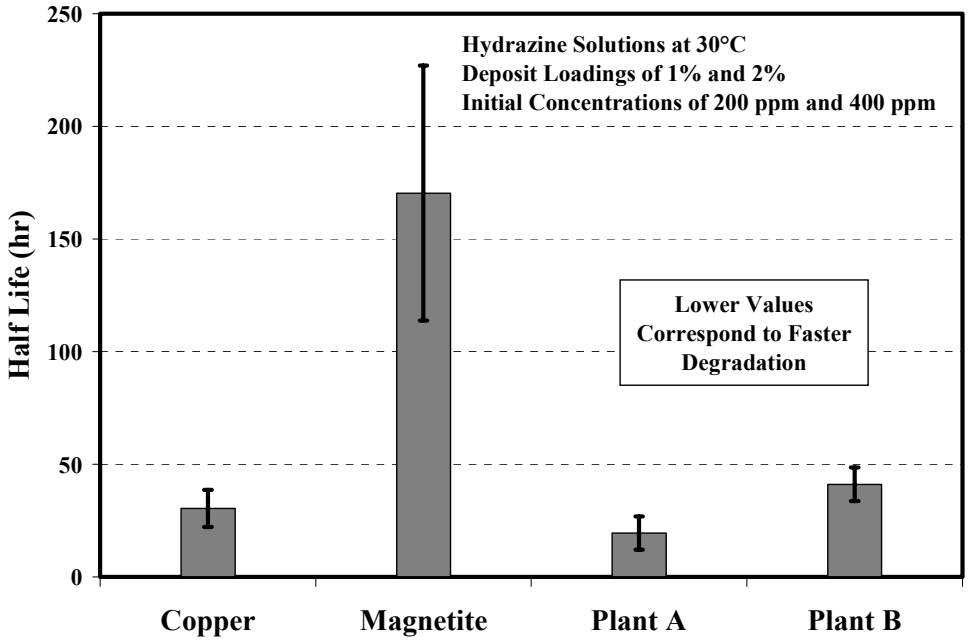

Figure 3-53
Hydrazine Decomposition at 30°C, Effect of Powder Type

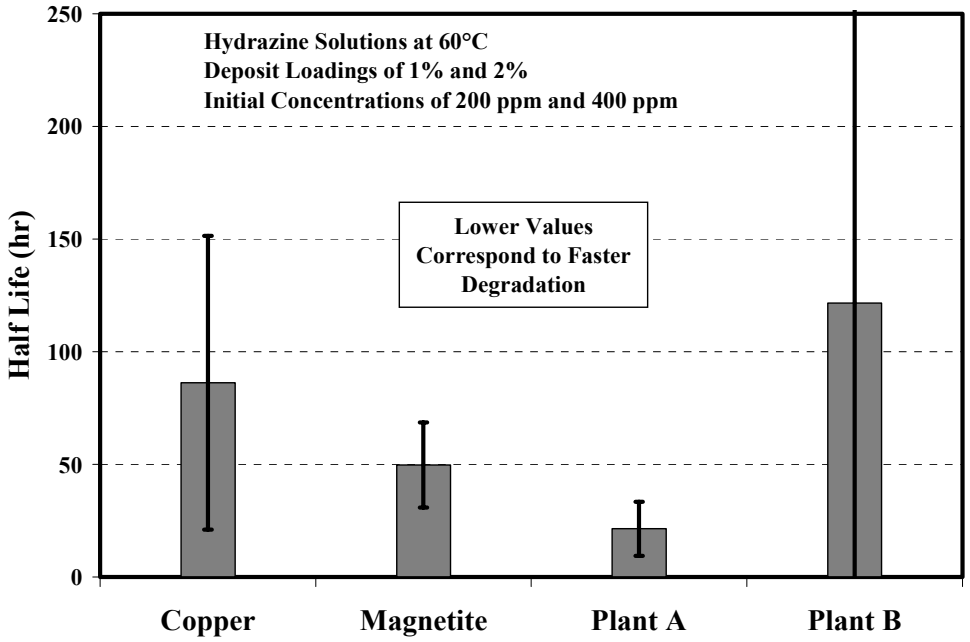

Figure 3-54
Hydrazine Decomposition at 60°C, Effect of Powder Type

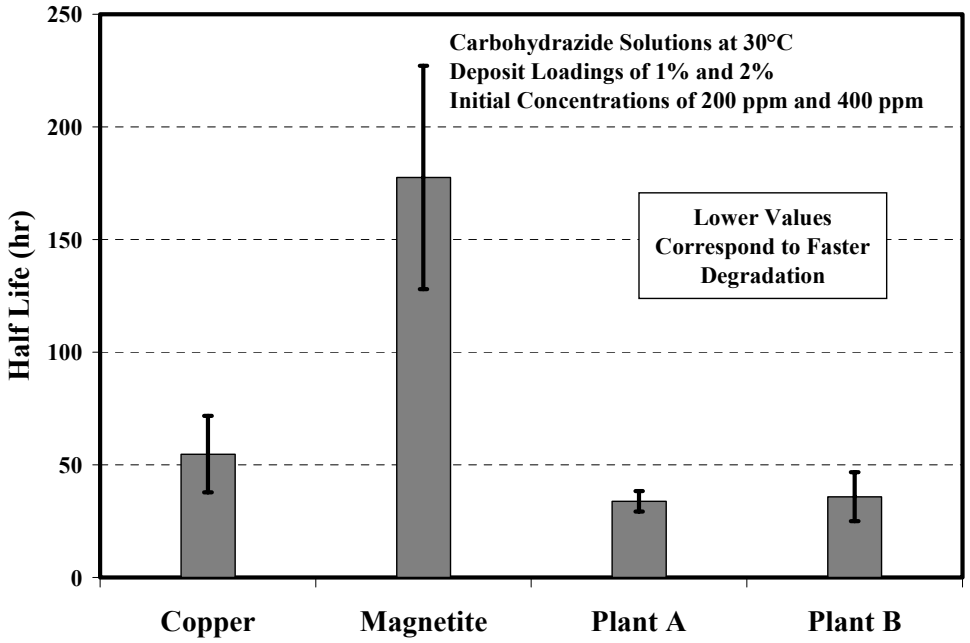

Figure 3-55
Carbohydrazide Decomposition at 30°C, Effect of Powder Type

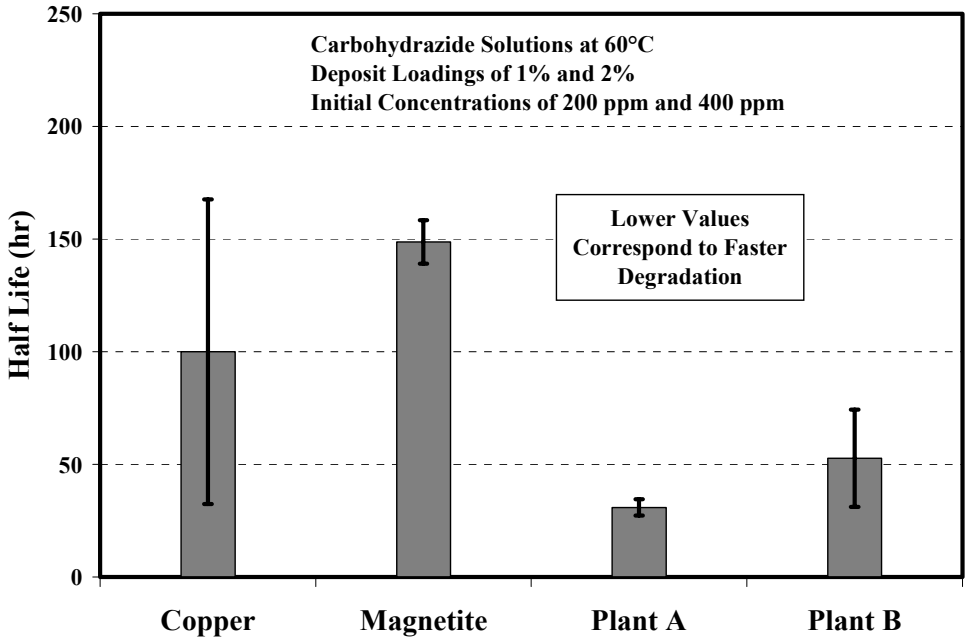

Figure 3-56
Carbohydrazide Decomposition at 60°C, Effect of Powder Type

Temperature

The effect of temperature on scavenger decomposition may be evaluated by comparing Figure 3-53 with Figure 3-54 (for hydrazine) and Figure 3-55 with Figure 3-56 (for carbohydrazide).

In the case of hydrazine, increasing the temperature from 30°C (86°F) to 60°C (140°F) does not affect the rate of decomposition in the presence of copper powder or secondary side deposits. In the presence of synthetic magnetite, an increase in temperature appears to significantly accelerate the decomposition of hydrazine. In general, there appears to be significantly more scatter in the half-life values measured at 60°C (140°F) compared to those measured at 30°C (86°F).

In the case of carbohydrazide, increasing the temperature from 30°C (86°F) to 60°C (140°F) does not appear to significantly change the decomposition rate. This is true even in the case of synthetic magnetite, which was not true for hydrazine. Therefore, carbohydrazide should be given consideration especially at plants which may experience relatively high layup temperatures.

Headspace

In the experiments described in Table 3-2 and discussed above, the solution volume entirely filled the test volume and was separated from the surrounding atmosphere. This limited the amount of oxygen that was available to react with the scavenger present in the solution. However, during wet layup of steam generators, it is possible that the upper portions of the steam generator may be filled with air, although most US plants use nitrogen blankets when manways

and piping valves are closed. The presence of air (which may exist if, for instance, upper bundle access is required) may accelerate decomposition of oxygen scavengers. Additional tests, described in Table 3-3 to Table 3-5, were conducted to determine if an air containing headspace influenced the decay of hydrazine.

The results of the experiments with hydrazine at 30°C (86°F) in the absence of deposits (described in Table 3-3) are shown in Figure 3-51. Although there is considerable scatter in the data, there appears to be a trend of increasing stability as the ratio of the headspace volume to the solution volume is decreased. Figure 3-52 shows similar results for experiments at 60°C (140°F) (described in Table 3-5). At 60°C (140°F), the decomposition of hydrazine (in the absence of deposits) is significantly accelerated by the presence of air in the head space. It is not clear if the volume of the headspace, relative to the volume of the solution, is a significant factor.

Figure 3-57 shows the effect of headspace on the decomposition of hydrazine at 60°C (140°F) in the presence of copper powder. The data in this figure indicates that the presence of an air filled headspace significantly accelerates the decomposition of hydrazine. This is expected to be due to the continued replenishment of oxygen to the solution. The concentration of oxygen in air (~20%) is high compared to the equilibrium concentration in water (~7 ppm at room temperature). Therefore, even small volumes of air can constitute large reservoirs for oxygenation of the liquid phase.

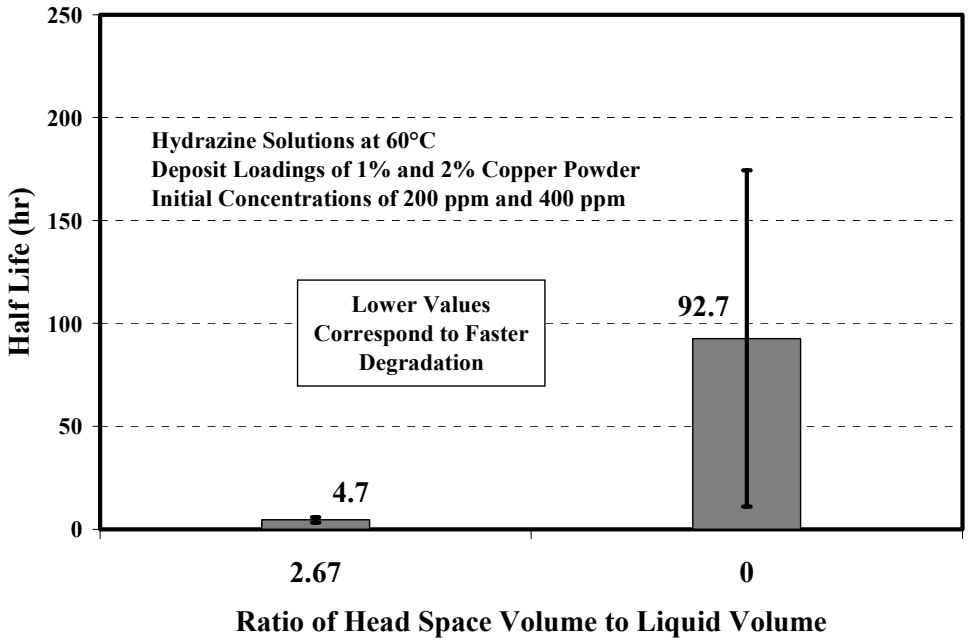

Figure 3-57
Hydrazine Decomposition at 60°C, Effect of Headspace, Copper Powder

Modeling Decomposition of Oxygen Scavengers in Deposits

As discussed in the previous section, Scavenger Decomposition (page 3-40), when evaluating the effects of oxygen scavengers on oxidation and reduction, it is important to note that in critical areas, such as the interiors of crevices or tube scales, the scavenger concentration may be significantly less than that in the bulk secondary side solution due to decomposition in the deposits. To evaluate the relevance of such decomposition, a combination diffusion and reaction model was developed. The details of the model are given in Appendix A. The model predicts that the concentration of the scavenger, relative to the concentration in the bulk is given by the following equation:

$$\frac{C}{C_b} = 1 - \sum_{n=0}^{\infty} \frac{\frac{4}{(2n+1)\pi}}{\phi^2 + \left(\frac{2n+1}{2}\pi\right)^2} \left[\phi^2 + \left(\frac{2n+1}{2}\pi\right)^2 e^{-\left\{\phi^2 + \left(\frac{2n+1}{2}\pi\right)^2\right\}\theta} \right] \sin\left(\frac{2n+1}{2}\pi x\right) \qquad (3\text{-}14)$$

Equation 3-14 assumes that decomposition of scavenger only takes place inside porous deposits. It requires the input of one nondimensional parameter, the Thiele Modulus (ϕ), defined by Equation 3-12 as a function of the deposit thickness (L, the distance between the bulk and the tube surface), the scavenger decomposition rate (k_d, equivalent to $ln(2)/t_{½}$, where $t_{½}$ is the scavenger half life) and the effective diffusivity of the scavenger through the porous deposit (D_{eff}). The relative concentration is then a function of the nondimensional time (θ), which is equivalent to the ratio of real time (t) to the characteristic time (Θ), which is equivalent to the square of the deposit thickness (L) divided by the effective diffusivity (D_{eff}). The time relationships are given in the following equation:

$$\theta = \frac{t}{\Theta} = \frac{t}{\frac{L^2}{D_{eff}}} \qquad (3\text{-}15)$$

The diffusion of oxygen scavengers into deposits was examined for the following three different geometries:

- freespan tube scale
- packed crevices
- sludge piles

The required data for describing these geometries are the depth of the deposit (L), the porosity (ε) and the tortuosity (τ). Table 3-6 shows the values of these parameters considered in the current analysis. The length scales were chosen to represent typical values, but also to demonstrate the effect of this parameter on scavenger distribution within the deposit. The porosities chosen are based on analysis of numerous secondary side deposits conducted for nuclear plants by Dominion Engineering, Inc. The tortuosity is typical of porous media and chosen to reflect the data available in the literature [15 and 16].

Table 3-6
Characteristics of Geometries Considered

Location	*L* (cm)	ε	τ
Scale	0.005	0.2	3
Crevice	0.5	0.1	3
Sludge Pile	1.5	0.1	3

In each of the three geometries listed above, the diffusion and decomposition of two different oxygen scavengers were considered: hydrazine and carbohydrazide. The physical properties of the two scavengers required for the calculation are the decomposition reaction constant (k_d) and the diffusivity in water (D). The values used in this evaluation for these parameters are given in Table 3-7. Note that these are the values for a temperature of approximately 25°C (77°F). The reaction rate constants (k_d) are calculated from the half-life values according to the following equation:

$$k_d = \ln(2)t_{1/2} \tag{3-16}$$

The half-life values are estimates taken from the data presented in Figure 3-53 (for hydrazine) and Figure 3-55 (for carbohydrazide). The diffusivities were calculated from data available in the literature (see Appendix B).

Table 3-7
Physical Properties of the Oxygen Scavengers Considered

Scavenger	Half Life (hr)	k_d (1/s)	D (cm^2/s)
Hydrazine	25	7.7×10^{-6}	1.8×10^{-5}
Carbohydrazide	40	4.8×10^{-6}	1.3×10^{-5}

When the deposit properties given in Table 3-6 are combined with the chemical properties given in Table 3-7 six sets of parameters are generated, as shown in Table 3-8. The effective diffusivity (D_{eff}) is the rate of diffusion through a porous media and is determined from the nominal diffusivity (a property of the chemical) and the nature of the porous media using the following equation:

$$D_{eff} = D\frac{\varepsilon}{\tau} \tag{3-17}$$

The Thiele Modulus, ϕ, is given by Equation 3-12. The characteristic time, Θ, is derived from the following equation:

$$\Theta = \frac{L^2}{D_{eff}} \tag{3-18}$$

Table 3-8
Scavenger Decomposition Cases Considered

Scavenger	Location	D_{eff} (cm^2/s)	ϕ	Θ (s)	Θ (hr)	Θ (day)
Hydrazine	Crevice	3.1×10^{-7}	2.5	8.2×10^{5}	230	9.4
	Tube Scale	1.2×10^{-6}	0.013	20	5.7×10^{-3}	2.4×10^{-4}
	Sludge Pile	6.1×10^{-7}	5.3	3.7×10^{6}	1.0×10^{3}	42
Carbohydrazide	Crevice	2.2×10^{-7}	2.3	1.1×10^{6}	320	13
	Tube Scale	8.7×10^{-7}	0.012	29	8.0×10^{-3}	3.3×10^{-4}
	Sludge Pile	4.4×10^{-7}	5.0	5.2×10^{6}	1.4×10^{3}	60

From the parameters shown in Table 3-8, it can be concluded that the cases for tube scale are not of interest. The Thiele Moduli for these cases are very small, indicating that the concentration distribution is dominated by the reaction rate. In other words, diffusion is much faster than decomposition. Therefore, the concentration everywhere within the deposit will be roughly the same as the concentration in the bulk, since new scavenger from the bulk is transported into the deposit as fast as it is consumed by decomposition. The Thiele Moduli for the crevice and the sludge pile are on the order of unity, indicating that diffusion and decomposition both influence the concentration distribution within the deposit. In these cases, the characteristic time, Θ, is long (on the order of days), indicating that the concentration profile in the deposit will change with time over a period that is meaningful with respect to plant operations related to layup and startup. Therefore, the four relevant cases from Table 3-8 were investigated using Equation 3-14. These cases were:

- Hydrazine in a crevice
- Hydrazine in a sludge pile
- Carbohydrazide in a crevice
- Carbohydrazide in a sludge pile

Each of these cases is discussed below. For the purposes of evaluating the results of applying Equation 3-14 to these cases it was assumed that the bulk concentration was 400 ppm. However, Equation 3-14 does not depend on the bulk concentration, since it evaluates concentrations relative to the bulk. Thus the results presented below as relative concentrations apply to any initial bulk concentration.

Hydrazine in a Crevice

Figure 3-58 shows the solutions to Equation 3-14 for hydrazine diffusing into and reacting in a packed crevice for several values of θ, the dimensionless time. Four curves give the concentration as a function of the position in the crevice at four different times (equivalent to 2.3 hours, 11.5 hours, 23 hours and 47 days). The solutions plotted in the figure show behavior typical of solutions to Equation 3-14 in the following ways:

- The concentration at the bottom of the crevice (x=1) is the lowest at all times.
- The concentrations at all positions gradually approach the steady state value (closely approximated by θ=5).
- In the initial stages, the concentration near the bottom is approximately zero.

One aspect of the solution that is unique to this particular solution is the steady state value of the concentration at the crevice bottom. Even after a very long time (47 days) the concentration at the bottom of the crevice is only one sixth of the bulk concentration.

Figure 3-59 shows the concentration at the bottom of the crevice as a function of time. As assumed in the initial conditions used to obtain Equation 3-14 (see Appendix A), the crevice is initially devoid of hydrazine. As time progresses, the concentration gradually increases. As the concentration nears the steady state concentration, the rate of increase slows. Eventually, the concentration becomes nearly constant at approximately the steady state concentration. In the particular case examined here, that concentration is approximately one sixth of the bulk concentration, or about 65 ppm. The steady state value is reached at a dimensionless time of approximately 0.5, corresponding to an actual time of about 100 hours.

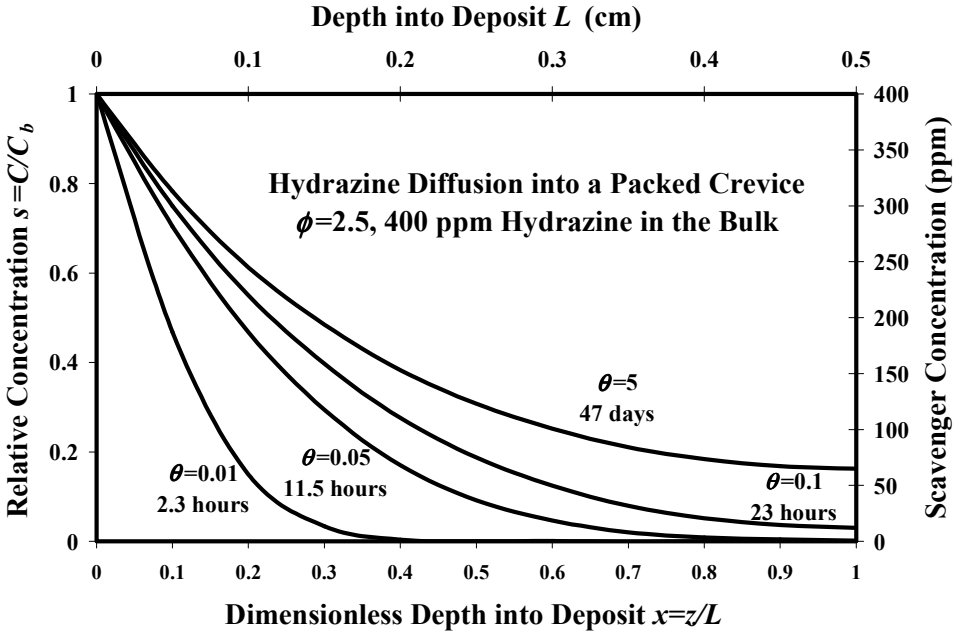

Figure 3-58
Hydrazine Diffusion into a Crevice, Concentration as a Function of Position

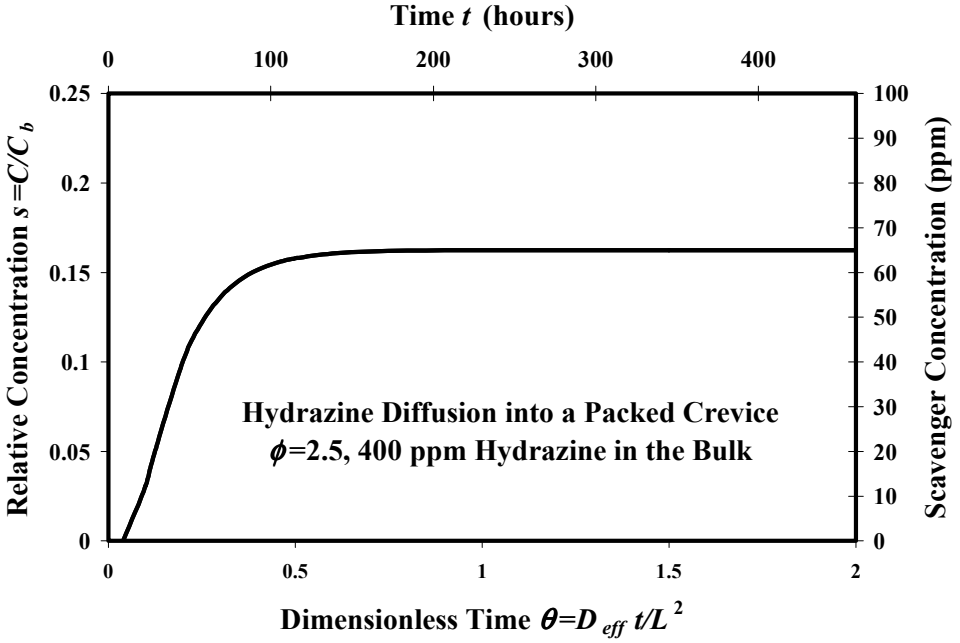

Figure 3-59
Hydrazine Concentration at the Bottom of a Crevice as a Function of Time

Hydrazine in a Sludge Pile

Figure 3-60 and Figure 3-61 show a similar analysis for hydrazine diffusion into and reaction in a sludge pile having the physical characteristics given in Table 3-6. Again, the curves display behavior typical of solutions to Equation 3-14. Of particular note is the concentration of hydrazine at the bottom of the sludge pile as shown in Figure 3-61. The concentration there approximates the steady state value after the dimensionless time has reached about 0.25, corresponding to a real time of about 15 days. However, the steady state concentration at the bottom of the sludge pile is less than 1% of the bulk concentration. This indicates that in typical wet layup situations the tubesheet and the tube to tubesheet crevices are exposed to less than 1% of the bulk concentration of hydrazine.

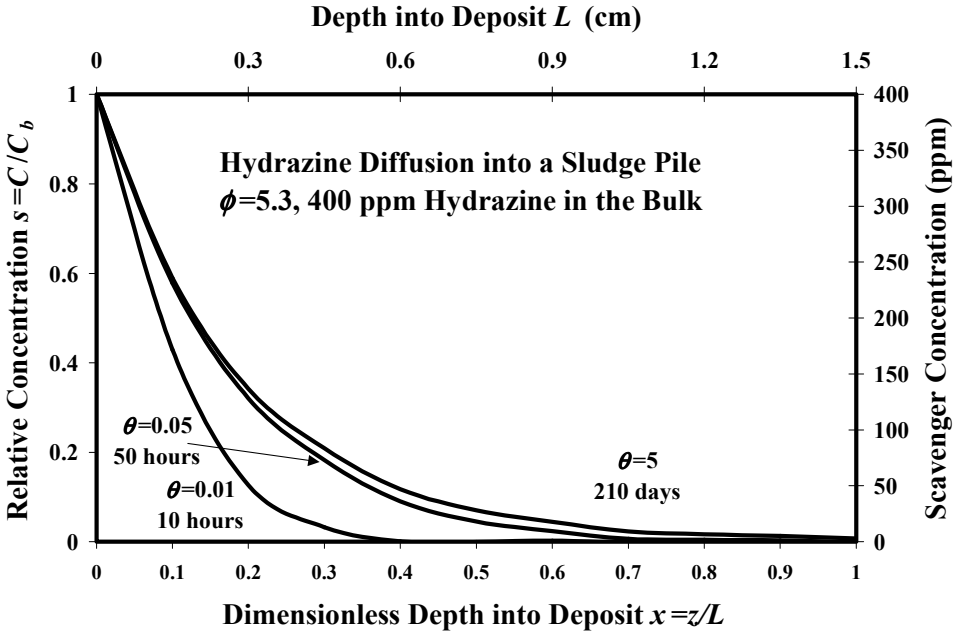

Figure 3-60
Hydrazine Diffusion into a Sludge Pile, Concentration as a Function of Position

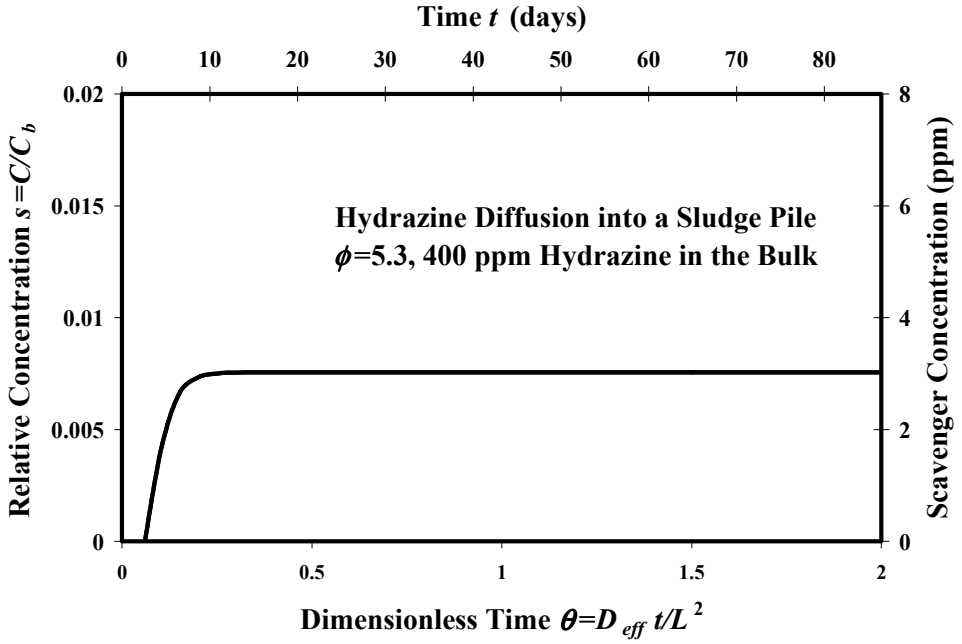

Figure 3-61
Hydrazine Concentration at the Bottom of a Sludge Pile as a Function of Time

Carbohydrazide in a Crevice

Figure 3-62 and Figure 3-63 show the calculated concentrations of carbohydrazide in a crevice based on Equation 3-14 and Table 3-6. The results are similar to those for hydrazine in a crevice, save that the concentrations are slightly higher in the crevice due to the longer half-life of carbohydrazide.

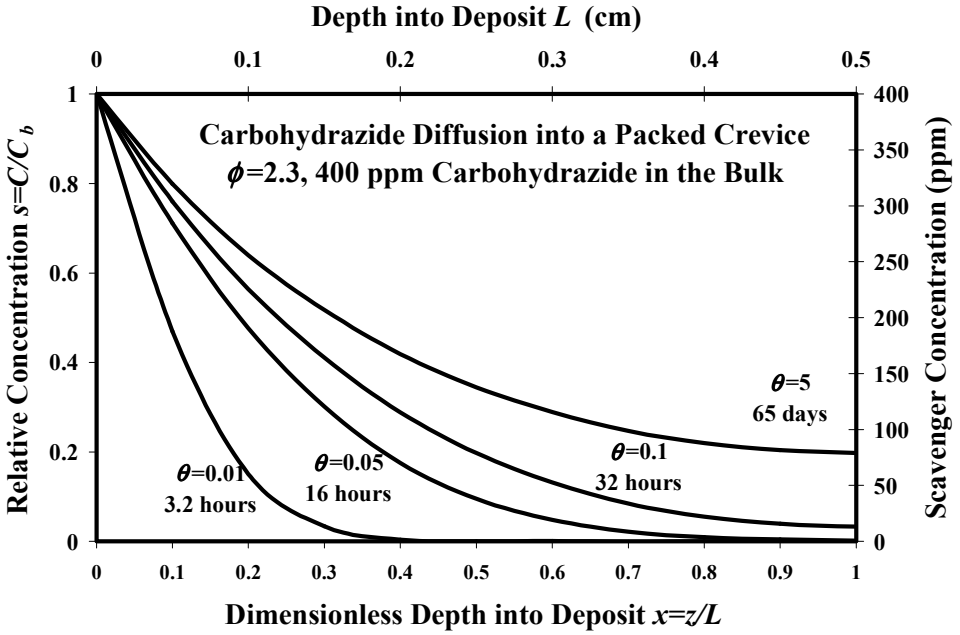

Figure 3-62
Carbohydrazide Diffusion into a Crevice, Concentration as a Function of Position

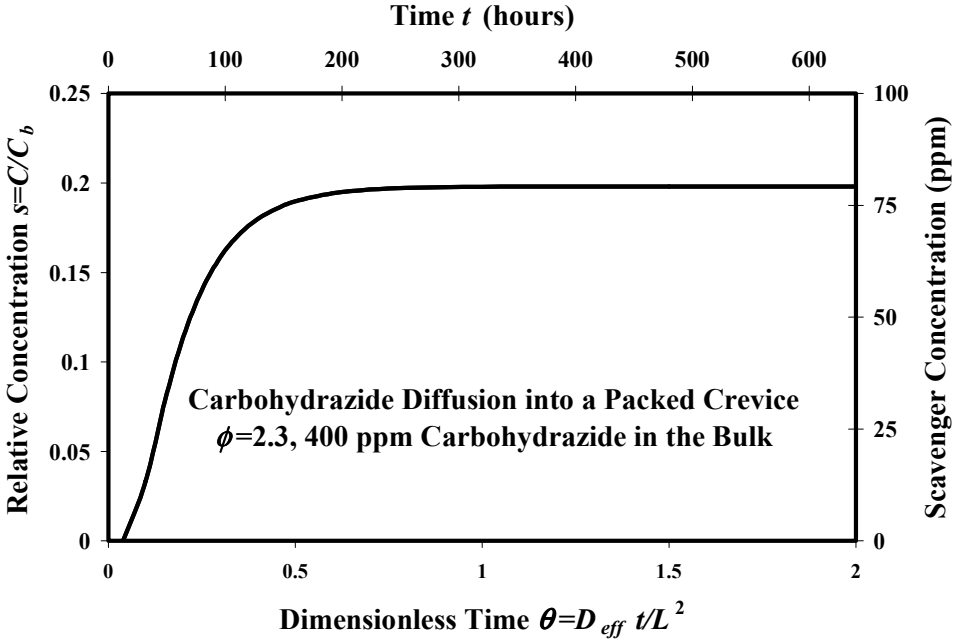

Figure 3-63
Carbohydrazide Concentration at the Bottom of a Crevice as a Function of Time

Carbohydrazide in a Sludge Pile

Figure 3-64 and Figure 3-65 show the results of a similar analysis for carbohydrazide diffusion into and decomposition in a sludge pile. Like the case for hydrazine, the concentration at the bottom of the pile is significantly less than the concentration in the bulk. The steady state concentration at the bottom of the sludge pile is about 1% of that in the bulk.

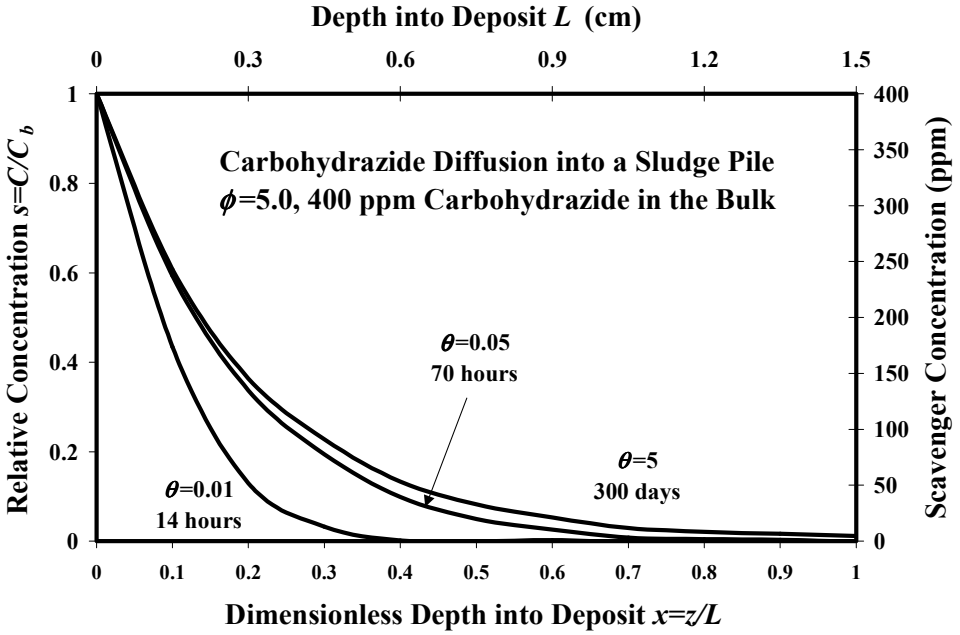

Figure 3-64
Carbohydrazide Diffusion into a Sludge Pile, Concentration as a Function of Position

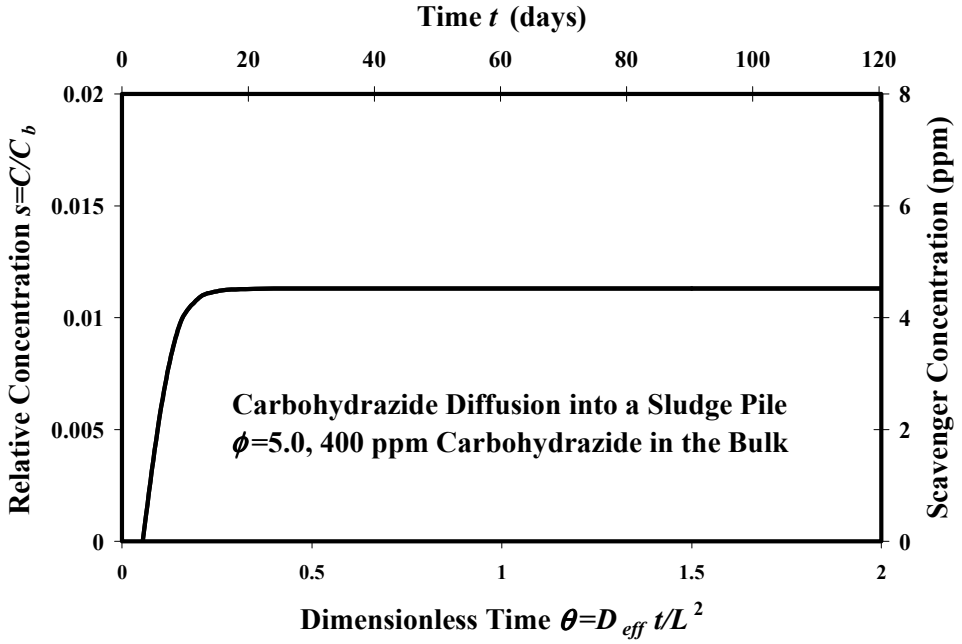

Figure 3-65
Carbohydrazide Concentration at the Bottom of a Sludge Pile as a Function of Time

Decomposition Modeling Conclusions

The following conclusions can be drawn from the analyses described above:

- mass transport limits the concentration of hydrazine or carbohydrazide in crevices and sludge piles
- in tube scale, by contrast, mass transport limits are small

The effects observed in the modeling could limit the reduction of oxidized species in the following two ways:

- elimination of the reduction reaction
- retardation of the reduction reaction

If the transport limits lower the concentration of scavenger deep in the deposits to zero for an extended period of time, no reduction will take place. For example, Figure 3-61 shows that the concentration of hydrazine at the bottom of a sludge pile is zero while the dimensionless time, θ, is less than about 0.06. This corresponds to a real time of about 2.6 days. If a plant were to fill the steam generator after a dry layup and begin startup in less than 2.6 days, no reduction whatsoever of oxides would be expected to occur.

If transport limits lower the concentration of scavenger deep in deposits to some concentration above zero, but less than the bulk concentration, reduction of oxides in crevices and the sludge pile would be expected to proceed at a rate proportional to the concentration of scavenger in the

deposit. Thus, for the case of hydrazine in a sludge pile (see Figure 3-61) where the hydrazine is expected to be at 3 ppm for a bulk concentration of 400 ppm, the rate of reduction of oxides would be expected to be two orders of magnitude slower than would be the case for boldly exposed oxides. In this scenario, an aggressive reduction campaign (such as Test 2, in Figure 3-35) which used 50 ppm of hydrazine during startup would actually only be as effective as a less aggressive campaign (such as Test 1 in Figure 3-35) which used only 0.5 ppm of hydrazine.

4
APPLICATION EXAMPLES

As discussed above in Section 1 (see page 1-7), a plant-specific evaluation of the status of reducible metal oxides (RMOs) should proceed through the following five steps:

- Review plant deposit characterization results.
- Summarize the shutdown, layup and startup protocols.
- Estimate the oxidation of deposit species during shutdown.
- Estimate the reduction of RMOs during startup.
- Estimate the amount of RMOs present at the start of operation.

The data presented in this report are meant to support the third and fourth steps, evaluating the oxidation and reduction of deposit species. In order to aid plant chemists in applying these data to their own practices, several application examples are evaluated in this section.

First, specific periods of the outage are examined. These include examples for estimating deposit species oxidation during the following three main types of environment:

- Atmospheric exposure
- Wet layup
- Sludge lancing

Second, a brief explanation is given on how the estimated oxidation thicknesses from each period during the outage are summed. Finally, two typical startup sequences are examined in order to estimate the extent to which RMOs might be reduced.

Specific Outage Periods

The purpose of collecting data on oxidation rates in several different environments (*e.g.*, atmospheric, high pH aqueous and deaerated aqueous) is to estimate the total degree of oxidation during the various periods during an outage. The recommended strategy for this estimation is to divide the outage into discrete periods, during each of which the environment on the secondary side of the steam generator is reasonably constant. Once this division is made, the extent of oxidation in each of the periods can be estimated. The extent of oxidation for the entire outage is then given by the sum of the extents for each period. Thus any outage can be viewed as the sum of a sequence of basic exposure types, primarily atmospheric, layup chemistry and sludge lancing chemistry. In order to illustrate this estimation technique, several sample periods have been evaluated. These evaluations are presented in the sections below.

Atmospheric Exposure

Case A-1

In Case A-1, the steam generator is exposed to air at 60°C (140°F) for 3 days. Under these conditions, the deposit species which oxidizes the most is copper. Equation 3-1 gives the oxide thickness, *x*, in nanometers as a function of time, *t*, in seconds. In order to evaluate this equation, the parameters *A* and *B* must be known. Their values are given in Equations 3-4 and 3-7, respectively. These equations require the use of the constants given in Equations 3-6 and 3-8. Since the temperature of interest is above the break-point temperature T_o=57.5°C (135.5°F), the *high T* values of the parameters are used. The following equations show the calculation of the parameters *A* and *B*:

$$A = A_{high\ T} e^{\frac{-E_{act\ A\ high\ T}}{RT}} = 1.45 \text{ x } 10^{16}\ nm\ \ e^{\frac{-1.06 \text{ x } 10^5 \frac{J}{mol}}{8.314 \frac{J}{molK} 333K}} = 0.34\ nm \tag{4-1}$$

$$B = B_{high\ T} e^{\frac{-E_{act\ B\ high\ T}}{RT}} = \frac{3.29 \text{ x } 10^{-19}}{s}\ \ e^{\frac{1.03 \text{ x } 10^5 \frac{J}{mol}}{8.314 \frac{J}{molK} 333K}} = \frac{0.0047}{s} \tag{4-2}$$

These values can then be used in Equation 3-1 to calculate the oxide thickness developed during this stage of the outage. The result is the following equation:

$$\begin{aligned} x = A \ln(Bt+1) &= 0.34\ nm\ \ \ln\left(0.0047\ 3\ days \frac{24\ hours}{day} \frac{3600\ s}{hour} + 1\right) \\ &= 0.34\ nm \ln(1218.24+1) = 2.4\ nm \end{aligned} \tag{4-3}$$

Thus for an atmospheric exposure of 3 days at 60°C (140°F) approximately 2.4 nm of oxide might be expected to form on copper particles in the deposits on the secondary side. It should be noted that the previous EPRI study [6] has shown that the matrix surrounding typical steam generator deposit copper inclusions (typically consisting of magnetite, Fe_3O_4) does not present a barrier to oxidation. Therefore, the predicted oxide thickness is valid for deposits in all locations within the steam generator.

Case A-2

In Case A-2, the steam generator is exposed to air for 14 days at a temperature of 30°C (86°F). Once again, the logarithmic law of Equation 3-1 is used. First the constants *A* and *B* are calculated as follows:

$$A = A_{low\,T} e^{\frac{-E_{act\,A\,low\,T}}{RT}} = 93.2\ nm\ \ e^{\frac{-1.63 \times 10^4 \frac{J}{mol}}{8.314 \frac{J}{molK} 303 K}} = 0.14\ nm \tag{4-4}$$

$$B = B_{low\,T} e^{\frac{-E_{act\,B\,low\,T}}{RT}} = \frac{1.57 \times 10^{-5}}{s}\ \ e^{\frac{1.60 \times 10^4 \frac{J}{mol}}{8.314 \frac{J}{molK} 303 K}} = \frac{0.0090}{s} \tag{4-5}$$

Note that 30°C (86°F) is below the break-point temperature of 57.5°C (135.5°F). Therefore, the *low T* values, given in Equations 3-6 and 3-8, are used.

Using these values in the logarithmic law (Equation 3-1) yields the following:

$$\begin{aligned} x &= A \ln(Bt+1) = 0.14\ nm\ \ \ln\left(0.0090\,12\ days \frac{24\ hours}{day} \frac{3600\ s}{hour} + 1\right) \\ &= 0.14\ nm \ln(9331.2+1) = 1.3\ nm \end{aligned} \tag{4-6}$$

Comparison of Case A-1 and Case A-2

A comparison of Cases A-1 and A-2 shows that of the two parameters differing between the cases (duration and temperature), the temperature is by far the most important. Even though the deposits in Case A-2 were exposed for 4 times as long as those for Case A-1, they were only oxidized half as much. Mathematically, this is evident from the logarithmic law (Equations 3-1, 4-3 and 4-6). In this expression, the oxide thickness, *x*, is only logarithmically dependent on the time, whereas it is linearly dependent on the constant *A*, which is in turn exponentially dependent on the temperature. Physically, the dependence on time is weak because a semi-protective oxide layer develops quickly, leading to slow oxidation at long times, whereas increasing the temperature makes the oxide layer more permeable, allowing more oxidation.

These results lead to the conclusion that during periods of atmospheric exposure, maintaining a low temperature is more important to limiting oxidation of deposits than keeping the exposure short in duration.

Wet Layup

Case W-1

In Case W-1, a steam generator is placed in wet layup for ten days under the following conditions:

- Dissolved oxygen = 10 ppb
- Temperature = 50°C (122°F)

- pH = 9.0, with hydrazine

The first step in evaluating this case is to estimate the oxidation rate. Figure 3-2 shows the oxidation rate of copper in a low oxygen solution with pH=9 at various temperatures. The oxidation rate for 50°C (122°F) can be read from this graph as approximately 0.6 nm/day. However, the values given in Figure 3-2 are for oxygen concentrations at 200 ppb. As discussed on page 3-4, the oxidation rate is expected to decrease linearly with the oxygen concentration. Therefore, the oxidation rate at 10 ppb must be calculated. The following equation demonstrates this calculation:

$$\begin{aligned} Actual\ Oxidation\ Rate &= \frac{Actual\ DO}{200\ ppb} Oxidation\ Rate\ at\ 200\ ppb\ DO \\ &= \frac{10\ ppb}{200\ ppb} 0.6 \frac{nm}{day} = 0.03 \frac{nm}{day} \end{aligned} \tag{4-7}$$

From the oxidation rate and the layup duration, the total oxidation is calculated as follows:

$$x = Oxidation\ Rate \cdot Layup\ Duration = 0.03 \frac{nm}{day} 10\ days = 0.3\ nm \tag{4-8}$$

Case W-2

In Case W-2, a steam generator is placed in wet layup for seven days under the following conditions:

- Dissolved oxygen = 100 ppb
- Temperature = 40°C (104°F)
- pH = 10, with ethanolamine

Again, the first step is to consult Figure 3-2. At 40°C (104°F) Figure 3-2 indicates that deposits in a low oxygen solution will oxidize at a rate of approximately 0.4 nm/day. However, two corrections must be made to this estimate, a pH correction (Figure 3-2 gives data for pH=9, the actual solution is pH=10) and a dissolved oxygen concentration (Figure 3-2 is for DO=200 ppb, the actual solution is 100 ppb).

In order to correct for pH, Figure 3-4 must be consulted. For ethanolamine, the oxidation rate is slightly higher at pH=10 than it is at pH=8.5. Figure 3-4 indicates that the oxidation rate increases approximately 15% when the pH is raised from 9 to 10 with ethanolamine. An overestimation of the oxidation rate would be considered conservative, so a 20% increase will be assumed here. Thus the estimated oxidation rate (without the oxygen concentration correction) is given by the following calculation:

$$\begin{aligned} Oxidation\ Rate_{corrected\ for\ pH} &= (1+20\%)Oxidation\ Rate_{pH=9} \\ &= 1.2 \cdot 0.4 \frac{nm}{day} = 0.5 \frac{nm}{day} \end{aligned} \tag{4-9}$$

In order to correct for oxygen concentration, Equation 4-7 is again used:

$$\begin{aligned} Actual\ Oxidation\ Rate &= \frac{Actual\ DO}{200\ ppb} Oxidation\ Rate\ at\ 200\ ppb\ DO \\ &= \frac{100\ ppb}{200\ ppb} 0.5 \frac{nm}{day} = 0.25 \frac{nm}{day} \end{aligned} \tag{4-10}$$

Finally, the total oxidation is estimated using the rate and the duration as follows:

$$x = Oxidation\ Rate \cdot Layup\ Duration = 0.25 \frac{nm}{day} 7\ days = 1.8\ nm \tag{4-11}$$

Case W-3

In case W-3, a steam generator is placed in wet layup for five days under the following conditions:

- Dissolved oxygen = aerated
- Temperature = 30°C (86°F)
- pH = 10, with morpholine

The first step is to utilize Figure 3-2. For an aerated solution (oxygen saturated) at pH=10 at 30°C (86°F), the oxidation rate is given as 0.1 nm/day. Since this pH and oxygen concentration are given directly in the figure, no additional corrections are needed.

The total oxidation during this period is given by the following calculation:

$$x = Oxidation\ Rate \cdot Layup\ Duration = 0.1 \frac{nm}{day} 5\ days = 0.5\ nm \tag{4-12}$$

Comparison of Cases W-1, W-2 and W-3

As indicated by the above analysis, the oxidation rate under wet layup is a function of the pH, temperature and oxygen concentration. However, the dependence on these parameters is fairly simple and a rate is easily calculated using the experimental data presented above in Section 3. It

is important to note that in general, all dependencies are linear, including the total oxidation as a function of time (unlike the case for atmospheric exposure). Therefore, lowering the temperature, raising the pH, lowering the oxygen or shortening the layup period can all have a significant impact on the total oxide formed during layup.

Sludge Lancing

Case S-1

In Case S-1, a steam generator is sludge lanced for 24 hours with water at the following conditions:

- Dissolved oxygen = aerated
- Temperature = 30°C (86°F)
- pH = 7

Figure 3-2 gives the oxidation rate at these conditions as 0.9 nm/day. These conditions are directly indicated in the figure, so no further corrections are required and the total oxidation can be calculated as follows:

$$x = Oxidation\ Rate \cdot Layup\ Duration = 0.9 \frac{nm}{day} 1\ day = 0.9\ nm \tag{4-13}$$

Summing the Outage Periods

In order to estimate the total oxidation that takes place during an outage, the oxidation during the various periods are estimated and summed. In theory, this is a simple process but in practice, it may be complicated by different sections of the steam generator experiencing different environments. For example, during top-of-tubesheet sludge lancing, deposits in the bottom of the steam generator may be exposed to aerated neutral water while the upper bundle is exposed to warm air.

Two strategies exist for dealing with periods when the portions of steam generator are simultaneously exposed to different environments. These are as follows:

- Separate calculations for different regions
- Conservative choices

The first option, separate calculations for different regions, involves dividing the steam generator into a small number of separate regions for the purposes of the oxide calculation. The procedure for each region would be the same using the different environmental conditions as inputs. The calculations would be performed as descried above, but would be redone separately for each region.

The second option is to make only one calculation, but for each period to assume that all the deposits are oxidized to the same extent as those subjected to the most oxidizing environment. For example, if a top-of-tubesheet sludge lancing is performed, tubesheet deposits are likely to be exposed to a more oxidizing environment (neutral pH, aerated water) than the upper bundle (air). Therefore, a conservative assumption is made that all of the deposits (including upper bundle deposits) were oxidized to the same extent that the tubesheet deposits were oxidized. This results in a single estimate that is high for many regions of the steam generator but never low.

Startup Sequences

Once an assessment of the extent of deposit oxidation during an outage has been made, a similar assessment regarding the extent of oxide reducible by the startup procedure should take place. This assessment should be based on a comparison of a plant-specific startup protocol to one of the autoclave tests described above in Section 3 (see page 3-33). To demonstrate how this may be accomplished, two cases are examined below using two of the startup data sets collected in an informal survey of plant practices (see Appendix C).

It should be noted that, unlike the case for oxidation, the reduction of reducible metal oxides (RMOs) can be significantly retarded by the deposit matrix. As discussed above in Section 3 (see page 3-40) RMOs deep in crevices or sludge piles can be exposed to significantly lower concentrations of oxygen scavengers due to decomposition of the scavenger. Therefore, in the cases analyzed below, two separate evaluations are made, one for exposed deposits (such as free span scale) and one for occluded deposits (such as deposits in crevices or at the bottom of top-of-tubesheet sludge piles).

Case R-1

The temperature and hydrazine profiles during the startup sequence considered in Case R-1 are shown in Figure 4-1 and Figure 4-2. By inspection of Figure 4-1 it can be seen that the temperature profile is quite similar to Autoclave Test 1. Inspection of Figure 4-2 shows that the bulk hydrazine concentration at Plant A was on the same order of magnitude as that used in Autoclave Test 1. Early in the startup, when temperatures were low, the hydrazine concentration was somewhat lower than in Autoclave Test 2. Later in the startup, the hydrazine concentrations were slightly higher. In general, the startup sequence at Plant A was comparable to the startup sequence used in Autoclave Test 2 and the extent of reduction of RMOs in boldly exposed deposits is expected to have been roughly equivalent, *i.e.*, about 16 nm (see Figure 3-35).

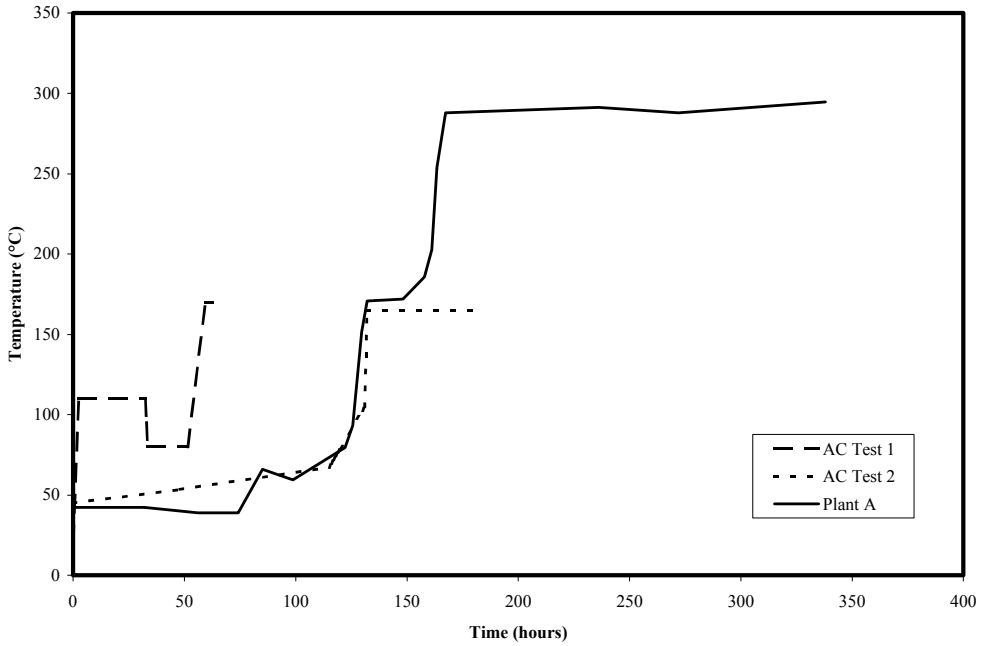

Figure 4-1
Temperature During Startup at Plant A Compared to Autoclave Tests 1 and 2

Because oxygen scavengers decompose as they diffuse into deposits, RMOs located deep in deposits are not subjected to the same environment as boldly exposed deposits. Therefore, a separate analysis is required to assess the extent of RMO reduction deep in deposits. For Plant A, the case of deposits under a top-of-tubesheet sludge pile is considered. As shown above in Figure 3-61, the concentration at the bottom of a typical sludge pile (1.5 cm thick with a porosity of 10%) is 0.0075 times the bulk concentration. (Details about calculated reduction factors for specific deposits are given in Section 3, starting on page 3-62, or in Appendix A.) Figure 4-2 shows the levels of hydrazine predicted for the bottom of the sludge pile. These levels are significantly lower than those in Autoclave Test 1 (0.5 ppm). However, the duration of exposure during the startup at Plant A is significantly longer than the exposure during Autoclave Test 1. Assuming a linear rate of reduction and a linear dependence on the hydrazine concentration (both assumptions stemming from the first order kinetics of the reduction reaction), the RMO reduction at the bottom of the sludge pile in the startup at Plant A would be expected to be about half of the reduction in Autoclave Test 1. Since Autoclave Test 1 reduced about 8 nm of oxide, the Plant A startup would reduce approximately 4 nm of oxide under the sludge pile.

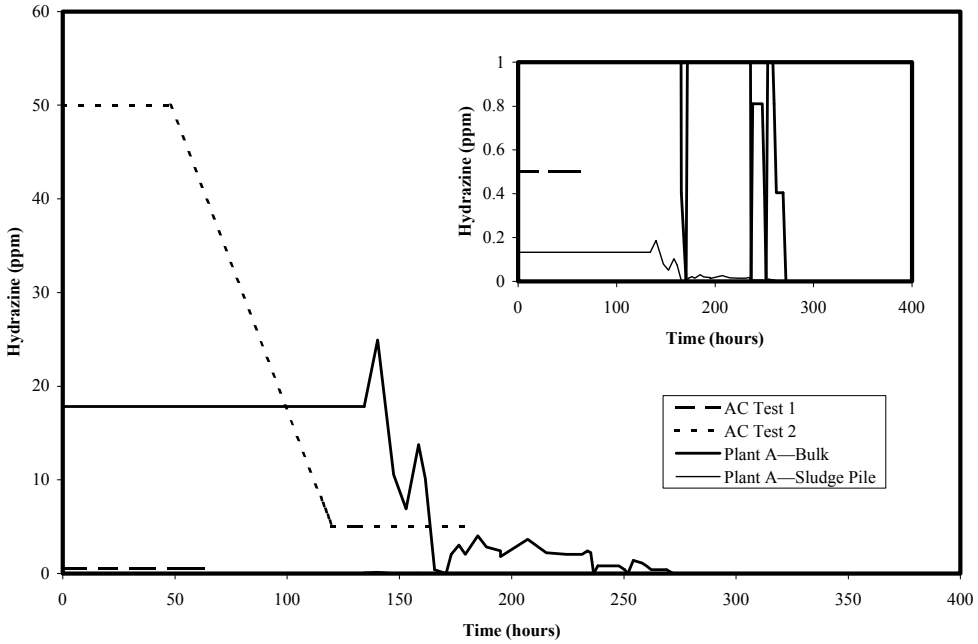

Figure 4-2
Hydrazine Concentrations During Startup at Plant A Compared to Autoclave Tests 1 and 2

Case R-2

The temperature and hydrazine concentration profiles for a recent startup at Plant C are given in Figure 4-3 and Figure 4-4, respectively, along with comparable data from Autoclave Tests 1 and 2. Inspection of Figure 4-3 shows that the temperature during startup at Plant C was roughly comparable to that during Autoclave Test 1. Likewise, inspection of Figure 4-4 indicates that the hydrazine concentration at Plant C was comparable to that during Autoclave Test 1. The longer duration and higher concentration at Plant C would lead to more RMO reduction at Plant C than during Autoclave Test 1, which reduced 8 nm of copper oxide (see Figure 3-35).

In occluded deposits, hydrazine concentrations will be reduced due to decomposition. In a typical crevice (0.5 cm deep with a porosity of 10%), the hydrazine concentration will be approximately 0.16 times the bulk concentration (see Figure 3-59). (Details about calculated reduction factors for specific deposits are given in Section 3, starting on page 3-62, or in Appendix A.) Figure 4-4 shows the concentrations of hydrazine calculated to be present at the bottom of a crevice during the startup of Plant C. The hydrazine concentrations are approximately one fifth of those used during Autoclave Test 1. Therefore, given that Test 1 lasted approximately as long as the startup at Plant C, the RMO reduction deep in a crevice at Plant C is expected to have been on the order of 1.6 nm (one fifth of the 8 nm observed in Autoclave Test 1).

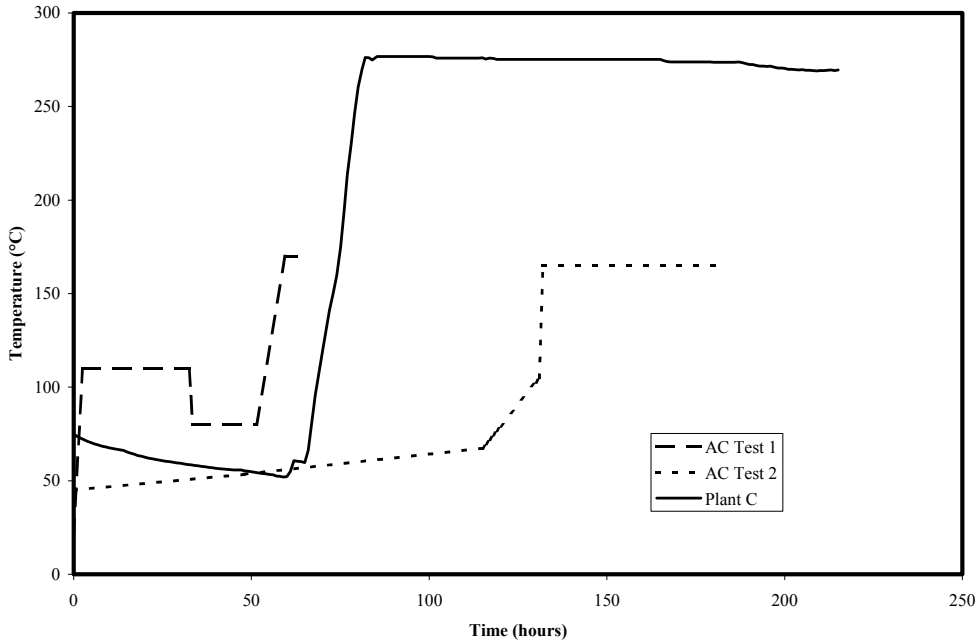

Figure 4-3
Temperature During Startup at Plant C Compared to Autoclave Tests 1 and 2

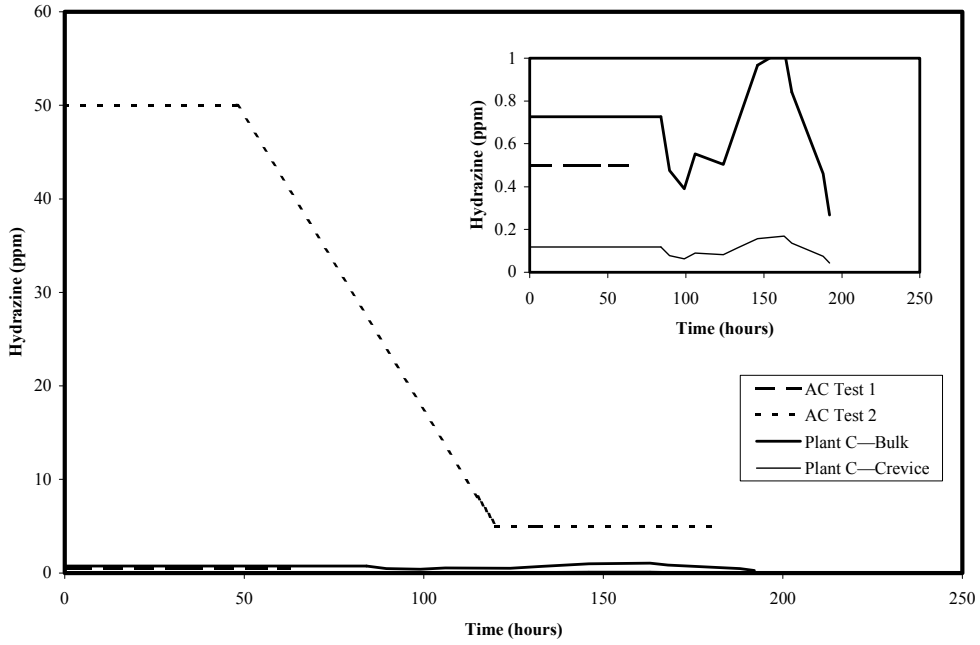

Figure 4-4
Hydrazine Concentrations During Startup at Plant C Compared to Autoclave Tests 1 and 2

Summary

In the sections above, examples of the application of the data presented in Section 3 are given. Assessing the total impact of an outage on RMOs on the secondary side of the steam generator goes through four steps:

- Assessment of RMOs formed during outage periods
- Summation of RMO formation during the outage
- Assessment of RMO reduction during startup
- Comparison of RMO formation with RMO reduction

Assessing the impact of any remaining RMOs or optimization of an outage schedule requires integration of additional data including maintenance requirements, steam generator replacement schedule and deposit characterization.

5
RECOMMENDATIONS FOR FURTHER STUDY

The results of this study can be used by plant personnel to predict the degree of oxidation of secondary side deposits during shutdown and layup and the extent to which the consequent reducible metal oxides are reduced during startup. However, this knowledge is not completely sufficient for the evaluation of the oxidation and reduction impact of shutdown, layup and startup practices.

In order to evaluate the effect of reducible metal oxides on long-term steam generator tube integrity, three pieces of data are required:

- The extent of oxidation present during operation
- The influence of the oxides on the electrochemical potential
- The influence of the electrochemical potential on tube degradation

From the data presented in this report the extent of oxidation during shutdown and layup and after startup can be assessed. Numerous other researchers have addressed the influence of the potential on tube degradation. However, there is very little data in the literature regarding the influence of the extent of oxidation on the potential. The most extensive study is Reference 2, which examines the effect of the bulk concentration of synthetic oxides on the electrochemical potential.

The studies performed in Reference 2 and in most other published investigations address only the bulk concentration of synthetic oxides. However, the factor that is most likely to influence the electrochemical potential is the surface area of the oxide film, regardless of whether it is formed on synthetic oxides or is grown on metal particles. Although it has not been demonstrated experimentally, it is unlikely that the core of a solid particle will significantly influence the chemistry of the surrounding solution.

Because most experimental work cited in the literature has investigated the effect of the addition of synthetic oxide particles, the possible mitigating effect of other compounds (perhaps magnetite, Fe_3O_4) has not been adequately investigated. In steam generator deposits copper particles are generally surrounded by a magnetite matrix. Although previous investigations [6] have shown that this matrix is unlikely to affect the interaction of dissolved oxygen with copper in deposits, the effect of the matrix on the electrochemical influence of copper oxides has not been determined. As shown in Figure 2-1, the Fe/Fe_3O_4 couple has a potential that is well below the potential of the Cu/Cu_2O, Cu/CuO and Fe_3O_4/Fe_2O_3 couples. It is possible that the presence of magnetite in intimate contact with copper oxide may suppress the deleterious effects of the copper oxide.

In addition to the uncertainties regarding the effects of surface area and other surrounding oxides, there is uncertainty about the distance through which reducible metal oxides can exert their deleterious effects. In part this may be related to the interaction of these compounds with magnetite. Copper particles in typical steam generator tube scale exists primarily as segregated inclusions, close to, but generally not actually touching, the steam generator tubes. The distance through which such inclusions can influence the electrochemical potential at the tube surface has not been determined.

Any new research in this field should attempt to answer the following questions:

- What is the proper measure of oxide concentration with respect to tube degradation? Is it oxide thickness, oxide mass per liquid volume, oxide area per tube area, some other measurement or a combination of several measurements?
- How does the electrochemical potential depend on the oxide concentration (measured properly)?
- What is the correct length scale over which to evaluate the effect of reducible metal oxides?
- How does the intimate contact of potential raising and potential lowering oxides affect the local electrochemical potential experienced by steam generator tubes?

Additionally, the transport of RMOs from the balance of plant during early power operation was not within the scope of the work performed in preparing this report. Based on the work done in this report, it appears that oxides developed in place in steam generators can be adequately reduced by the use of low oxygen levels and high levels of oxygen scavengers during startup. However, it is known that the levels of RMOs brought into the steam generator during early power operation (power ascension) are high relative to transport during steady-state full power operation. Reducing these RMOs before they concentrate in crevice areas (*e.g.*, by the use of high levels of hydrazine) may be of even more importance than reducing the RMOs developed in place in the steam generators. Therefore, experiments and modeling of formation, transport and reduction of these RMOs should be the subject of further work.

6
REFERENCES

1. Outokumpu HSC Chemistry for Windows Version 3.0, Outokumpu Research Oy, Poir, Finland, 1997.

2. R.J. Jacko, Corrosion Evaluation of Thermally Treated Alloy 600 Tubing in Primary and Faulted Secondary Water Environments, EPRI NP-6721-SD, June 1990.

3. W.H. Cullen and M.J. Partridge, *Susceptibility of Alloys 600 and 690 to Acidified Sulfate and Chloride Environments*, EPRI TR-104045, June 1994.

4. A. Kishida, H. Takamatsu, H. Kitamura, S. Isobe, K. Onimura, K. Arioka, T. Hattori, T. Arai and M. Sato, "The Cause and Remedial Measures of Steam Generator Tube Intergranular Attack in Japanese PWR," *3rd Int. Symposium on Environmental Degradation of Materials in Nuclear Power Systems—Water Reactors*, Traverse City, September 1987.

5. *Source Book on Limiting Exposure to Startup Oxidants*, EPRI, Palo Alto, CA:1999. TR-112967.

6. *The Oxidation and Reduction of Copper in Steam Generator Deposits: Under Startup, Layup and Startup Conditions*, EPRI, Palo Alto, CA: 2000. 1001204

7. Eriksen, T.E., P. Ndalamba and I. Grenthe, "Short Communication on the Corrosion of Copper in Pure Water," Corrosion Science, 29:10, 1241, 1989.

8. *Proceedings: 1999 EPRI Workshop on Startup Oxidant Control: Chattanooga, Tennessee, Januaary 19-20, 1999*, EPRI, Palo Alto, CA: 1999. TR-112815.

9. *PWR Secondary Water Chemistry Guidelines—Revision 5*, EPRI, Palo Alto, CA: 2000. TR-102134-R5.

10. J. Schubert and W. Zerlick, "Ways to Avoid Plugging and Leaks in Water-Cooled Generator Stator Windings," EPRI Conference on Maintaining the Integrity of Water Cooled Stator Windings, Atlanta, Georgia, June 5-6, 1995. TR-105504.

11. *Recommendations for Hydrazine and Carbohydrazide Levels during Layup as a Function of pH*, Draft Report for the EPRI Secondary Water Guidelines Committee, Dominion Engineering, Inc., February 2000.

12. Pourbaix, M., *Atlas of Electrochemical Equilibria in Aqueous Solutions*, NACE, Houston, TX, 1974.

13. *ASTM Method D1385, Standard Test Method for Hydrazine in Water*

14. M.Blanco, J. Coello, H. Iturriaga, S. Maspoch and E.Rovira Talanta, 1992, 39(10), p1313-1316.

15. Millet, P.J. and J.M. Fenton, "Measurement of Effective Diffusion Coefficients for Chloride Salts in Nonprotective Magnetite," *Corrosion*, **46:9**, 710, 1990.

16. Froment, G.F. and K.B. Bischoff, *Chemical Reactor Design and Analysis*, John Wiley and Sons, New York, 1990

A
APPENDIX A: MODELING OXYGEN SCAVENGER DECOMPOSITION IN STEAM GENERATOR DEPOSITS

Purpose

During layup and operation of PWR steam generators, oxygen scavengers such as hydrazine or carbohydrazide are added to the secondary side fluid in order to reduce the level of dissolved oxygen and retard corrosion of the steam generator construction materials. An auxiliary function of the oxygen scavengers is to keep secondary side deposits in a highly reduced state. When deposits become oxidized from copper to copper oxide or from magnetite to hematite, they may raise the corrosion potential of the underlying construction material.

Steam generator deposits generally contain copper inclusions, even in nominally copper free plants, due to the presence of copper as a tramp element. Copper is known to catalyze the decomposition of hydrazine and carbohydrazide. Therefore, it is possible that in deep crevices, the scavenger, though present in the bulk secondary water, may decompose before it can diffuse through the deposit layer. This calculation provides the means to determine the concentration profile of hydrazine along the diffusion path into a deposit layer.

Because there are several different situations to which this calculation may be applied (diffusion through tube scale, diffusion into a crevice, layup and full-power operating conditions, *etc*.) the calculation is made symbolically. Choices for the various parameters may be substituted at will into the derived equations.

Summary of Results

Two equations were derived. The first gives the steady state concentration of oxygen scavenger anywhere in a porous deposit as a function of the position and the Thiele Modulus (a measure of the relative importance of diffusion and reaction kinetics). The second equation gives the transient concentration anywhere in a porous deposit as a function of position, elapsed time and the Thiele Modulus.

Project Input Requirements

The equations are derived symbolically to allow their use in several situations. For a given analysis the following parameters would be required:

D_{bulk} the diffusivity of hydrazine (or carbohydrazide) in water

ε the void fraction of the deposit

τ the tortuosity of the deposit

C_b the bulk concentration of oxygen scavenger

L the thickness of the scale or depth of crevice

k_d the scavenger decomposition rate constant

References

A.1. H.B. Dwight, Tables of Integrals and Other Mathematical Data, MacMillan Publishing Co., Inc., New York, 1957.

A.2. G.E. Meyers, Analytical Methods in Conduction Heat Transfer, Genium Publishing Corporation, Schenectady, 1987.

Assumptions

Several assumptions are made in modeling the simultaneous decay and diffusion of oxygen scavengers into tube scale. The details of the assumptions and their justifications are listed below.

Single Dimensional Diffusion

It is assumed that the diffusion of oxygen scavenger into the scale is one-dimensional. That is, the concentration of oxygen scavenger varies only in the direction normal (perpendicular) to the scale surface. Strictly speaking, this is known to be false. For example, at a corner such as the edge of a support plate, oxygen scavenger will diffuse into the scale from both sides of the corner. Likewise, transport is not strictly one dimensional through scale on rounded surfaces, like tubes. However, if the thickness of the scale is small compared to the curvature of the surface, it can be closely approximated by a flat surface.

Porous Scale Network

Tube scale and other deposits have a porous nature. It is assumed that these structures can be modeled as porous media. This means that rather than trying to predict the transport of oxygen scavenger down a long and twisted path, the diffusion is modeled using tortuosity (τ) and void fraction (ε) parameters. The effective diffusivity in the direction of average diffusion (*i.e.* normal to the scale/bulk interface, rather than along a single pore) is given by:

$$D_{eff} = D_{bulk} \frac{\varepsilon}{\tau} \qquad \text{(A-1)}$$

The values of the tortuosity and void fraction are expected to change depending on the type of deposit under investigation and are therefore left as input parameters for specific applications of this calculation.

First Order Reaction Rate

The decomposition of oxygen scavengers is catalyzed by the presence of copper. It is likely that this is a surface reaction. However, it is assumed here that within the scale, the decomposition of oxygen scavenger can be modeled as a first order reaction with respect to the concentration of the oxygen scavenger. The reaction rate is thus characterized by a pseudo-first order reaction rate constant (k_d). Experimental evidence has shown that this is an appropriate way to model the decomposition of oxygen scavengers.

Bulk Uniformity

Although it is likely that, if considerable oxygen scavenger is being degraded within the scale, that there will be a scavenger depleted layer just outside the scale, it is assumed that the concentration of scavenger immediately outside the scale is the same as in the bulk of the secondary side fluid. The degree to which the secondary side bulk mass exceeds that of the fluid in the pores of the deposits is considerable. Therefore, it is unlikely that there will be a significant depletion of the bulk fluid scavenger by decomposition in the pores. This assumption will tend to slightly overestimate both the concentration of scavenger in the pores and the overall rate at which scavenger is consumed by the decomposition reaction.

Pore Bottom

At the pore bottom, the furthest point from the bulk fluid interface, the consumption of scavenger is assumed to be zero. Although, if the bottom of the pore is physically similar to its walls, there will be some decomposition of oxygen scavenger there, the area at the pore's end is small compared to the area of its walls. Therefore, the decomposition of scavenger that takes place on the pore end is very small compared to that which is degraded on the walls. The consumption at the end is therefore negligible. Given the impermeability of the pore's end, there will therefore be no significant consumption of scavenger at the end of the pore. Over a wide range of temperatures, the decomposition reaction is much faster than the reduction of oxides. Therefore, scavenger consumption by metal oxides has been neglected.

Constant Physical Properties

The concentrations of scavenger in the pore and in the bulk are assumed to be small enough that they do not significantly affect the properties of the secondary side fluid. Thus the diffusivity and the reaction rate constant are assumed to be independent of the scavenger concentration. Considering the small quantities of scavenger even in the bulk (less that 0.05%) this assumption is valid given that the oxygen scavengers do not significantly alter the physical properties of water even when present in greater quantities.

Analysis

The analysis consists of four parts:

- Derivation of the governing differential equation
- Derivation of the steady-state solution
- Derivation of the transient solution
- Validation of the transient solution

These four parts are given in the sections below.

Differential Equation

Under the assumptions given above, transport of oxygen scavenger through steam generator deposits is described by a partial differential equation for the concentration of oxygen scavenger (C):

$$D_{eff}\frac{\partial^2 C}{\partial z^2} - k_d C = \frac{\partial C}{\partial t} \tag{A-2}$$

where z is the distance into the scale, t is the elapsed time (beginning when the oxygen scavenger concentration is first raised to layup levels), and, as defined above, C is the time and position dependent concentration of oxygen scavenger, k_d is the decomposition reaction rate constant and D_{eff} is the effective diffusivity.

The boundary conditions on the differential equation are given by the assumptions discussed above. By the assumption of bulk uniformity the boundary condition at z=0 (the scale/bulk interface) is given by:

$$C(0,t) = C_b \tag{A-3}$$

where C_b is the uniform bulk concentration of oxygen scavenger. At the bottom of the pore (z=L), the boundary condition is given by the assumption that there is no consumption of oxygen scavenger at the pore bottom. Mathematically, this is given by:

$$\left.\frac{\partial C}{\partial z}\right|_{z=L} = 0 \qquad \text{for all } t \tag{A-4}$$

where L is the length from the scale-bulk interface to the pore bottom. The length L is equivalent to the thickness of the scale or the depth of the crevice.

To completely determine the concentration of oxygen scavenger, the only additional information required is an initial condition. Since the change over from operating chemistry to layup chemistry involves a significant increase in the concentration of oxygen scavenger, the initial condition is assumed to be a bulk concentration of oxygen scavenger at layup levels (C_b) and a pore concentration of oxygen scavenger at zero. The initial condition is then given by:

$$C(z > 0,0) = 0 \tag{A-5}$$

The differential equation, boundary conditions and initial condition completely define the oxygen scavenger concentration anywhere in the pore at any time. This particular equation is easily solved using a modified separation of variables technique. The equilibrium concentration can also be easily calculated.

Equilibrium Concentrations

At equilibrium, the concentration of oxygen scavenger does not change with time. The partial differential equation given in Equation A-2 then simplifies to an ordinary differential equation:

$$D_{eff}\frac{d^2C}{dz^2} - k_d C = 0 \tag{A-6}$$

In order to simplify the solution of the differential equation, it is convenient to substitute non-dimensional variables into the equation. The following definitions are made:

$$s \equiv \frac{C}{C_b} \qquad x \equiv \frac{z}{L} \qquad \phi \equiv L\sqrt{\frac{k_d}{D_{eff}}} \tag{A-7}$$

The parameter s is a dimensionless concentration. The parameter x is a dimensionless length. The parameter ϕ is the Thiele Modulus or the ratio of the decomposition rate to the diffusion rate. For large values of ϕ, decomposition is fast relative to diffusion making diffusion the rate-limiting step. For small values of ϕ, the decomposition reaction is the rate-limiting step.

If the non-dimensional definitions are substituted into the differential equation, it is reduced to:

$$\frac{d^2s}{dx^2} - \phi^2 s = 0 \tag{A-8}$$

with the boundary conditions:

$$s(x = 0) = 1 \tag{A-9}$$

indicating that at the scale-bulk interface the oxygen scavenger concentration is equal to the bulk concentration, and:

$$\left.\frac{ds}{dx}\right|_{x=1} = 0 \tag{A-10}$$

indicating that at the pore bottom, there is no consumption of oxygen scavenger.

The differential equation is satisfied by the general solution:

$$s = a\cosh(\phi\, x) + b\sinh(\phi\, x) \tag{A-11}$$

where *a* and *b* are unknown constants. The unknown constants must be determined by substituting the values given by the boundary conditions into the general solution. At the scale-bulk interface, substituting the boundary condition into the general solution yields:

$$s = 1 = a\cosh(\phi\, 0) + b\sinh(\phi\, 0) = a\cdot 1 + b\cdot 0 = a \tag{A-12}$$

At the pore bottom, the boundary condition is given as a differential. Therefore the general solution must be differentiated. This yields:

$$\frac{ds}{dx} = a\phi\sinh(\phi\, x) + b\phi\cosh(\phi\, x) \tag{A-13}$$

Substituting the boundary condition at the pore bottom into the derivative of the general solution gives:

$$\left.\frac{ds}{dx}\right|_{x=1} = 0 = a\phi\sinh(\phi\, 1) + b\phi\cosh(\phi\, 1) = a\phi\sinh(\phi) + b\phi\cosh(\phi) \tag{A-14}$$

This equation can be rearranged to determine *b*. Substituting in the fact that *a*=1 (Equation A-12), yields:

$$b = \frac{-\sinh(\phi)}{\cosh(\phi)} \tag{A-15}$$

The derived values of *a* and *b* can now be substituted into the general solution of the differential equation to give the value of the non-dimensional concentration, *s*, at all positions:

$$s = \cosh(\phi\, x) - \frac{\sinh(\phi)}{\cosh(\phi)}\sinh(\phi\, x) \tag{A-16}$$

In this form, the equilibrium concentration of the oxygen scavenger can be expressed as a function of position and the Thiele Modulus, ϕ.

Transient Analysis

The solution of the differential equation given in Equation A-2 takes several steps. First the equation and boundary conditions are non-dimensionalized to simplify the solution. Next, a general solution is assumed using undetermined functions of time. The undetermined functions must then be solved for using the initial condition. Additionally, several integral identities will be needed at various stages of the solution. The solution will be broken into the following steps:

- Non-Dimensionalization and General Solution
- Integral Identities
- Solution of Undetermined Functions
- Construction of the Particular Solution

Non-Dimensionalization and General Solution

The transient analysis is completed by solving the partial differential equation given in Equation A-2.

Returning to the original partial differential equation,

$$D_{eff}\frac{\partial^2 C}{\partial z^2} - k_d C = \frac{\partial C}{\partial t} \tag{A-17}$$

allows the calculation of the time dependent concentration. The solution is simplified by making the following substitutions:

$$y \equiv 1 - \frac{C}{C_b} \qquad x \equiv \frac{z}{L} \qquad \phi \equiv L\sqrt{\frac{k_d}{D_{eff}}} \qquad \theta = \frac{D_{eff}}{L^2}t \tag{A-18}$$

Making these substitutions, the partial differential equation becomes:

$$\frac{\partial^2 y}{\partial x^2} + \phi^2(1-y) = \frac{\partial y}{\partial \theta} \tag{A-19}$$

while the boundary conditions become:

$$y(\theta,0)=1 \tag{A-20}$$

and

$$\left.\frac{\partial y}{\partial x}\right|_{x=1}=0 \qquad \text{for all } \theta \tag{A-21}$$

The initial condition is:

$$y(x,0)=1 \tag{A-22}$$

The partial differential equation thus formulated has the general solution:

$$y=\sum_{n=0}^{\infty}a_n(\theta)\sin\left(\frac{2n+1}{2}\pi\, x\right) \tag{A-23}$$

where a_n are undetermined functions of θ, which must be solved for using the initial condition.

Integral Identities

In order to solve the differential equation it is necessary to evaluate several integrals. In order to make the solution easier to follow, the evaluation of these integrals is conducted here.

The first integral identity required is [Reference A.1, Equation 858.41]:

$$\int_0^1 \sin^2\left(\frac{2n+1}{2}\pi\, x\right)dx=\frac{1}{2} \tag{A-24}$$

The second integral identity required is:

$$\int_0^1 \sin\left(\frac{2n+1}{2}\pi\, x\right)dx=\frac{2}{(2n+1)\pi}\left\{-\cos\left(\frac{2n+1}{2}\pi\, x\right)\right\}\Bigg|_{x=0}^{x=\frac{2n+1}{2}\pi}=\frac{2}{(2n+1)\pi} \tag{A-25}$$

The third integral uses the general solution of y and the fact that the sine function in that definition is an orthogonal function. The integral of the product of two orthogonal functions is zero unless the functions are the same [Reference A.2]. This property is used in the derivation of the integral identity below.

$$\int_0^1 y \sin\left(\frac{2m+1}{2}\pi\, x\right) dx = \int_0^1 \left\{\sum_{n=0}^{\infty} a_n \sin\left(\frac{2n+1}{2}\pi\, x\right)\right\} \sin\left(\frac{2m+1}{2}\pi\, x\right) dx$$

$$= \int_0^1 a_n \sin^2\left(\frac{2n+1}{2}\pi\, x\right) dx \qquad \text{by orthogonality}$$

$$= a_n \int_0^1 \sin^2\left(\frac{2n+1}{2}\pi\, x\right) dx$$

$$= a_n \frac{1}{2} \qquad \text{by Equation (A-24)} \qquad \text{(A-26)}$$

The fourth integral identity necessary must be solved by multiple integration by parts. Note that the third integral identity just derived is necessary for the solution of the fourth integral.

$$\int_0^1 \frac{\partial^2 y}{\partial x^2} \sin\left(\frac{2n+1}{2}\pi\, x\right) dx = \left\{\sin\left(\frac{2n+1}{2}\pi\, x\right)\frac{\partial y}{\partial x}\right\}\Bigg|_{x=0}^{x=1} - \int_0^1 \frac{\partial y}{\partial x} \cos\left(\frac{2n+1}{2}\pi\, x\right)\frac{2n+1}{2}\pi\, dx$$

$$= -\frac{2n+1}{2}\pi \int_0^0 \frac{\partial y}{\partial x} \cos\left(\frac{2n+1}{2}\pi\, x\right) dx$$

$$= -\frac{2n+1}{2}\left\{y \cos\left(\frac{2n+1}{2}\pi\, x\right)\Bigg|_{x=0}^{x=1} + \int_0^0 y \sin\left(\frac{2n+1}{2}\pi\, x\right)\frac{2n+1}{2}\pi\, dx\right\}$$

$$= -\left(\frac{2n+1}{2}\pi\right)^2 \int_0^1 y \sin\left(\frac{2n+1}{2}\pi\, x\right) dx = -\left(\frac{2n+1}{2}\pi\right)^2 \frac{1}{2} a_n \qquad \text{(A-27)}$$

Solution of Undetermined Functions

To solve for the undetermined functions a_n, the integral identity given by Equation A-26 is rearranged to yield:

$$a_n = 2\int_0^1 y \sin\left(\frac{2n+1}{2}\pi x\right) dx \qquad \text{(A-28)}$$

Differentiating with respect to θ, yields:

$$\frac{da_n}{d\theta} = 2\int_0^1 \frac{\partial y}{\partial \theta} \sin\left(\frac{2n+1}{2}\pi x\right) dx \tag{A-29}$$

Substituting Equation A-19 into Equation A-29 gives:

$$\frac{da_n}{dt} = 2\int_0^1 \left[\frac{\partial^2 y}{\partial x^2} + \phi^2(1-y)\right] \sin\left(\frac{2n+1}{2}\pi x\right) dx \tag{A-30}$$

Separating the addition terms in the integral in Equation A-30 gives:

$$\frac{da_n}{d\theta} = 2\int_0^1 \frac{\partial^2 y}{\partial x^2} \sin\left(\frac{2n+1}{2}\pi x\right) dx + 2\phi^2 \int_0^1 \sin\left(\frac{2n+1}{2}\pi x\right) dx - 2\phi^2 \int_0^1 y \sin\left(\frac{2n+1}{2}\pi x\right) dx \tag{A-31}$$

The three integral terms in Equation A-31 are (from left to right) the three identities give by Equations A-27, A-25 and A-26. Substituting these identities into Equation A-31 gives:

$$\frac{da_n}{d\theta} = -\left(\frac{2n+1}{2}\pi\right)^2 + 2\phi^2 \frac{2}{(2n+1)\pi} - 2\phi^2 \frac{1}{2} a_n \tag{A-32}$$

which rearranged gives:

$$\frac{da_n}{d\theta} = \left[-\phi^2 - \left(\frac{2n+1}{2}\pi\right)^2\right] a_n + \frac{4\phi^2}{(2n+1)\pi} \tag{A-33}$$

In order to simplify the solution of the differential equation, it is convenient to make the following substitutions:

$$b_n \equiv -\phi^2 - \left(\frac{2n+1}{2}\pi\right)^2 \qquad\qquad c_n \equiv \frac{4}{(2n+1)\pi} \tag{A-34}$$

Substituting these definitions into Equation A-33 gives a simple differential equation:

$$\frac{da_n}{d\theta} = b_n a_n + c_n \phi^2 \tag{A-35}$$

The solution of this equation requires an initial condition for a_n. This is provided by substituting the value of θ=0 into Equation A-28, and noting that by Equation A-20, y=0 when θ=0. The initial condition is then given by:

$$a_n(0) = 2\int_0^1 \sin\left(\frac{2n+1}{2}\pi x\right)dx = 2\frac{2}{(2n+1)\pi} = \frac{4}{(2n+1)\pi} = c_n \tag{A-36}$$

The solution to Equation A-35 is as follows:

$$\int_0^\theta \frac{da_n}{b_n a_n + c_n\phi^2} = \int_0^\theta d\theta$$

$$\frac{1}{b_n}\ln\left(b_n a_n + c_n\phi^2\right)\Big|_{\theta=0}^{\theta} = \frac{1}{b_n}\ln\left(\frac{b_n a_n + c_n\phi^2}{b_n c_n + c_n\phi^2}\right) = \theta$$

$$\frac{b_n a_n + c_n\phi^2}{b_n c_n + c_n\phi^2} = e^{b_n\theta}$$

$$b_n a_n + c_n\phi^2 = \left(b_n c_n + c_n\phi^2\right)e^{b_n\theta}$$

$$a_n = -\frac{c_n\phi^2}{b_n} + \frac{b_n c_n + c_n\phi^2}{b_n}e^{b_n\theta}$$

$$a_n = \frac{c_n}{b_n}\left[-\phi^2 + \left(b_n + \phi^2\right)e^{b_n\theta}\right] \tag{A-37}$$

Substituting in the definitions given by Equation A-34 gives:

$$a_n = \frac{\dfrac{4}{(2n+1)\pi}}{\phi^2 + \left(\dfrac{2n+1}{2}\pi\right)^2}\left[\phi^2 + \left(\frac{2n+1}{2}\pi\right)^2 e^{-\left\{\phi^2 + \left(\frac{2n+1}{2}\pi\right)^2\right\}\theta}\right] \tag{A-38}$$

Construction of the Particular Solution

The functions a_n defined by Equation A-38 can now be substituted into the general solution given by Equation A-23 to give an explicit expression for y:

$$y = \sum_{n=0}^{\infty} \frac{\frac{4}{(2n+1)\pi}}{\phi^2 + \left(\frac{2n+1}{2}\pi\right)^2} \left[\phi^2 + \left(\frac{2n+1}{2}\pi\right)^2 e^{-\left\{\phi^2 + \left(\frac{2n+1}{2}\pi\right)^2\right\}\theta} \right] \sin\left(\frac{2n+1}{2}\pi x\right) \qquad \text{(A-39)}$$

Combining the definitions of s (Equation A-7) and y (Equation A-18) gives the transient non-dimensional concentration as a function of the non-dimensional time (θ) and the non-dimensional distance into the scale (x) for a given value of the Thiele Modulus (ϕ):

$$\begin{aligned} s &= \frac{C}{C_b} = 1 - y \\ &= 1 - \sum_{n=0}^{\infty} \frac{\frac{4}{(2n+1)\pi}}{\phi^2 + \left(\frac{2n+1}{2}\pi\right)^2} \left[\phi^2 + \left(\frac{2n+1}{2}\pi\right)^2 e^{-\left\{\phi^2 + \left(\frac{2n+1}{2}\pi\right)^2\right\}\theta} \right] \sin\left(\frac{2n+1}{2}\pi x\right) \end{aligned} \qquad \text{(A-40)}$$

Validation

Because of the complexity of the transient solution, it is useful to analyze a few test cases to ensure that the derived solution behaves in a way that is not counterintuitive. Three test cases were analyzed. These were as follows:

- Comparison with the steady state solution (ϕ=1; θ=5)
- Comparison of solutions with different values of ϕ (ϕ=5, 2, 1, 0.5 or 0.2; θ=5)
- Comparison of solutions at different times (ϕ=1; θ=0.01, 0.1, 0.5, 1 and 5)

Each of these cases was examined qualitatively to validate Equation A-40. For the purpose of these validation cases and for the cases given in the main body of the report, solutions to Equation A-40 were generated using the sum of terms up to and including n = 6. The solution to Equation A-40 becomes increasingly unstable as ϕ becomes large or as θ becomes small. If n > 6 terms are truncated, the solutions are stable and accurate if ϕ is not much larger than 5 and if θ is not much smaller than 0.01. Only solutions with $\phi \leq 5$ and $\theta \geq 0.01$ were considered.

Figure A-1 shows a comparison of the steady state solution (Equation A-16) and the transient solution (Equation A-40) at θ=5, which is comparable to infinity for the case considered. A value of ϕ=1 was selected for this test case because at this value reaction and diffusion phenomena are roughly of equal influence and the solution is most likely to display any calculation errors. From the figure, it is evident that there is strong agreement between the two solutions. The boundary conditions are also met since s=1 at x=0 (as required by Equation A-20) and the slope of the curve is zero (*i.e.*, horizontal) at x=1 (as required by Equation A-21).

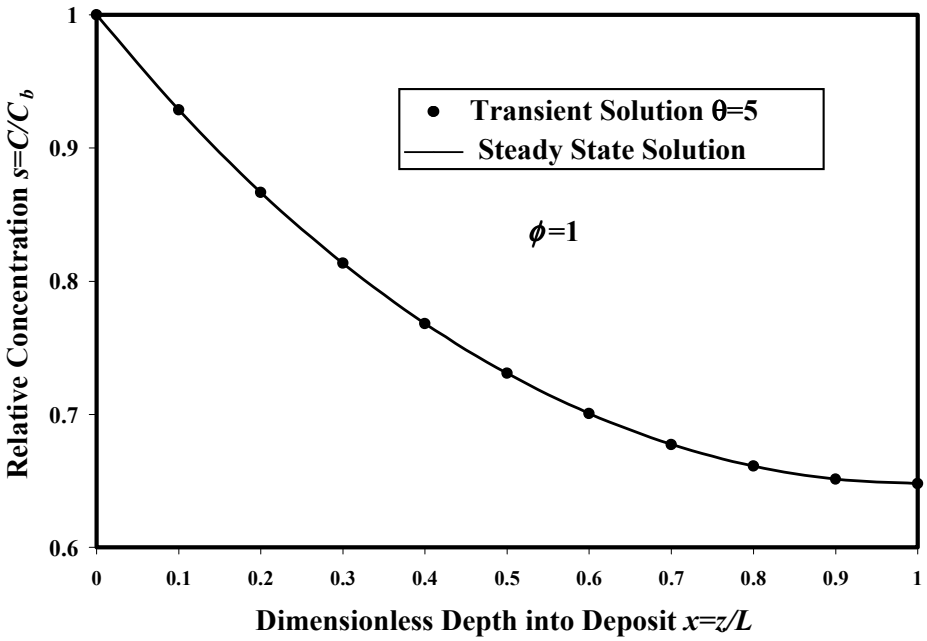

Figure A-1
Comparison of Steady State and Transient Solutions (θ=5, ϕ=1)

Figure A-2 shows solutions to Equation A-40 for $\theta = 5$ and various values of ϕ. For relatively large values of ϕ, there is a significant difference in concentration between the bulk and the inside of the crevice. This is as expected, since a large ϕ value implies that diffusion is the rate limiting factor. From the definition of ϕ (Equation A-18) it is clear that three different conditions (or a combination of the three) can lead to a large value of ϕ. These three conditions are as follows:

- The crevice is very deep (L is large)
- The decomposition reaction is very fast (k_d is large)
- Diffusion is very slow (D is small)

When considered separately, it is clear that each of these three conditions would be expected to lead to a low concentration of scavenger in the crevice. Conversely, the following three conditions (or a combination of the three) will lead to a low value of ϕ:

- The crevice is very shallow (L is small)
- The decomposition reaction is very slow (k_d is small)
- Diffusion is very fast (D is large)

Each of these conditions would lead to a relatively constant concentration of scavenger in the crevice. This is reflected in the test cases in Figure A-2 for $\phi = 0.5$ and $\phi = 0.2$. The behavior of the transient solution conforms with intuitive expectations with respect to changes in the value of ϕ.

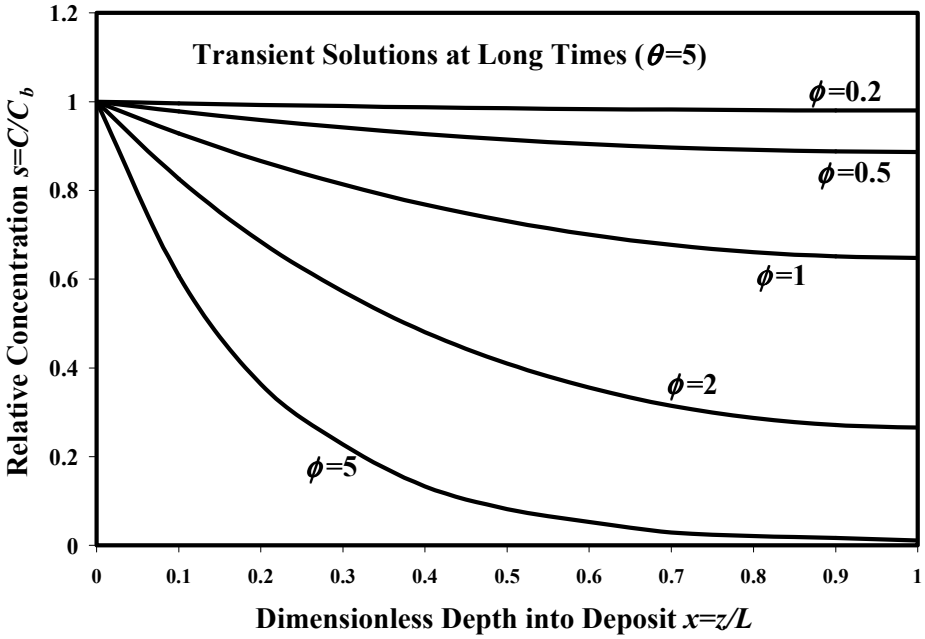

Figure A-2
Transient Solutions at Long Times (θ=5) for Different Values of ϕ

Figure A-3 shows solutions to Equation A-40 for different dimensionless times (θ) for $\phi = 1$. At times close to zero ($\theta = 0.01$), the scavenger concentration in the crevice is close to zero, as required by the initial condition (Equation A-22). As time progresses, the concentration in the portions of the crevice closest to the bulk (low x) slowly increases. At the bottom of the crevice ($x = 1$), the concentration starts at zero and slowly rises to the final steady state value. At every time, the concentration at the mouth of the crevice ($x = 0$) is 1, satisfying the first boundary condition (Equation A-20). At every time, the slope of the curve (the concentration gradient) is 0 at the bottom of the crevice ($x = 1$), satisfying the second boundary condition (Equation A-21).

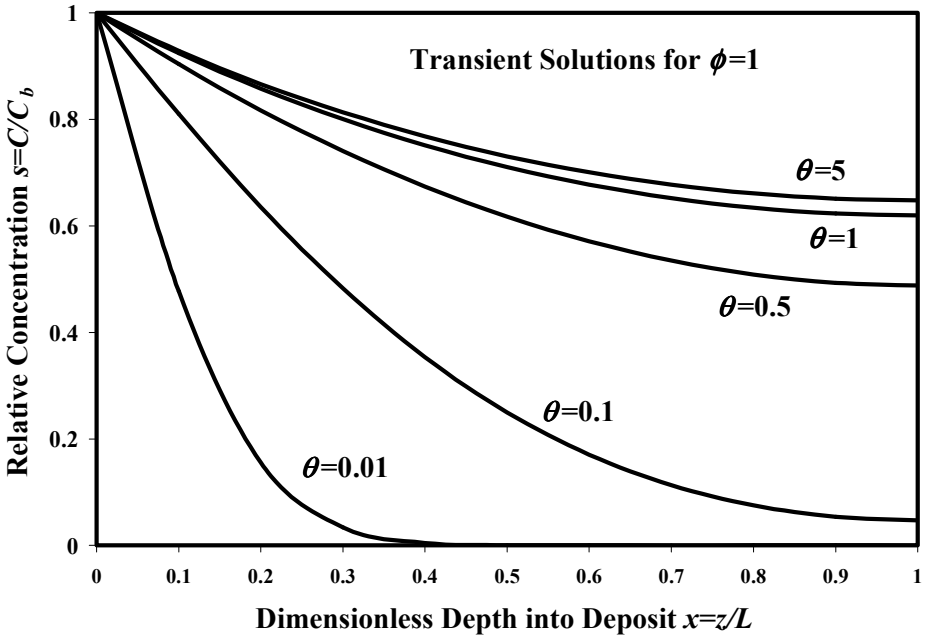

Figure A-3
Transient Solutions at Multiple Times for $\phi = 1$

The solution given by Equation A-40 satisfies the validation tests and satisfactorily gives the expected qualitative behavior of the system.

B
APPENDIX B: CALCULATION OF THE DIFFUSIVITIES OF OXYGEN SCAVENGERS

Purpose

The purpose of this calculation is to provide estimated values of the diffusivities of hydrazine and carbohydrazide in water.

Summary of Results

The calculation predicts the following diffusivities for hydrazine and carbohydrazide:

$$D_{hydrazine} = 2.52 \text{ x } 10^{-5} \frac{cm^2}{s} \tag{B-1}$$

$$D_{carbohydrazide} = 3.01 \text{ x } 10^{-5} \frac{cm^2}{s} \tag{B-2}$$

Project Input Requirements

Diffusivity of ammonia [B.1]:

$$D_{ammonia} = 2.0 \text{ x } 10^{-5} \frac{cm^2}{s} \tag{B-3}$$

Densities of hydrazine [B.1], carbohydrazide [B.2] and ammonia [B.1]:

$$\rho_{hydrazine} = 1.011 \frac{g}{cm^3} \tag{B-4}$$

$$\rho_{carbohydrazide} = 1.616 \frac{g}{cm^3} \tag{B-5}$$

$$\rho_{ammonia} = 0.618 \frac{g}{cm^3} \tag{B-6}$$

Molecular weights of water [B.1], hydrazine [B.1], carbohydrazide [B.2] and ammonia [B.1]:

$$MW_{water} = 18 \tag{B-7}$$

$$MW_{hydrazine} = 32 \tag{B-8}$$

$$MW_{carbohydrazide} = 90 \tag{B-9}$$

$$MW_{ammonia} = 17 \tag{B-10}$$

Viscosity of water [B.1]:

$$\eta_{water} = 0.85\ cP \tag{B-11}$$

Association factor of water [B.1]:

$$\phi_{water} = 2.6 \tag{B-12}$$

Assumptions

The method of the calculation is to assume that the diffusivity of hydrazine and carbohydrazide is similar to that of ammonia. This assumption is based on the similarity of the chemistry of the three molecules. The method further assumes that the diffusivity of the three species can be accurately described by the Wilke-Change equation given in Reference B.1.

Calculation

The calculation is based on the Wilke-Chang equation, which is given in Reference B.1 as:

$$D = 7.4\ x\ 10^{-8}\ \frac{\left(\phi_{water} MW_{water}\right)^{\frac{1}{2}} T}{\eta_{water} V^{0.6}} \tag{B-13}$$

where T is the absolute temperature and V is the molar volume of water. The molar volume can be calculated from the density and the molecular weight by the following equation:

$$V = \frac{MW}{\rho} \tag{B-14}$$

The molar volumes of the three diffusing species are given in Table B-1.

Table B-1
Determination of Molecular Volumes

Substance	MW	Density (g/cm^3)	Mol Vol (cm^3/mol)
Ammonia	17	0.618	27.5
Hydrazine	32	1.011	31.7
Carbohydrazide	90	1.616	55.7

Given the input data and the molecular volumes listed above, Equation B-13 can be evaluated for each compound as follows:

$$D_{ammonia} = 7.4\ x\ 10^{-8}\ \frac{(2.6\,18)^{\frac{1}{2}}303}{0.85\ \ 27.5^{0.6}} = 2.47 \text{ x } 10^{-5}\ \frac{cm^2}{s} \tag{B-15}$$

$$D_{hydrazine} = 7.4\ x\ 10^{-8}\ \frac{(2.6\,18)^{\frac{1}{2}}303}{0.85\ \ 31.7^{0.6}} = 2.27 \text{ x } 10^{-5}\ \frac{cm^2}{s} \tag{B-16}$$

$$D_{carbohydrazide} = 7.4\ x\ 10^{-8}\ \frac{(2.6\,18)^{\frac{1}{2}}303}{0.85\ \ 55.7^{0.6}} = 1.62 \text{ x } 10^{-5}\ \frac{cm^2}{s} \tag{B-17}$$

However, Reference B.1 gives the diffusivity of ammonia in water as $2.0 \text{x} 10^{-5}$ cm^2/s. Although Equation B-15 gives a reasonable estimate, correcting Equation B-13 by a factor of 0.8 would yield a more accurate prediction. Since hydrazine and carbohydrazide interact with water in a way similar to ammonia, correcting Equations B-16 and B-17 by a factor of 0.8 would most likely improve the accuracy of the estimate of the diffusivity. Making that correction yields the following results:

$$D_{hydrazine} = 0.8 \cdot 2.27 \text{ x } 10^{-5}\ \frac{cm^2}{s} = 1.8 \text{ x } 10^{-5}\ \frac{cm^2}{s} \tag{B-18}$$

$$D_{carbohydrazide} = 0.8 \cdot 1.62 \text{ x } 10^{-5}\ \frac{cm^2}{s} = 1.3 \text{ x } 10^{-5}\ \frac{cm^2}{s} \tag{B-19}$$

Equations B-18 and B-19 represent the best available estimates of the diffusivities of hydrazine and carbohydrazide.

References

B.1. Perry, R.H. and D.W. Green, *Perry's Chemical Engineers' Handbook, Sixth Edition*, McGraw-Hill Book Company, New York, 1984.

B.2. Kurzer, F. and M. Wilkinson, "The Chemistry of Carbohydrazide and Thiocarbohydrazide," *Chemical Reviews*, **70:1**, 111, 1970.

C
APPENDIX C: TYPICAL SECONDARY SIDE STARTUP CONDITIONS

Introduction

A limited survey of secondary side startup conditions was conducted. Responses were obtained from 5 US units. Four of these provided secondary side chemistry data from recent startups; one provided their current startup chemistry procedure with some supplementary data from a recent startup. Responses were also obtained from two foreign units, which provided data on recent startups. The startup dates ranged from 1997 to 2001.

The survey requested the following secondary-side chemistry data as functions of time from plant personnel:

- Temperature
- Oxygen concentration
- Hydrazine (or other scavenger) concentration
- pH

The extent of the information provided varied from unit to unit. Summaries of the information provided are given below.

Startup Data

In total, seven plants (A through G) provided data on the chemistry of recent startups. Three of these plants provided data from two startups. The data from the first 6 of these plants are shown in graphical form in Figure C-1 through Figure C-32.

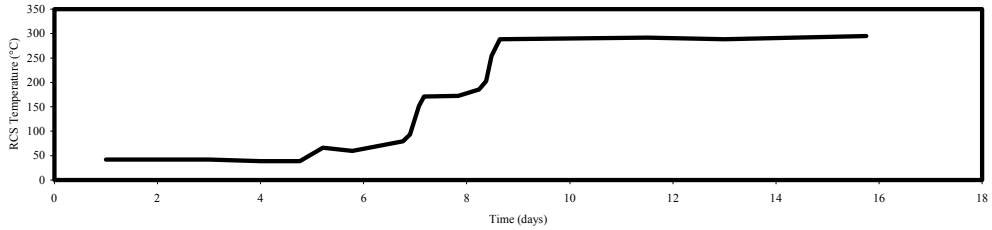

Figure C-1
Plant A, Startup 1: Temperature as a Function of Time

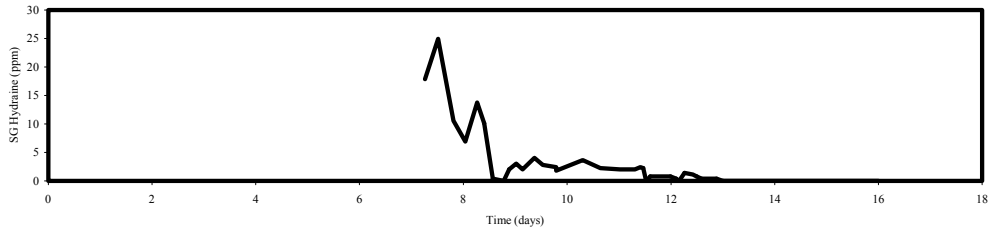

Figure C-2
Plant A, Startup 1: Hydrazine as a Function of Time

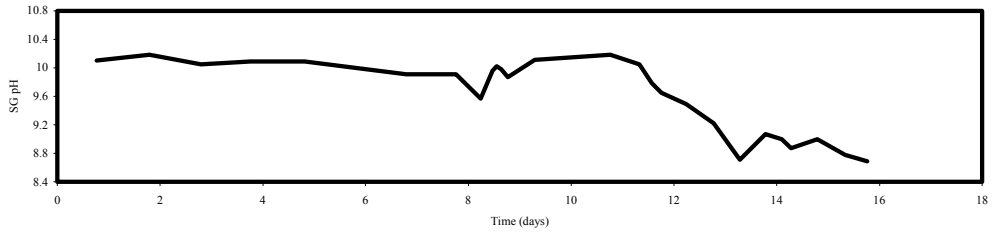

Figure C-3
Plant A, Startup 1: pH as a Function of Time

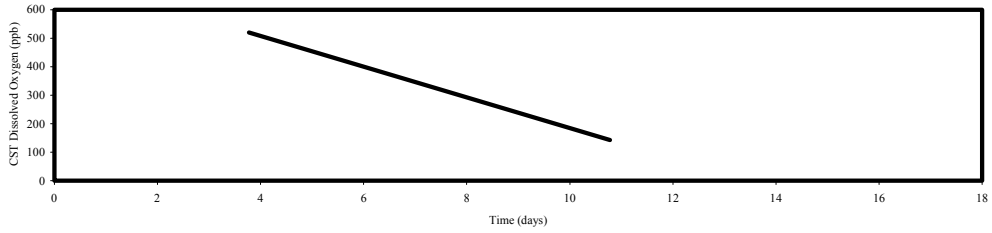

Figure C-4
Plant A, Startup 1: Dissolved Oxygen as a Function of Time

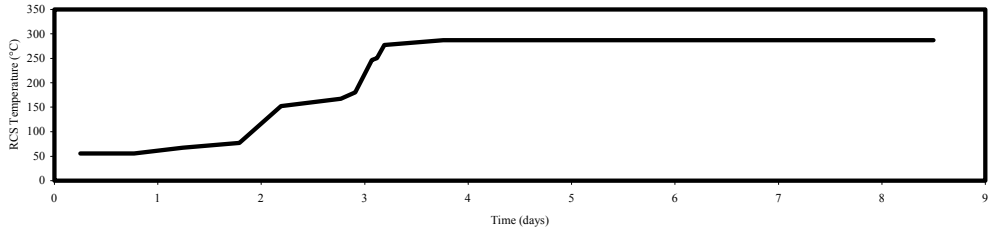

Figure C-5
Plant A, Startup 2: Temperature as a Function of Time

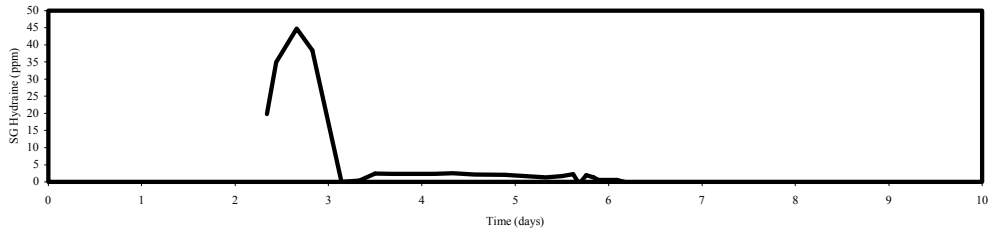

Figure C-6
Plant A, Startup 2: Hydrazine as a Function of Time

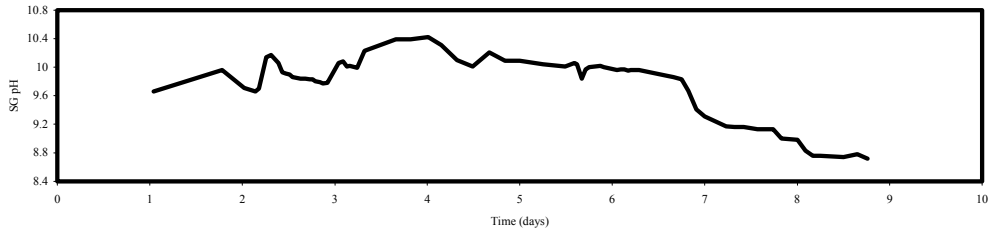

Figure C-7
Plant A, Startup 2: pH as a Function of Time

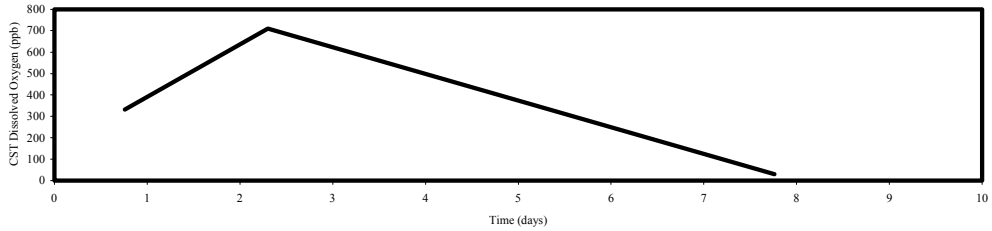

Figure C-8
Plant A, Startup 2: Dissolved Oxygen as a Function of Time

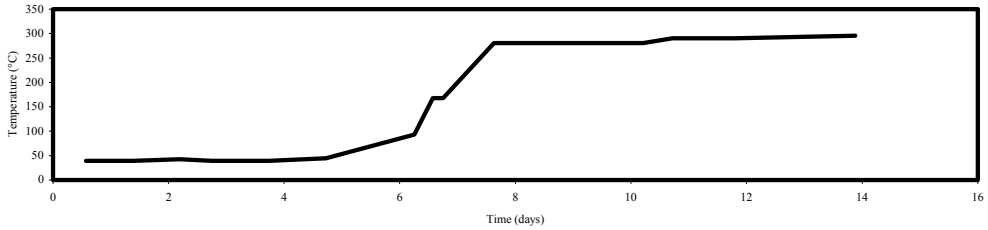

Figure C-9
Plant B, Startup 1: Temperature as a Function of Time

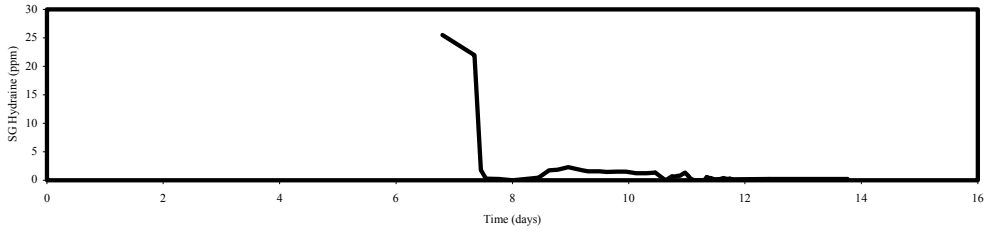

Figure C-10
Plant B, Startup 1: Hydrazine as a Function of Time

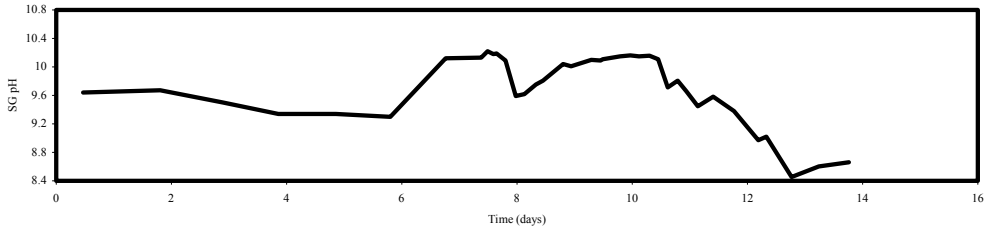

Figure C-11
Plant B, Startup 1: pH as a Function of Time

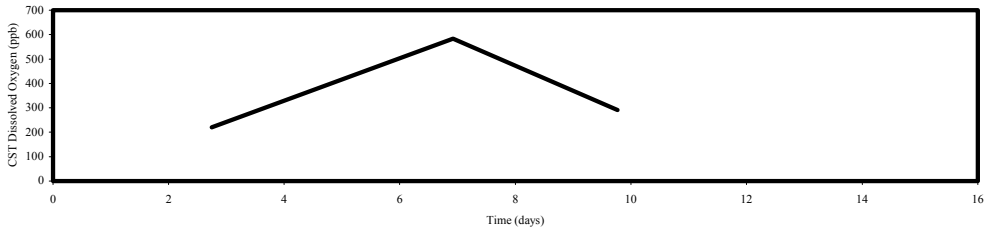

Figure C-12
Plant B, Startup 1: Dissolved Oxygen as a Function of Time

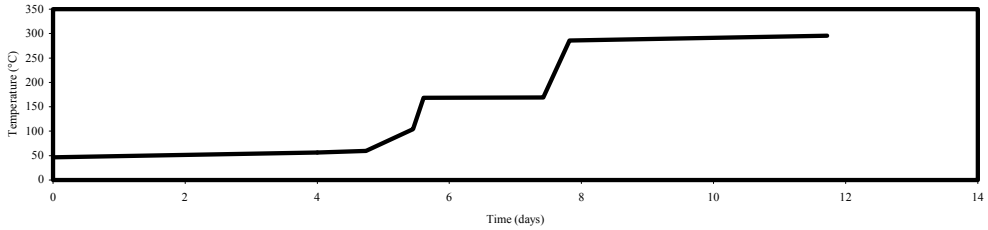

Figure C-13
Plant B, Startup 2: Temperature as a Function of Time

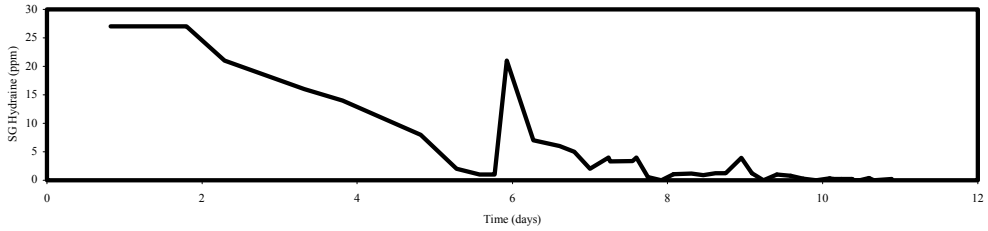

Figure C-14
Plant B, Startup 2: Hydrazine as a Function of Time

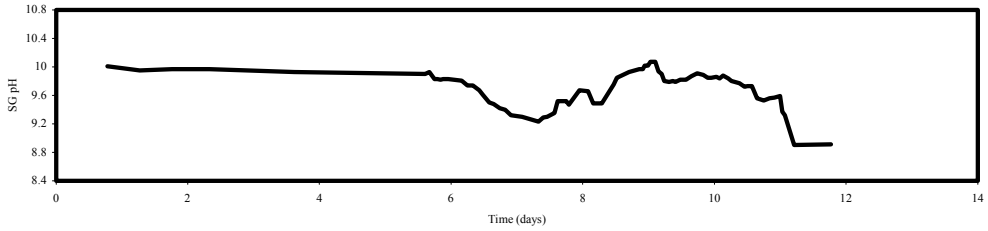

Figure C-15
Plant B, Startup 2: pH as a Function of Time

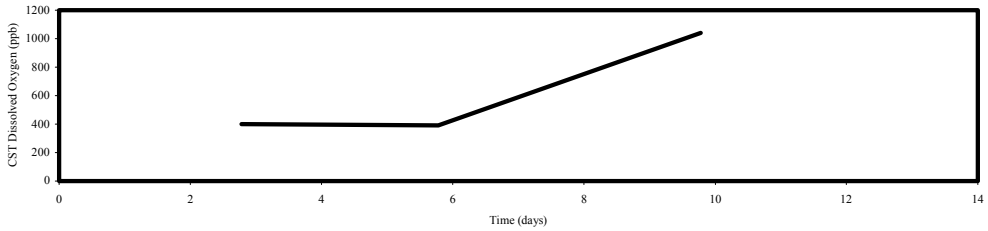

Figure C-16
Plant B, Startup 2: Dissolved Oxygen as a Function of Time

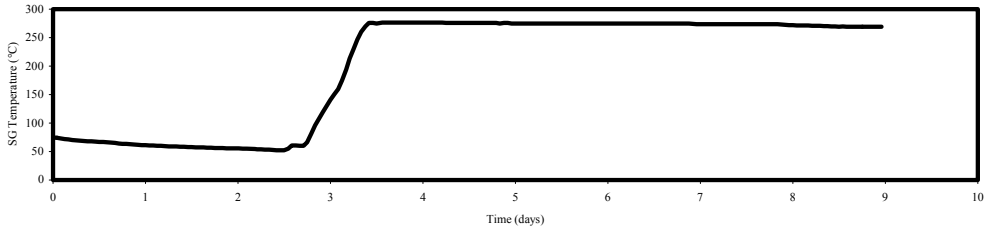

Figure C-17
Plant C: Temperature as a Function of Time

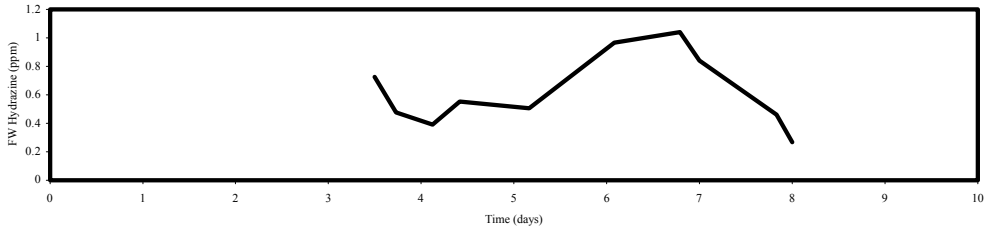

Figure C-18
Plant C: Hydrazine as a Function of Time

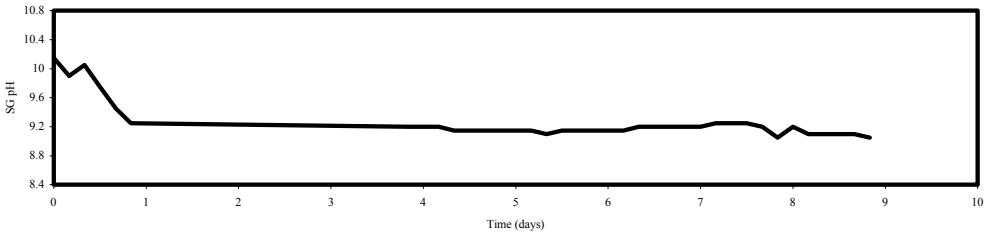

Figure C-19
Plant C: pH as a Function of Time

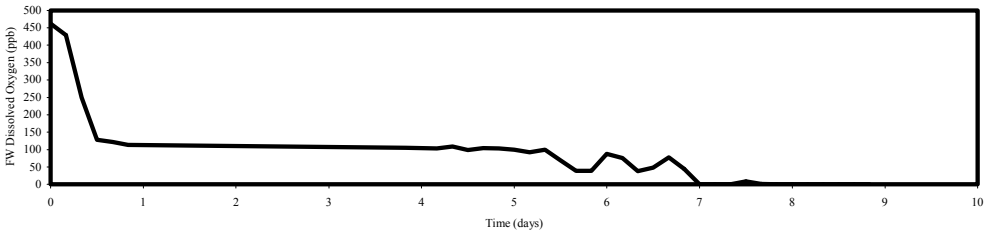

Figure C-20
Plant C: Dissolved Oxygen as a Function of Time

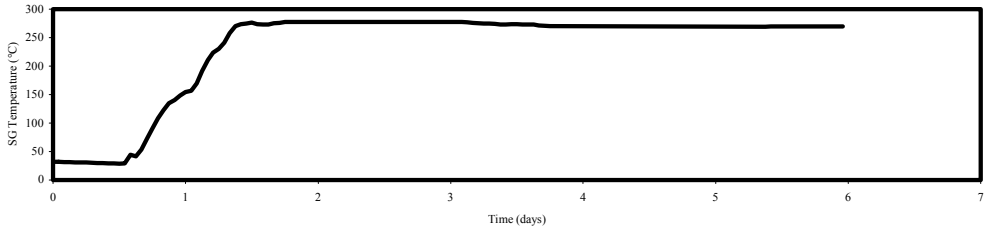

Figure C-21
Plant D, Startup 1: Temperature as a Function of Time

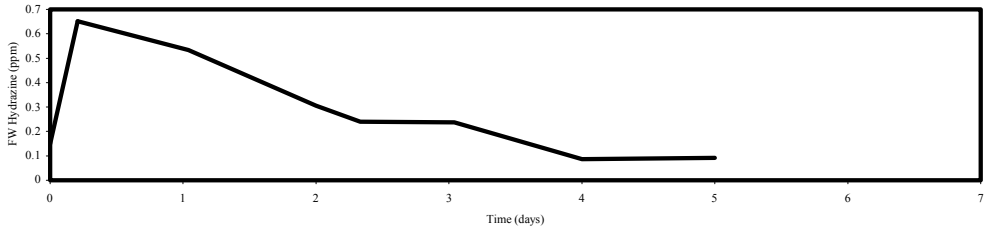

Figure C-22
Plant D, Startup 1: Hydrazine as a Function of Time

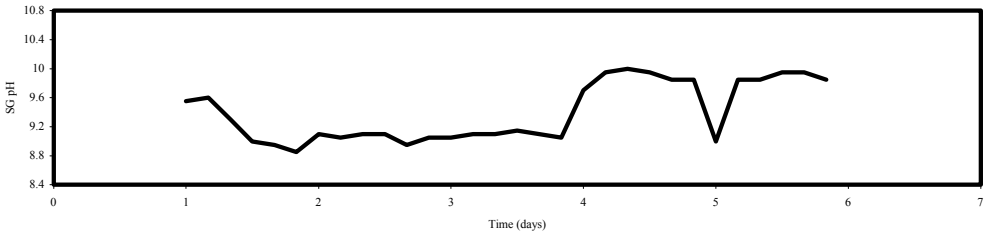

Figure C-23
Plant D, Startup 1: pH as a Function of Time

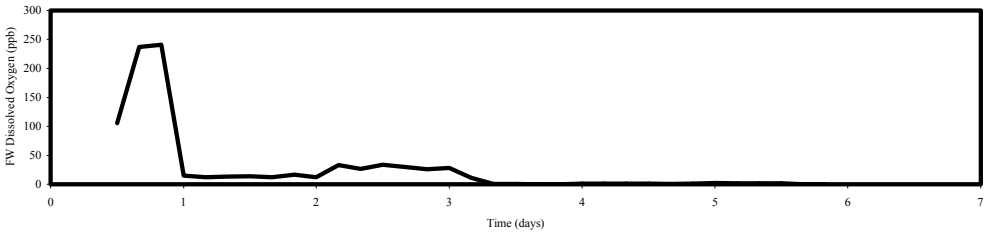

Figure C-24
Plant D, Startup 1: Dissolved Oxygen as a Function of Time

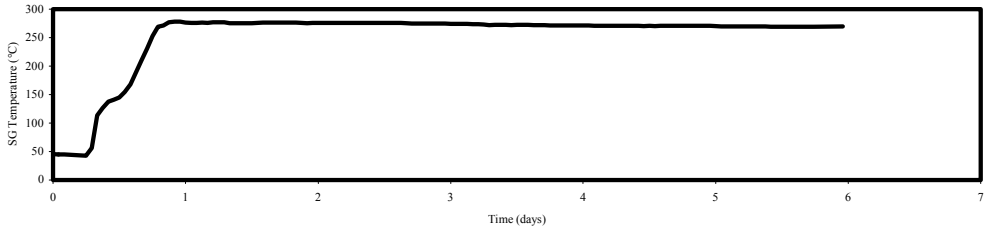

Figure C-25
Plant D, Startup 2: Temperature as a Function of Time

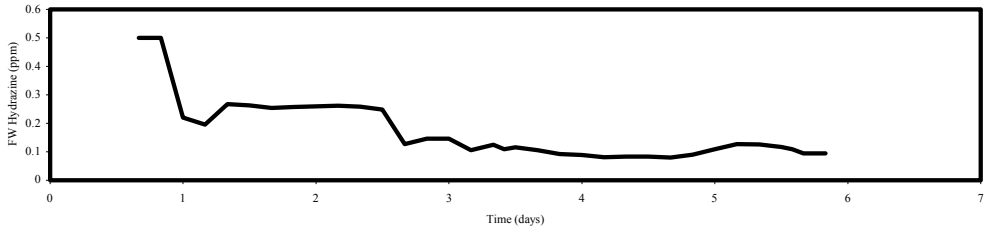

Figure C-26
Plant D, Startup 2: Hydrazine as a Function of Time

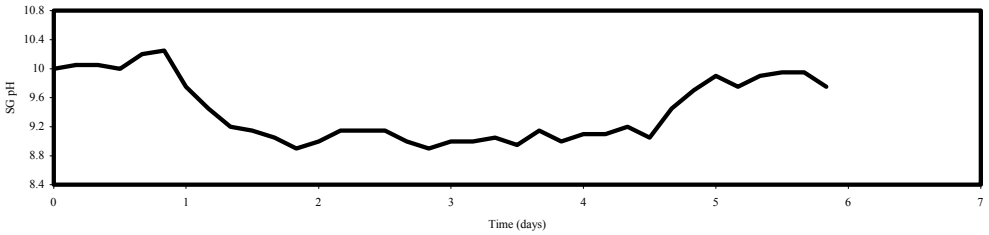

Figure C-27
Plant D, Startup 2: pH as a Function of Time

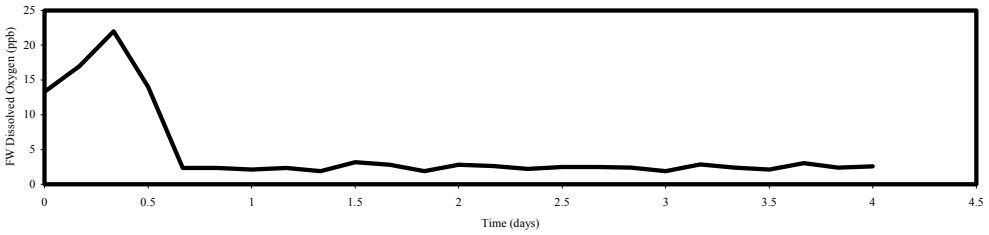

Figure C-28
Plant D, Startup 2: Dissolved Oxygen as a Function of Time

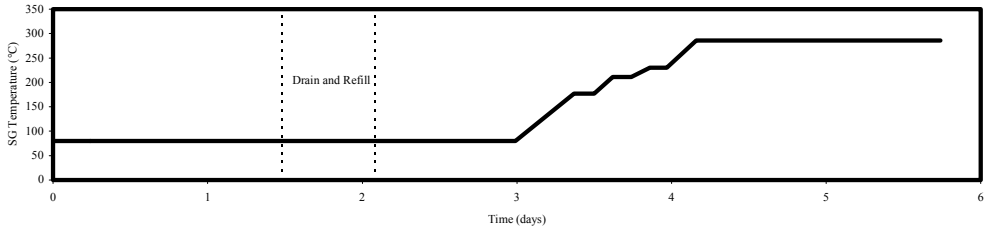

Figure C-29
Plant E: Temperature as a Function of Time

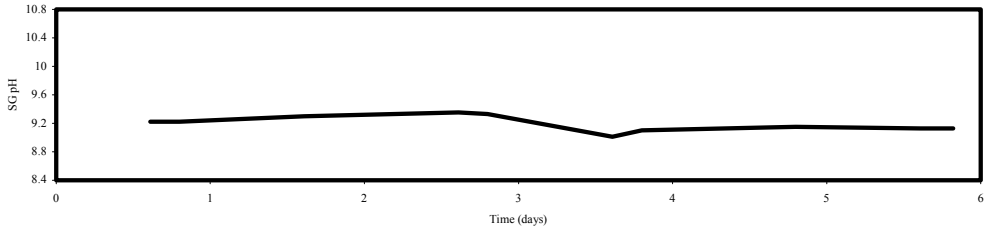

Figure C-30
Plant E: Hydrazine as a Function of Time

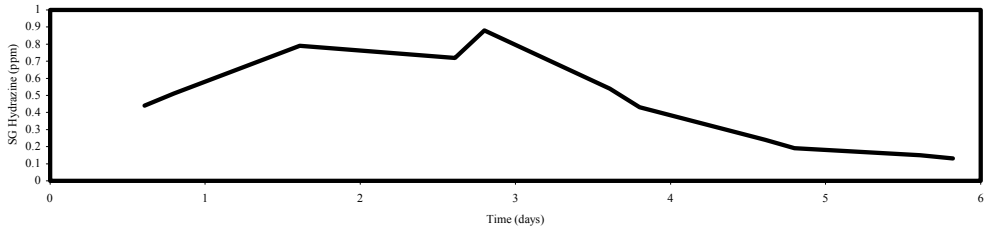

Figure C-31
Plant E: pH as a Function of Time

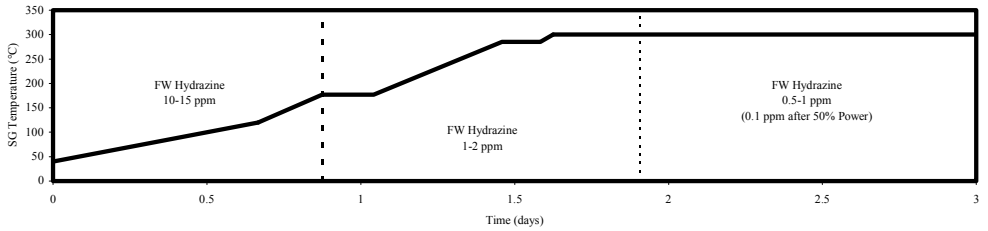

Figure C-32
Plant F: Temperature as a Function of Time

Plant G provided the feedwater specifications used during startup. The relevant specifications with respect to deposit oxidation and reduction are as follows:

- pH > 9
- DO < 100 ppb
- Hydrazine > 8 times DO or 100 ppb (whichever is higher)

These specifications were supplemented by the following information regarding a recent outage:

- At the commencement of heatup (65°C—146°F), the SG hydrazine concentration was about 30 to 60 ppm.
- After a few days the SG hydrazine concentration had fallen to about 17 ppm.
- When the temperature had reached 292°C (558°F), the SG hydrazine concentration was approximately zero.

Target:
Nuclear Power

About EPRI

EPRI creates science and technology solutions for the global energy and energy services industry. U.S. electric utilities established the Electric Power Research Institute in 1973 as a nonprofit research consortium for the benefit of utility members, their customers, and society. Now known simply as EPRI, the company provides a wide range of innovative products and services to more than 1000 energy-related organizations in 40 countries. EPRI's multidisciplinary team of scientists and engineers draws on a worldwide network of technical and business expertise to help solve today's toughest energy and environmental problems.

EPRI. Electrify the World

Printed on recycled paper in the United States of America

1003591

EPRI • 3412 Hillview Avenue, Palo Alto, California 94304 • PO Box 10412, Palo Alto, California 94303 • USA
800.313.3774 • 650.855.2121 • askepri@epri.com • www.epri.com